AIGARS EKERS

Fizikas maģistrs / Master of Physics

ENERĢIJAS PĀRDEVES UN JONIZĀCIJAS PROCESI SĀRMU METĀLU MOLEKULU UN ATOMU SADURSMĒS

ENERGY TRANSFER AND IONISATION PROCESSES IN COLLISIONS OF ALKALI METAL MOLECULES AND ATOMS

Promocijas darbs / Promotion work

Latvijas Universitāte / University of Latvia

Rīga - 1999

Disertācijā iekļauto publikāciju saraksts

A list of publications included in the dissertation

[Dis1] **A. Ekers**, "*A study of Na(4d) + Na(3s) inelastic collisions*", Proceedings of the Latvian Academy of Sciences B **7/8**, 130 (1995).

[Dis2] Luo Caiyan, **A. Ekers**, J. Klavins, and M. Jansons, "*Studies of inelastic cross section in Rb(7S) + Rb(5S) collisions*", Physica Scripta **53**, 306 (1996).

[Dis3] **A. Ekers**, M. Głódź, J. Szonert, B. Bieniak, K. Fronc, and T. Radelitski, "*Inelastic cross sections and natural lifetimes for the $6^2D_{3/2,5/2}$ and $8^2S_{1/2}$ states of Rb*", Eur. Phys. J. D (submitted).

[Dis4] **A. Ekers** and J. Alnis, "*Non-dipole excitation transfer between the 6^2S and 4^2D states in potassium*", Latv. J. Phys. Techn. Sci. (1999) in press.

[Dis5] J. Klavins, M. Jansons, **A. Ekers**, Luo Caiyan, and S. Svanberg, "*Ionization in collisions between excited sodium dimers and atoms*", Chem. Phys. Lett. **228**, 346 (1994).

[Dis6] **A. Ekers**, O. Kaufmann, K. Bergmann, J. Alnis, and J. Klavins, "*Vibrational effects in $Na_2(A^1\Sigma_u^+,v')$ + $Na(3p_{3/2})$ associative ionization*", Chem. Phys. Lett. (1999) in press.

[Dis7] **A. Ekers**, O. Kaufmann, M. Keil, and K. Bergmann, "*Associative ionization in collisions of electronically excited Na atoms with vibrationally excited $Na_2(v'')$ molecules*", Eur. Phys. J. D (submitted).

Original Paper: Atomic & Molecular Physics

PROCEEDINGS OF THE LATVIAN ACADEMY OF SCIENCES. Section B, 1995, no. 7/8 (576/577), pp. 130–132.

A STUDY OF Na(4d) + Na(3s) INELASTIC COLLISIONS

A. Ekers

Institute of Atomic Physics and Spectroscopy, University of Latvia:
Raiņa bulv. 19, Rīga, LV-1586 LATVIA

In the Na 4d state, the J=5/2 component was selectively excited, and a population of $5s_{1/2}$ was observed. The solution of balance equations showed that the cross-section for the excitation transfer process Na(4d) + Na(3s) → Na(5s) + Na(3s) is about $10^{-15}cm^2$. The presented treatment of balance equations allowed to determine ET cross-sections for both the 4d J=3/2 and J=5/2 components, relatively to 4d fine structure mixing cross-sections, even when only one J component was directly excited and when fluorescence from this level could not be detected.

PACS number: 34.50.

Received September 27, 1995

Recommended for publication by Māris Jansons, Full Member of the Latvian Academy of Sciences

1. INTRODUCTION

Recently, it was shown [1] that the excitation transfer (ET) process between rubidium atomic *7s* and *5d* states proceeds at a relatively large cross-section ($\sigma = 8\times10^{-15}$ cm^2). Alkali *s* and *d* states are not directly connected with the ground state by electric dipole transitions. Therefore, the well known dipole-dipole interaction can be neglected in processes of this kind, and other interactions must exist which are able to provide high efficiency of the ET. This suggested to investigate other alkali atoms.

In the present work, ET between the sodium atomic *4d* and *5s* states was studied:

$$Na(4d_{3/2,5/2}) + Na(3s_{1/2}) \rightarrow Na(5s_{1/2}) + Na(3s_{1/2}) + \\ + \Delta E(+1348\,cm^{-1}). \qquad (1)$$

In *4d* state, only the *J=5/2* component was selectively excited, using single frequency ring dye laser radiation on transition $3p_{3/2} \rightarrow 4d_{5/2}$ (cf. Fig. 1). The *3p* state population was achieved by non-resonant collision induced absorption of photons of the same wavelength:

$$Na(3s_{1/2}) + Na(3s_{1/2}) + h\nu \rightarrow Na(3p_{1/2,3/2}) + Na(3s_{1/2}). \qquad (2)$$

Such a method of excitation has, for instance, been applied to achieve *6d* state in caesium [2].

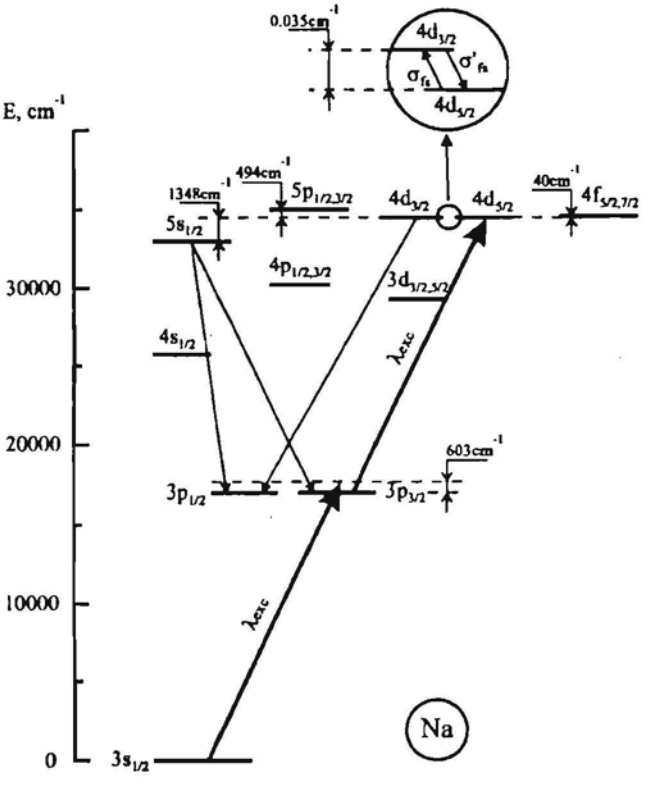

Fig. 1. Partial term diagram of a sodium atom, showing the exciting laser at λ_{exc} = 568.8 nm (thick arrowlines) and the detected LIF transitions (thin arrowlines). The fine structure of the *4d* state is shown magnified (in a circle), together with the corresponding mixing cross-sections σ_{fs} and σ'_{fs}.

2. EXPERIMENT

The experiment was carried out in sodium vapour following the typical scheme for laser-induced fluorescence (LIF) experiments. The sodium vapour was contained in an alkali resistant glass cell with a sapphire window for laser beam entry. The vapour temperature varied between 280 and 340 °C, and the concentration N_0 of sodium ground state atoms was calculated from the vapour pressure [3]. Na atoms were excited by an unfocused beam ($\varnothing \simeq 2$ mm) of a single frequency cw ring dye laser (Coherent Radiation, model CR-699), with Rh6G dye and about 250 mW of output power. The LIF spectra were recorded with a monochromator (Carl Zeiss, model GDM1000), a photomultiplier tube (FEU-51) and a lock-in amplifier (home built).

3. RESULTS AND DISCUSSION

Fluorescence was detected on $5s_{1/2} \rightarrow 3p_{1/2,3/2}$ and $4d_{3/2} \rightarrow 3p_{1/2}$ transitions, and it was observable only when the laser radiation was in resonance with the $3p_{3/2} \rightarrow 4d_{5/2}$ transition. Hence, Na $5s_{1/2}$ state was not excited in the energy pooling process [4]:

$$Na(3p) + Na(3p) \rightarrow Na(5s) + Na(3s). \quad (3)$$

In fact, it was not possible to detect fluorescence from the laser excited $4d_{5/2}$ level, since the $4d_{5/2} \rightarrow 3p_{3/2}$ transition overlaps with scattered laser light, but $4d_{5/2} \rightarrow 4p_{3/2}$ is infrared, which was beyond the sensitivity of the photomultiplier.

There are two possibilities for populating the $5s_{1/2}$ state. One is direct ET from *4d* to *5s* state (1), since there is a crossing of diabatic terms of *4d+3s* and *5s+3s* configurations located at ca 11.5 a.u. [5]. Another possibility is ET from *4d* to *5p* with subsequent radiational transition to 5s:

$$Na(4d) + Na(3s) \rightarrow Na(5p) + Na(3s) + \\ + \Delta E(-494\ cm^{-1}), \quad (4)$$

$$Na(5p) \rightarrow Na(5s) + h\nu\ (A=1.36\times10^{6}s^{-1}). \quad (5)$$

In the first case, neglecting ET between *4d* and *4f* states, the process can be described by the following system of balance equations (steady state conditions assumed):

$$[\dot{5s}] = 0 = [4d_{3/2}]N_0\sigma_1 v + [4d_{5/2}]N_0\sigma_2 v - [5s]\frac{1}{\tau_{5s}}; \quad (6.1)$$

$$[\dot{4d_{3/2}}] = 0 = [4d_{5/2}]N_0\sigma_{fs} v - [4d_{3/2}]\{\sigma_1 + \sigma'_{fs} + \frac{1}{\tau_{4d}N_0 v}\}. \quad (6.2)$$

Here, σ_1 and σ_2 are the cross sections for ET $4d_{3/2} \rightarrow 5s_{1/2}$ and $4d_{5/2} \rightarrow 5s_{1/2}$ respectively; v is the mean velocity; N_0 is the density of ground state atoms; σ_{fs} and σ'_{fs} are the cross-sections for the fine structure mixing of *4d* state in collisions with ground state Na atoms; τ_{5s}, τ_{4d} are the lifetimes of *5s* and *4d* states. The square brackets denote the populations of the respective state. By expressing $[4d_{5/2}]$ from (6.2) and substituting it into (6.1), one can obtain

$$\frac{[5s_{1/2}]}{[4d_{3/2}]} = \left\{\sigma_1 + \sigma_2\left(\frac{\sigma_1}{\sigma_{fs}} + \frac{\sigma'_{fs}}{\sigma_{fs}}\right)\right\}\tau_{5s} v \cdot N_0 + \frac{\sigma_2}{\sigma_{fs}}\frac{\tau_{5s}}{\tau_{4d}}. \quad (7)$$

Multiplying and dividing both sides of eq. (7) by transition probabilities $A(3s–5s)$ and $A(4d_{3/2}–3p_{1/2})$, we finally obtain

$$\eta(N_0) = \frac{n_q(5s \rightarrow 3p)}{n_q(4d_{3/2} \rightarrow 3p_{1/2})} = aN_0 + b, \quad (8)$$

where

$$a = \frac{A(5s-3p)}{A(4d_{3/2}-3p_{1/2})}\tau_{5s} v\left\{\sigma_1 + \sigma_2\left(\frac{\sigma_1}{\sigma_{fs}} + \frac{\sigma'_{fs}}{\sigma_{fs}}\right)\right\}; \quad (8')$$

$$b = \frac{A(5s-3p)}{A(4d_{3/2}-3p_{1/2})}\frac{\tau_{5s}}{\tau_{4d}}\frac{\sigma_2}{\sigma_{fs}}. \quad (8'')$$

Here, n_q are the quantum fluxes of corresponding transitions [$cm^{-3}\times s^{-1}$], which were measured relatively in the experiment that accounted for the spectral sensitivity of the detection system. The values for the lifetimes and the spontaneous transition probabilities can be found in [6].

The experimental η dependence on sodium atom ground state concentration N_0 is shown in Fig. 2. At extrapolation $N_0 \rightarrow 0$, η has a small value which corresponds to b in eq. (8). This residual value appears since fluorescence from the collision excited $4d_{3/2}$ level was measured instead of the signal from the laser excited $4d_{5/2}$ (fluorescence on the $4d_{5/2} \rightarrow 3p_{3/2}$ transition overlaps with scattered laser light).

Both parameters a and b of eq. (8) can be extracted from the experimental $\eta(N_0)$ dependence (see Fig. 2). Substitution of a and b into (8') and (8") gives the cross-sections for the ET process (1), relative to fine structure mixing cross-sections σ_{fs} and σ'_{fs} of the *4d* state:

$$\sigma_1 = 5.04 \times 10^{-15}cm^2 - 0.078\sigma'_{fs},$$

$$\sigma_2 = 0.085\sigma_{fs}.$$

Thus, the cross-sections σ_1 and σ_2 can be expressed by *4d* state fine structure mixing cross-sections. Unfortunately, values σ_{fs} and σ'_{fs} were not found in the existing literature, but for the lowest alkali *d* states they usually are in the range of $10^{-14}cm^2$. One can see that σ_1 and σ_2 are of an order of $10^{-15}cm^2$. Consideration of the ET between *4d* and *4f* states in balance equations (6.1) and (6.2) does not influence the value of σ_2; it

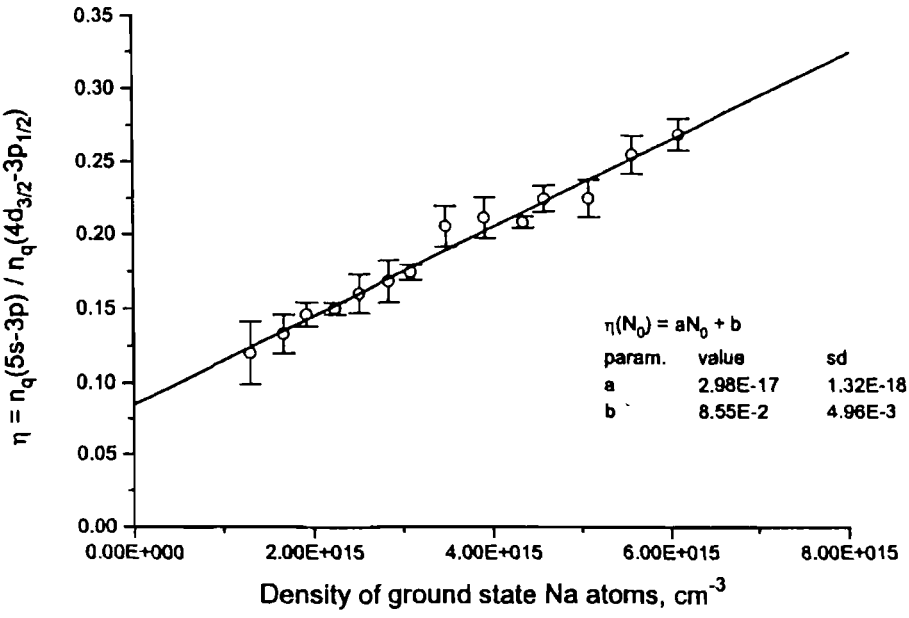

Fig. 2. Dependence of the ratio of $5s_{1/2}\rightarrow 3p_{1/2,3/2}$ to $4d_{3/2}\rightarrow 3p_{1/2}$ quantum fluxes (i.e., η) on the density N_0 of ground state Na atoms.

can only bring an additional error (maximally about 30%) in the value of σ_1.

If ET goes through the *5p* state (i.e., processes (4) and (5)), the solution of the balance equations gives $\sigma_{p2} = 0.19\sigma_{fs}$ for the cross-section of ET from $4d_{5/2}$ to *5p* (without distinguishing the fine structure of *5p*). It seems unlikely that the cross-section can be so high for an endoergic process (4). Nevertheless, to decide unambiguously whether process (1) or process (4) + (5) leads to the population of $5s_{1/2}$ state will be possible only after experimentation with IR detection on $5p\rightarrow 4s$ transition.

ACKNOWLEDGEMENTS

The experimental part of this work was carried out in the Institute of Experimental Physics of Warsaw University. I express my thanks to Prof. A. Kopystynska of the Warsaw University and Prof. M. Jansons of the University of Latvia for helpful discussions and support. I also wish to acknowledge the Komitet Badan Naukowych (Poland) that supported my stay in Warsaw.

REFERENCES

1. Luo, C., Ekers, A., Klavins, J., Jansons, M. (1996) *Physica Scripta* (in press).
2. Yabuzaki, T., Tam, A. C., Hou, M., Happer, W., Curry, S. M. (1978) *Opt. Commun.* **24**, 305.
3. Nesmayanov, A. N. (1963) *Vapour Pressure of the Chemical Elements* (Elsevier, Amsterdam).
4. Shvegzhda, Zh. L., Papernov, S. M., Janson, M. L. (1983) *Chem. Phys. Lett.* **101**, 187.
5. Henriet, A., Masnou-Seeuws, F. J., (1987) *Phys. B* **20**, 671.
6. Груздев, П. Ф. (1990) *Вероятности переходов и радиационные времена жизни уровней атомов и ионов* (Transition Probabilities and Radiative Lifetimes of Atomic and Ionic Levels) (Энергоатомиздат, Москва).

Physica Scripta. Vol. 53, 306–308, 1996

Studies of Inelastic Cross-Section in Rb(7S) + Rb(5S) Collisions

Luo Caiyan,[a] A. Ekers,[a, b] J. Klavins[b] and M. Jansons[b]

[a] Atomic Physics Division, Lund Institute of Technology, P.O. Box 118, S-221 00 Lund, Sweden
[b] Institute of Atomic Physics and Spectroscopy, University of Latvia, Rainis Blvd. 19, LV-1586 Riga, Latvia

Received April 26, 1995; accepted in revised form July 31, 1995

Abstract

The cross section $\sigma = (8 \pm 4) \times 10^{-15}\,\mathrm{cm}^2$ was determined for the Rb(7S) + Rb(5S) → Rb(5D) + Rb(5S) excitation energy transfer process, and the quenching cross section $\sigma_q = (2 \pm 1) \times 10^{-14}\,\mathrm{cm}^2$ for the Rb(5D) state in collisions with ground state Rb atoms. Applying rubidium quasi-molecular asymptotic potential curves at relatively large internuclear distances, a qualitative interpretation of the experimental results is presented. It is shown that the quenching of the Rb(5D) atoms in collisions may be explained by a reversed energy pooling process Rb(5D) + Rb(5S) → Rb(5P) + Rb(5P).

1. Introduction

In collision physics a great interest has always been paid to energy transfer (ET) processes proceeding at relatively large cross sections between levels, which are not directly connected with the atomic ground states by electric dipole transitions. In the present work the following ET process was studied:

$$\mathrm{Rb}(7S_{1/2}) + \mathrm{Rb}(5S_{1/2}) \rightarrow \mathrm{Rb}(5D_{3/2,\,5/2}) + \mathrm{Rb}(5S_{1/2}) + \Delta E(+607\,\mathrm{cm}^{-1}) \quad (1)$$

Since the optical electric dipole transition 5S → 7S in rubidium is forbidden, the 7S level had to be excited by means of the following process (cf. Fig. 1):

$$\mathrm{Rb}(5S_{1/2}) + \mathrm{Rb}(5S_{1/2}) + h\nu \rightarrow \mathrm{Rb}(5P_{3/2}) + \mathrm{Rb}(5S_{1/2}), \quad (2)$$

$$\mathrm{Rb}(5P_{3/2}) + h\nu \rightarrow \mathrm{Rb}(7S_{1/2}). \quad (3)$$

In process (2) the resonance state $\mathrm{Rb}(5P_{3/2})$ of rubidium was populated by collision-induced laser excitation. The corresponding cross section in the vicinity of the resonance transition could reach a high value (The calculated rate constant of the process (2) α is about $10^{-37}\,\mathrm{cm}^5$ [1]). The second photon of equal energy excited rubidium atoms from the state $\mathrm{Rb}(5P_{3/2})$ to Rb(7S) in the step process (3). This method of excitation has, for instance, been applied for reaching the 6D state in caesium [2]. It is important to note that fluorescence from the 7S and 5D levels could exist only in the cases when the laser wavelength in processes (2) and (3) was at resonance with the $5P_{3/2} \rightarrow 7S_{1/2}$ transition. This indicated that the Rb 5D state was not excited in the energy pooling process (3):

$$\mathrm{Rb}(5P_{3/2}) + \mathrm{Rb}(5P_{3/2}) \rightarrow \mathrm{Rb}(5D_{3/2,\,5/2}) + \mathrm{Rb}(5S_{1/2}) + \Delta E(-68\,\mathrm{cm}^{-1}), \quad (4)$$

which might act as a competing mechanism to process (1).

2. Experiment and results

The experiment was carried out in rubidium vapour following the typical scheme for laser-induced fluorescence experiments (LIF). The rubidium vapour was contained in an alkali resistant glass cell with a sapphire window. The temperature range in our experiment was 240 ~ 300 °C. Rb atoms were excited by a cw ring dye laser (Coherent Radiation, model CR-699) with Pyridine-2 dye and with about 160 mW of output power. The laser beam was focused (ca. 0.3 mm dia) into the rubidium cell. The LIF spectra were recorded by means of a monochromator (Jobin Yvon, model HR-100), a photomultiplier tube (Hamamatsu, model R943-02) and a lock-in amplifier. (Princeton Appl. Research, model HR-8).

Under steady-state conditions of excitation the balance equation for the excitation of $\mathrm{Rb}(5D_J)$ is as follows:

$$[5D] = 0 = [7S]N_0\sigma v - [5D]\tau^{-1} - [5D]N_0\sigma_q v. \quad (5)$$

Here, σ is the cross section of the ET collisional process (1), v is the mean relative velocity of the colliding atoms; σ_q is the cross section of Rb(5D) quenching by ground state rubidium atoms, N_0 is the rubidium concentration; $\tau = 250$ ns [4] (the radiative lifetime of 5D state). The square brackets in eq. (5) denote the population of the respective state. In eq. (5) the quenching of the 5D state only by rubidium atoms is considered. In our experiments the concentration of rubidium atoms was around $N_0 \leqslant 1.3 \times 10^{16}\,\mathrm{cm}^{-3}$,

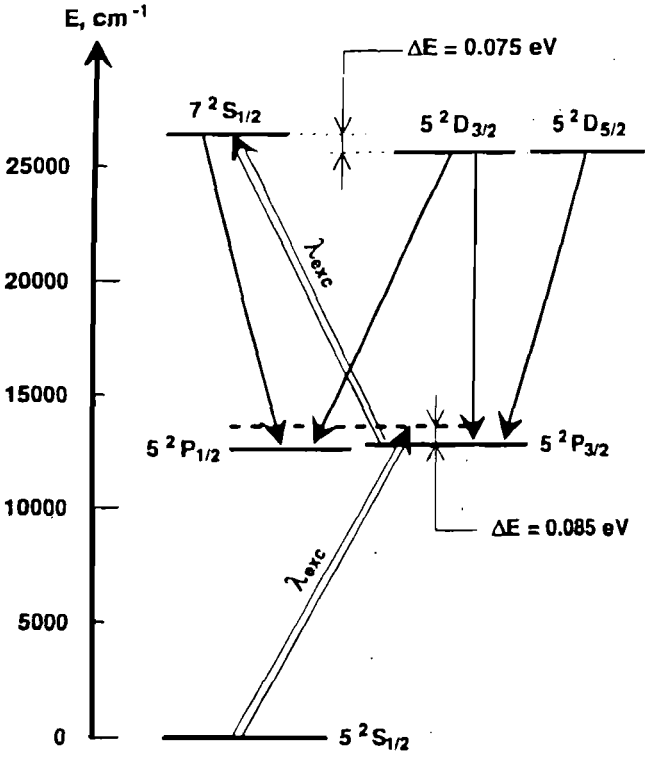

Fig. 1. Partial term diagram of the rubidium atom.

which corresponds to densities of rubidium molecules $[Rb_2] \leqslant 7.5 \times 10^{13}\,cm^{-3}$. At such relatively low Rb_2 concentrations, as compared to Rb atom concentrations, one might neglect quenching of Rb(5D) by Rb_2 molecules. This was also suggested by Sasso *et al.* [5] in caesium experiments, which showed that quenching of Cs(5D) in collisions with ground state atoms dominates over quenching by collisions with caesium dimers. The expression (5) can be transformed to the following way:

$$\eta = \frac{n(5D_J \to 5P_{1/2})}{n(7S_{1/2} \to 5P_{1/2})} = \frac{A}{A'} \frac{\sigma}{(N_0 v\tau)^{-1} + \sigma_q}, \tag{6}$$

where n are the quantum fluxes of the corresponding transitions $[cm^{-3} \times s^{-1}]$, which were measured relatively in the experiment accounting for the spectral sensitivity of the detection system. The transition probabilities $A = 2.5 \times 10^6\,s^{-1}$ and $A' = 2.0 \times 10^6\,s^{-1}$ [4], correspond to $5D \to 5P$ and $7S_{1/2} \to 5P_{1/2}$ transitions. The experimental value for η in dependence on ground state Rb atom concentration N_0 is shown in Fig. 2.

ET and quenching cross sections were determined by adjusting the parameters σ and σ_q in eq. (6) for optimum fit to the experimental data $\eta(N_0)$ (The solid line is a fitted curve in Fig. 2). The following values were obtained: $\sigma = 8 \times 10^{-15}\,cm^2$ and $\sigma_q = 2 \times 10^{-14}\,cm^2$. The estimated accuracy of the results is $\pm 50\%$, as obtained from statistical treatment of experimental points, which includes the fitting uncertainty and systematic errors. The concentration of rubidium ground state atoms was calculated from the vapour pressure obtained by using the Nesmayanov formula [6].

The total σ and σ_q values obtained correspond to the energy transfer and quenching of both fine structure components $J = 3/2$, $5/2$ of the Rb atom $5D_J$ state. The cross sections of collisional transitions between both components are $\sigma_{fs}(5/2 \to 3/2) = 2.9 \times 10^{-14}\,cm^2$ and $\sigma'_{fs}(3/2 \to 5/2) = 4.4 \times 10^{-14}\,cm^2$ [7]. At the given experimental Rb atom concentrations ($N_0 = 3 \times 10^{15} \sim 1.3 \times 10^{16}\,cm^{-13}$) the collisional mixing between $5D\ J = 3/2$ and $J = 5/2$ components takes place considerably faster than radiative relaxation of the $5D_{3/2,\,5/2}$ state. After the determination of the cross sections of each fine-structure component separately, their ratio was found to be consistent with the statitical weights $(\sigma(D_{5/2})/\sigma(D_{3/2}) \cong 1.5)$.

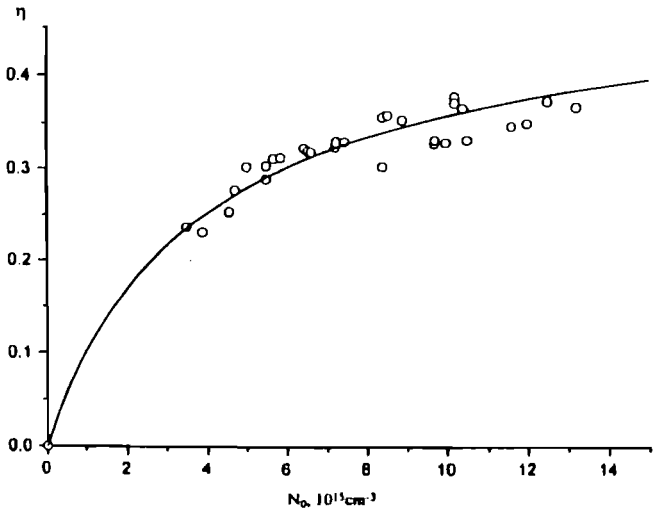

Fig. 2. Dependence of the ratio of $5D \to 5P$ and $7S \to 5P$ fluorescence intensities (i.e., η) on density of ground-state Rb atoms N_0: 0 – experiment; solid line – best fit of eq. (6), which correspond to $\sigma = 8 \times 10^{-15}\,cm^2$ and $\sigma_q = 2 \times 10^{-14}\,cm^2$.

We also estimated that the cross section of the endothermic process reverse to (1), namely

$$Rb(5D_J) + Rb(5S_{1/2}) \to Rb(7S_{1/2}) + Rb(5S_{1/2}) + \Delta E(-607\,cm^{-1}) \tag{7}$$

is of an order of $10^{-16}\,cm^2$. This is considerably less than the cross section of the 5D state quenching $\sigma_q = 2 \times 10^{-14}\,cm^2$. This indicates that the process (7) does not constitute the dominating mechanism in the quenching of the 5D state.

3. Discussion and conclusion

The large cross sections obtained in the present work lead to the conclusion that, in the processes discussed, ET takes place at relatively large internuclear distances. Barbier and Cheret [3] found the potential curves of the rubidium quasi molecule for the 5D–5S and 5P–5P configurations in asymptotic approximation at the values of $R \sim 20$–55 a.u. Using the results obtained by Bezuglov *et al.* [8] the behaviour of the 7S–5S configuration potential curves were estimated. At internuclear distances $R \approx 54 \sim 56$ a.u. the 0_g^+ terms of the 7S–5S and 5D–5S configurations show avoided crossing with the 0_g^+ term of the Rb^+Rb^- molecular ion (cf. Fig. 3, region I). As a result of the interaction of the states the energy transfer may take place from the 7S to the 5D state, and between the components $J = 3/2$ and $J = 5/2$ of the 5D state. At internuclear distance $R \approx 15$ a.u. another non-adiabatic region is situated (Fig. 3, region II), where we get a quasi-crossing between the 0_g^+ terms of the 7S–5S and 5D–5S configurations. As a result of radial motion of the nuclei non-adiabatic transitions may be induced between the 0_g^+ terms of equal symmetry ($\Delta\Omega = 0$), which may lead to energy transfer to the 5D $J = 5/2$ state.

Discussing the quenching of the 5D state we have neglected the quenching resulting from the process (7) and collisions with Rb_2 molecules. So there remains only one quenching process with an energy defect below $1000\,cm^{-1}$,* which may be responsible for quenching of the 5D state. This is, a reversed energy pooling process

$$Rb(5D_J) + Rb(5S_{1/2}) \to Rb(5P_{3/2}) + Rb(5P_{3/2}) + \Delta E(+68\,cm^{-1}). \tag{8}$$

A process of this type has been observed by Yabuzaki *et al.* [2] in cesium. If the process (8) is the only one which determines the quenching of the 5D state, then, according to the detailed balancing principle, the cross section of the direct energy pooling process (4) $\sigma_{EP} = 2.1 \times 10^{-14}\,cm^2$ was found from $\sigma_q = 2 \times 10^{-14}\,cm^2$. This is in fair agreement with results obtained by Barbier and Cheret [3] for the same energy pooling process (4): $\sigma_{EP} = 1 \times 10^{-14}\,cm^2$ (theoretical) and $\sigma_{EP} = 3 \times 10^{-14}\,cm^2$ (experimental). This provides us with sufficient reason to consider that the quenching of the Rb 5D state is connected with non-adiabatic

* The energy defects ΔE for the energy transfer from 5D to the next nearest 4F and 6P levels are $1088\,cm^{-1}$ and $+1911\,cm^{-1}$, respectively.

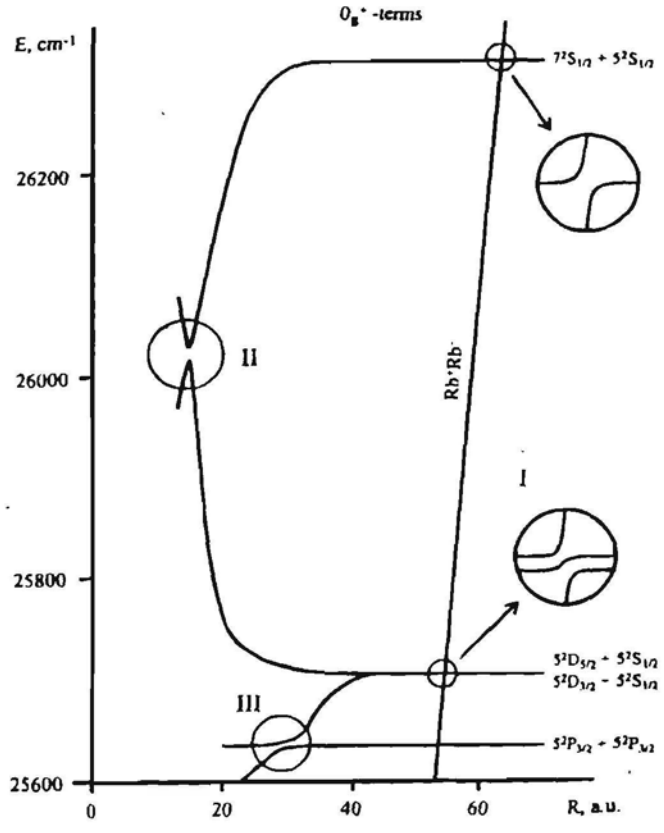

Fig. 3. Principal asymptotic potential curves of Rb_2 quasi-molecule in terms of Hund's (c) coupling. For clarity, 0_g^+ terms are displayed only. The location of the avoided crossing II is estimated without considering dispersion interaction.

transitions between terms of equal symmetry of the D–S and P–P configurations (cf. Fig. 3, region III). Transitions between the above terms have been analysed in [3, 8]. The present paper offers a qualitative description of the possible processes. A calculation of the potential curves will provide a theoretical determination of the contribution of each non-adiabatic region to the resulting transition probability of ET. This work is in progress at present.

Acknowledgements

This work was supported by the Swedish Natural Research Council and the Latvian Science Council. Help by V. Grushevsky in clarifying theoretical aspects of the problem and the support by S. Svanberg are gratefully acknowledged.

References

1. Ostrouhova, I. I., Smirnov, B. M. and Shlyapnikov, G. V., Sov. Phys. – JETP **46**, 86 (1977).
2. Yabuzaki, T., Tam, A. C., Hou, M., Happer, W. and Curry, S. M., Opt. Commun. **24**, 305 (1978).
3. Barbier, L. and Cheret, M., J. Phys. B: At. Mol. Phys. **16**, 3213 1983).
4. Gruzdev, P. F., "Transition probabilities and lifetimes of atomic and ionic levels" (Energoatomizdat., Moscow 1990).
5. Sasso, A. *et al.*, Phys. Rev. **A45**, 1670 (1992).
6. Nesmayanov, A. N., "Vapour Pressure of the Chemical Elements" (Elsevier, Amsterdam 1963).
7. Parker, J. W., Schuessler, H. A., Hill, R. H. Jr and Zollars, B. G., Phys. Rev. **A29**, 617 (1984).
8. Bezuglov, N. N., Borodin, V. M., Klucharev, A. N., Skrebov, V. N. and Janson, M. L., in: "Plasma Chemistry" (Energoatomizdat., Moscow 1987), vol. 13, p. 3.

Inelastic Cross Sections and Natural Lifetimes for the $6^2D_{3/2,5/2}$ and $8^2S_{1/2}$ States of Rb.

A. Ekers[a], M. Glódź[b], J. Szonert[b], B. Bieniak[b], K. Fronc[b], T. Radelitski[b]

[a] Institute of Atomic Physics and Spectroscopy, University of Latvia, Raina bulv. 19, LV1586 Riga, Latvia; e-mail: ekers@physik.uni-kl.de

[b] Institute of Physics, Polish Academy of Sciences, Al. Lotników 32/46, 02-668 Warsaw, Poland; e-mail: glodz@ifpan.edu.pl

Abstract

The results of an experimental study of population dynamics following excitation of $6^2D_{5/2,3/2}$ and $8^2S_{1/2}$ states of rubidium are reported. Excitation transfer and quenching cross sections in collisions with ground state rubidium atoms, and natural lifetimes have been measured. The experiment was performed in a vapour cell, using pulsed two-photon excitation and photon counting detection. The analysis of time dependent signals was based on a rate equation model in which transitions induced by thermal radiation have been accounted for. The measurements yielded following results: (1) 6^2D state J-mixing cross section: $\sigma^{Rb\ Rb}_{6D_{5/2}\rightarrow 6D_{3/2}}$ = 9.2(2.1)×10^{-14}cm^2; (2) cross sections for $8^2S\rightarrow 6^2D$ excitation transfer process: $\sigma^{Rb\ Rb}_{8S\rightarrow 6D}$ = 3.4(1.2)×10^{-14}cm^2; (3) quenching cross sections: $\sigma^{Rb\ Rb}_{q.8S}$ = 12.8(3.4)×10^{-14}cm^2, $\sigma^{Rb\ Rb}_{q.6D_{3/2}}$ = 22.8(2.9)×10^{-14}cm^2, $\sigma^{Rb-Rb}_{q.6D_{5/2}}$ = 14.1(5.7)×10^{-14}cm^2; (4) radiative lifetimes: τ_{8S} = 161(3) ns, $\tau_{6D_{3/2}}$ = 256(4) ns, $\tau_{6D_{5/2}}$ = 249(5) ns.

PACS: 34.50.Fa, 32.70.Cs, 32.50.+d

1 Introduction

The purpose of the present work has been to study the $8^2S_{1/2}$ and 6^2D_J states of Rb atoms with respect to the population/depopulation processes such as radiative decay and collisions which result in quenching and in excitation transfer between the states concerned.

Total collisional quenching cross sections for the rubidium ^2S and ^2D states as well as J-mixing ($nlJ \rightarrow nlJ'$ transition) cross sections for ^2D states have recently been discussed in a review [1], where results of theoretical approaches to describe various collisional processes are confronted with experimental data. Existing theoretical treatments based on the quasifree electron model explain the n-dependence of quenching cross sections for high n values. However, most of the measurements have been performed for states with relatively low n-values, for which such model does not hold. In the absence of theoretical data many authors compare experimental J-mixing and quenching cross sections with geometrical ones.

Collisional excitation transfer (ET) processes other than the quasielastic fine structure mixing have also been studied extensively during the last 30 years. Much effort has been devoted to understanding the so called energy pooling (EP) in alkalis, in which the excitation energy of two colliding resonance atoms is transferred to higher excited states:

$$X^*(^2P) + X^*(^2P) \rightarrow X^{**}(n^2l) + X(^2S), \qquad (1)$$

and to ET in heteronuclear collisions, in which the excitation is transferred from one type of atom to another. The most recent studies in this field concern m_J and velocity selective EP cross sections in sodium [2], J selective measurements of EP in caesium combined with thorough rate equation analysis with respect to various factors (e.g., radiation trapping, optical pumping etc.), which may influence the experimentally measured values of the cross sections [3,4], and ET involving heteronuclear collision partners [5,6]. The common feature of the above mentioned processes is that the colliding particles in entrance and exit channels are connected with their ground states or with each other by electric dipole transitions, and the ET is determined mainly by the dipole-dipole interaction [7,8,9,10], although it has been noted [2], that higher terms of multipole expansion may also be of importance.

The situation becomes different when one considers ET between the atomic ^2S and ^2D states (hereafter referred to as *S-D transfer*), in processes of the type

$$X^*(^2S) + X(^2S) \leftrightarrow X^*(^2D) + X(^2S), \qquad (2)$$

where atoms in neither channel possess dipole coupling. One may expect that in this case the ET will be weak as determined by an interaction other than the dipole-dipole.

To our knowledge only a few experiments have been conducted on S-D transfer. A very high cross section ($\sigma_{8S \rightarrow 6D} = 6.7 \times 10^{-13} \mathrm{cm}^2$) had been reported in [11] for the S-D transfer process

$$Rb(8^2S) + Rb(5^2S) \rightarrow Rb(6^2D) + Rb(5^2S) + \Delta E = +358 \mathrm{cm}^{-1}. \qquad (3)$$

Yet another study considers ET between the 7^2S and 5^2D states of rubidium [12], and the measured experimental cross section $\sigma^{exp}_{7S\to 5D} = 8\times10^{-15}\text{cm}^2$ was in reasonable agreement with the theoretical value $\sigma^{th}_{7S\to 5D} = 5.0\times10^{-15}\text{cm}^2$ [13]. It should be noted, however, that in this case the rather high value of the S-D transfer cross section was caused by the dipole-dipole interaction due to near lying 5^2P+5^2P configuration, which introduced strong dipole coupling between the initial 7^2S+5^2S and final 5^2D+5^2S configurations of colliding atoms [13].

In sodium ET from 4^2D to 5^2S state was observed, and the corresponding cross section was determined to be of the order of 10^{-15}cm^2 [14]. In that case one may also expect a strong influence of the 3^2P+3^2P configuration, which lies between the 4^2D+3^2S and 5^2S+3^2S configurations.

For process (3), the influence of the 5^2P+5^2P configuration can be neglected, since it is located more than 3000 cm^{-1} below the initial and final configurations. The surprisingly high $\sigma_{8S\to 6D}$, reported in [11], exceeds by a factor of four the value of the geometrical cross section for 8^2S. Also the fact that in another study [15] the very same cross section was reported to be $6.1\times10^{-14}\text{cm}^2$, which is an order of magnitude smaller than that obtained in [11], suggested that process (3) has to be reconsidered.

The natural lifetimes of excited states of atoms were extensively measured over several decades with continuously increasing precision due to technical development, as well as increasing awareness of side-effects influencing the measured values. Procedures have been developed to account for distorting phenomena such as magnetic field and/or polarisation effects, thermal escape, and the presence of blackbody radiation (BBR) (see, e.g., [16,17]).

A compilation of a vast number of experimental lifetimes for alkali atoms is contained in the paper by Theodosiou [18], who presents results of calculations for $n^2S_{1/2}$, n^2P_J, n^2D_J and n^2F_J alkali states with $n\leq21$, and compares these lifetimes to the values measured by various authors and those calculated elsewhere. Theodosiou [18] and similarly Hansen [19] used a three term model potential. The first term, which is of different form in the two papers, represented the single-electron central field due to the nucleus and the core electrons, the second term accounted for core polarisation and the third for spin-orbit interaction. He et al. [20] used another simple model potential experienced by the valence electron. The agreement between theoretical and experimental lifetimes varies from state to state, which on the side of the experiment may be a consequence of neglecting one or another of above mentioned side effects affecting the measured values.

2 Experimental set-up and procedure

The experimental set-up is shown in Fig. 1. A Pyrex glass cell containing metallic rubidium was placed in a thermostabilised two-chamber oven, and the temperature of its upper part T_u was varied between 75 and 125°C. The temperature of the lower part of the cell was kept 5°C below the temperature of the main oven body. The resulting atomic number density N_{Rb} ranged from 5.5×10^{11} to 1.5×10^{13}cm^{-3}. N_{Rb} was calculated by treating Rb vapour in the upper part of the cell as an ideal gas at a temperature T_u and at a pressure determined by the temperature of the lower (colder) part with a droplet of Rb. Temperature-vapour pressure relation from [21] was used. The cell was surrounded with a two-fold shield to screen the Earth's and stray magnetic fields. Two photon excitation on either $5^2S_{1/2}\rightarrow8^2S_{1/2}$, $5^2S_{1/2}\rightarrow6^2D_{3/2}$ or $5^2S_{1/2}\rightarrow6^2D_{5/2}$ transitions was achieved by using radiation of an excimer laser pumped dye laser (Lumonics EX-520, HD-500, pyridine-1 dye, pulses of ca 7 ns duration, spectral width of ca 3 GHz). The linearly polarised laser beam was sent through the cell. The fluorescence was observed at right angles. A two lens optical system imaged the fluorescence region onto the horizontal slit of a monochromator (Carl Zeiss Jena SPM2, 1.5 mm slit, 6 nm spectral resolution). The fluorescence signals were detected with a cooled photomultiplier (Hamamatsu R943-02), and a multichannel scaler (EG&G PAR 914P, 5 ns channel width). In order to avoid polarisation effects, a properly oriented polarisation plane rotator in the laser beam path (54.7° from vertical orientation) and a vertically oriented polariser in the fluorescence path were used to provide the magic angle configuration. The fluorescence signals were monitored on $8^2S_{1/2}\rightarrow5^2P_{1/2}$, $6^2D_{5/2}\rightarrow5^2P_{3/2}$, and $6^2D_{3/2}\rightarrow5^2P_{1/2}$ transitions (607.1, 629.8, and 620.6nm respectively). Background signals were also registered (see sect. 4.1). Relative spectral sensitivity of the detection system was determined for the detected wavelengths by using a calibrated tungsten ribbon lamp. Strong fluorescence signals were attenuated by neutral density filters to assure detector linearity.

Besides the time resolved signals at certain fluorescence lines, also emission spectra were registered with a photon counter, by using a wide open time-gate and tuning the monochromator output wavelength to the vicinity of fluorescence lines of interest. The aim was to gather more information about spectral resolution and the origin of backgrounds. The spectra were taken with laser in resonance as well as detuned from the transitions.

3 Rate equations

3.1 *J*-mixing

Since the $6^2D_{3/2}$ and $6^2D_{5/2}$ levels are situated very close to each other (2.26 cm^{-1}), the *J*-mixing process can be treated in a framework of a quasi two-level system. The collisional ET rate from state $|i\rangle$ out of a two-level system, K_i^{out}, is included in the excited state total decay rate Γ_i,

$$\Gamma_i = \Gamma_i^{rad} + K_i^{out} + R_{i\to j}, \tag{4}$$

where Γ_i^{rad} denotes the radiative decay rate and $R_{i\to j}$ is the rate for ET from $|i\rangle$ to $|j\rangle$.

The thermally averaged cross sections $\sigma_{i\to j}$ considered in this paper are related to the relevant rates $R_{i\to j}$ as

$$R_{i\to j} = \sigma_{i\to j} N v, \tag{5}$$

where N is the number density of perturbing atoms, $v = \sqrt{8kT_u/\pi\mu}$ is the mean relative velocity of the colliding partners, μ is their reduced mass, and k - the Boltzmann constant.

At the relatively low densities of our experiment, which result in ET rates much smaller than the radiative decay rates, one can neglect the effects due to multiple collisions. Since the duration of the laser pulse was much smaller than the radiative lifetimes of the considered states, no deconvolution is necessary. In a two level system, the equations describing the evolution of population in the laser excited level $|2\rangle$ and the collisionally excited level $|1\rangle$ are:

$$\frac{dN_2}{dt} = -\Gamma_2 N_2; \tag{6a}$$

$$\frac{dN_1}{dt} = R_{2\to 1} N_2 - \Gamma_1 N_1. \tag{6b}$$

The detected fluorescence signals I_i are directly proportional to number density of atoms N_i in state $|i\rangle$:

$$I_i = \xi_i A_{iP} N_i \tag{7}$$

Here, A_{iP} denote Einstein coefficients for the observed transitions to the resonance states, and ξ_i accounts for the detection efficiency. Since the experimental signals were corrected according to the performed spectral calibration, a common factor $\xi=\xi_1=\xi_2$ characterises both I_1 and I_2.

For solving the system (6) we choose an initial condition $N_2(t=0)=N_{20}$, where $t=0$ corresponds to the incidence of a laser pulse. To account for background signals, as explained in Sect. 4.1, we assume also some small initial population $N_1(t=0)=N_{10}$ for level $|1\rangle$. The resulting expressions for I_2 and I_1 are:

$$I_2 = \xi A_{2P} N_{20} e^{-\Gamma_2 t}; \tag{8a}$$

$$I_1 = \xi A_{1P}\left(N_{10} e^{-\Gamma_1 t} + N_{20} \frac{R_{2\to 1}}{\Gamma_1 - \Gamma_2}\left(e^{-\Gamma_2 t} - e^{-\Gamma_1 t}\right)\right). \tag{8b}$$

In order to obtain the J-mixing rate and the corresponding cross section (eq. (5)), equations (8a) and (8b) have to be fitted to the registered fluorescence signals.

The J-mixing cross section can also be deduced by comparing the time integrals of sensitised ($\int_0^\infty I_1 \mathrm{d}t$) and direct ($\int_0^\infty I_2 \mathrm{d}t$) fluorescence signals, namely:

$$\eta = \frac{\int_0^\infty I_1 \mathrm{d}t}{\int_0^\infty I_2 \mathrm{d}t} = \frac{A_{1P}}{A_{2P}} \frac{1}{\Gamma_1}\left(\frac{N_{10}}{N_{20}}\Gamma_2 + R_{2\to 1}\right). \tag{9}$$

The assumption $N_{10}=0$ leads to the simple expression for the ET rate

$$R_{2\to 1} = \eta \Gamma_1 \frac{A_{2P}}{A_{1P}}. \tag{10}$$

3.2 $8^2S \leftrightarrow 6^2D$ transfer

In the course of analysis of the experimental data on $8^2S \leftrightarrow 6^2D$ ET we determined that the approximation of two levels interconnected by a single collisional ET rate is, unlike in the case of relatively strong J-mixing, not sufficient to correctly reproduce the shapes of the recorded time resolved signals. We found it necessary to include in the analysis additional processes which compete with the direct ET between 8^2S and 6^2D. The two principal ones are induced by BBR[*)], with involvement of the intermediate states 7^2P and 8^2P, while the third process comprises ET between 8^2S and 5^2F. For example, on laser excitation to the 8^2S state, besides the direct ET, the population is transferred to the 6^2D state through (*i*) absorption of a BBR photon on the $8^2S \to 8^2P$ transition followed by emission to the 6^2D state; (*ii*) emission

[*)] For Rydberg states the BBR driven transitions which strongly compete with the collisional ET are discussed in [22] and references therein.

from 8^2S to 7^2P state followed by absorption of a BBR photon on the $7^2P \rightarrow 6^2D$ transition; (*iii*) ET from 8^2S to 5^2F followed by $8^2S \rightarrow 5^2F$ radiative decay (see Fig.2).

In order to describe the time evolution of the population of relevant states, the equation system (8) is modified to

$$\frac{dN_2}{dt} = -\Gamma_2 N_2 ; \tag{11a}$$

$$\frac{dN_1}{dt} = -\Gamma_1 N_1 + R_{2\to 1} N_2 + \sum_k T_{k\to 1} N_k ; \tag{11b}$$

$$\frac{dN_k}{dt} = -\Gamma_k N_k + T_{2\to k} N_2 , \tag{11c}$$

where k denotes each of the three intermediate states 7^2P, 8^2P, 5^2F. For k corresponding to 7^2P and 8^2P, the rates T are expressed either as

$$T_{a\to b} = A_{ba}(g_a/g_b)\langle n_{ba}\rangle \tag{12a}$$

for absorption, or

$$T_{b\to a} = A_{ba}(1+\langle n_{ba}\rangle) \tag{12b}$$

for emission (spontaneous and induced). When k denotes the 5^2F state, T is the collisional rate $T_{8S\to 5F} \equiv R_{8S\to 5F}$ (or $T_{5F\to 8S} \equiv R_{5F\to 8S}$) for the case when 8^2S (or 6^2D) is directly excited. g_a, g_b are the statistical weights of the states and $\langle n_{ba}\rangle = 1/(\exp(E_{ba}/kT)-1)$ is the number of BBR photons per mode of energy E_{ba} equal to energy separation of the states.

By solving eqs. (11) with the initial conditions $N_2(t=0)=N_{20}$, $N_1(t=0)=N_k(t=0)=0$ one obtains for N_1:

$$N_1 = N_{20}\left(\frac{R_{2\to 1}}{\Gamma_2-\Gamma_1}\left(e^{-\Gamma_1 t}-e^{-\Gamma_2 t}\right) + \sum_k T_{2\to k}T_{k\to 1}\left(\frac{1}{(\Gamma_2-\Gamma_1)(\Gamma_k-\Gamma_1)}e^{-\Gamma_1 t} - \frac{1}{(\Gamma_2-\Gamma_k)(\Gamma_k-\Gamma_1)}e^{-\Gamma_k t} + \frac{1}{(\Gamma_2-\Gamma_k)(\Gamma_2-\Gamma_1)}e^{-\Gamma_2 t}\right)\right). \tag{13}$$

The fluorescence signals I_i are related to the corresponding populations N_i by (7). Note, that I_2 is described, as before, by the single exponential function (8a).

3.3 Collisional quenching and radiative lifetimes

The fit of the single exponential (8a) to the direct fluorescence signal gives the total decay rate for this state at a certain temperature. This rate is related to the radiative decay rate

and to the collisional quenching rate by (4). The procedure for extracting the natural lifetimes and quenching cross sections at the conditions of the experiment is described in section 4.3.

4 Results and analysis

4.1 *J*-mixing

To obtain the 6^2D state *J*-mixing cross section, $\sigma^{Rb\ Rb}_{6D_{5/2}\rightarrow 6D_{3/2}}$, the $6^2D_{5/2}$ state was excited, and both the direct fluorescence from $6^2D_{5/2}$ and the sensitised fluorescence from $6^2D_{3/2}$ were registered at various number densities of Rb atoms. For the sensitised fluorescence signals, which are much weaker than those of the direct fluorescence, the issue of background signals was very important. In order to identify the origin of the observed background, and to account for it, whenever necessary, the following steps were performed. First, the noise signal was measured with the laser light blocked. This noise from sources like laboratory stray light or electronic pick-up from the laser discharge and trigger was negligible. Second, the background was detected with the monochromator detuned from the line while laser remained on the resonance. This background was still very small, and it originated, most probably, from the $6^2D_{5/2}\rightarrow 5^2P_{3/2}$ fluorescence passing at the wing of the transmission profile of the monochromator with widely open slits set at $6^2D_{3/2}\rightarrow 5^2P_{1/2}$ transition wavelength. Finally, the background was monitored with the laser 2-photon energy detuned down from the $5^2S_{1/2}\rightarrow 6^2D_{3/2}$ resonance by the amount equal to the 6^2D state fine structure splitting (2.26 cm^{-1}) and with monochromator set at the $6^2D_{3/2}\rightarrow 5^2P_{1/2}$ transition. In this case, we observed some direct 2-photon excitation of the $6^2D_{3/2}$ state, which is most likely due to the excitation by broadband amplified spontaneous emission (ASE) present in the laser beam. The signal recorded in this way should imitate the background to the measured sensitised fluorescence when the laser is in resonance with the $5^2S\rightarrow 6^2D_{5/2}$ 2-photon transition. The presence of the above mentioned backgrounds was evidenced also by analysing, at different sensitivities, the time integrated fluorescence spectra.

To determine the *J*-mixing cross sections, eq. (8b) was fitted to the sensitised fluorescence signals (see Fig. 3a), from where $R_{21} = R_{6D_{5/2}\rightarrow 6D_{3/2}}$ was obtained. The parameters Γ_1, Γ_2, and ξN_{20} were obtained by fitting a single exponential (8a) (see sect 4.3). The relevant Einstein coefficients were taken according to oscillator strengths given in [23]. Contribution of the direct excitation by ASE to the sensitised fluorescence was accounted for by allowing the second fitting parameter in eq. (8b) $\xi N_{10}\neq 0$, which corresponds to direct

excitation of the $6^2D_{3/2}$ state during the laser pulse. In this way the admixture of the direct fluorescence from the $6^2D_{5/2}$ state, whose lifetime is very close to that of the $6^2D_{3/2}$, is also accounted for.

We also tried another approach, to compare the integrated signals according to eq. (9) and (10). To do this, the noise signals, detected in separate measurements at each temperature, were subtracted from sensitised fluorescence signals. Although the $R_{6D_{5/2}\to 6D_{3/2}}$ values obtained in this way did not differ significantly from those obtained by the former procedure, the scatter of points was larger. This suggests that the first method is more accurate, because it better compensates for an unknown amount of excitation by ASE.

By using the first approach, to fit the signal shapes, we also obtained strong evidence that there are no other mechanisms involved in the population transfer between the fine structure components except the direct collisional transfer. Otherwise it would be impossible to fit the shapes of the signals, since, according to (8b), they are determined exclusively by the decay rates Γ_1 and Γ_2 of the states involved in the ET process.

Within the relatively narrow range of variation of $v_{\text{Rb-Rb}}$ in the present experiment, the J-mixing cross section due to Rb-Rb collisions was not expected to exhibit any noticeable dependence on temperature, and therefore on N_{Rb}. However, in Fig. 4a a strong dependence of the cross section values defined as $R_{6D_{5/2}\to 6D_{3/2}}/N_{\text{Rb}}\, v_{\text{Rb-Rb}}$ (eq. (5)) on N_{Rb} is observed. This indicates that there is another process that contributes to the J-mixing and does not involve collisions with the ground state Rb atoms. Since the cell was well outgassed before filling it with rubidium, the only foreign element could be atmospheric helium which can penetrate through the glass in the process of cell ageing. We assumed therefore that the measured rate consists of two terms: $R_{6D_{5/2}\to 6D_{3/2}} = R^{\text{Rb-Rb}}_{6D_{5/2}\to 6D_{3/2}} + R^{\text{Rb-He}}_{6D_{5/2}\to 6D_{3/2}}$, where $R^{\text{Rb-Rb}}_{6D_{5/2}\to 6D_{3/2}}$ is the rate for J-mixing in collisions with ground state Rb atoms, and $R^{\text{Rb-He}}_{6D_{5/2}\to 6D_{3/2}}$ is the rate for J-mixing in collisions with He atoms (density N_{He}). Consequently,

$$\frac{R_{6D_{5/2}\to 6D_{3/2}}}{N_{\text{Rb}}\, v_{\text{Rb-Rb}}} = \sigma^{\text{Rb-Rb}}_{6D_{5/2}\to 6D_{3/2}} + \sigma^{\text{Rb-He}}_{6D_{5/2}\to 6D_{3/2}} N_{\text{He}} \sqrt{\frac{\mu_{\text{RbRb}}}{\mu_{\text{RbHe}}}}\, \frac{I}{N_{\text{Rb}}}, \qquad (14)$$

where μ_{RbRb} and μ_{RbHe} are the reduced masses of colliding pairs of atoms (Rb-Rb) and (Rb-He). The resulting J-mixing cross section, $\sigma^{\text{Rb-Rb}}_{6D_{5/2}\to 6D_{3/2}} = 9.2(2.1)\times 10^{14}\text{cm}^2$, obtained by fitting eq. (14) to the experimental points (solid line in Fig. 4a), is compared with the results of other studies in Table 1. Using the known cross section for J-mixing induced by He, $\sigma^{\text{Rb-He}}_{6D_{5/2}\to 6D_{3/2}} = 4.5(0.7)\times 10^{-14}\text{cm}^2$ [24], we deduce the number density of He in our experiment

to be N_{He}= 1.5(0.3)×10^{13}cm^{-3}, which is about one order of magnitude smaller than the helium atmospheric concentration. An independent estimate based on available data on transport of He through the pyrex glass [25] gave N_{He}= 2(1)×10^{13}cm^{-3}, which is in a very good agreement with the former value. Possible contribution of BBR mediated transfer to the J-mixing was evaluated to be negligible.

4.2 $8^2S \leftrightarrow 6^2D$ transfer

Attempts were made to determine the cross sections for ET between 8^2S and 6^2D in both directions. However, the analysis of time resolved fluorescence signals allowed to determine the cross section only for the ET from 8^2S to 6^2D. Due to the negative energy defect and unfavourable ratio of the statistical weights, the opposite ET process is expected to be by a factor of 18 less efficient. The signals recorded by our apparatus in the $6^2D \rightarrow 8^2S$ case appeared to be masked by extra competing processes, which could not be unambiguously accounted for.

4.2.1 ET from 8^2S to 6^2D

With the $8^2S_{1/2}$ state excited by laser pulses, the sensitized fluorescence signal consisted of dominant fluorescence from the $6^2D_{5/2}$ state (the $6^2D_{5/2} \rightarrow 5^2P_{3/2}$ transition), overlapped with a fluorescence from the $6^2D_{3/2}$ state (the $6^2D_{3/2} \rightarrow 5^2P_{3/2}$ transition). The other component of the doublet from the $6^2D_{3/2}$ state (the $6^2D_{3/2} \rightarrow 5^2P_{1/2}$ transition) was overlapped with the strong $8^2S_{1/2} \rightarrow 5^2P_{3/2}$ line owing to low spectral resolution and therefore could not be detected. With an assumption that both 6^2D_J states are populated according to their statistical weights, g_J, a relation between the measured signal $I_{6D}^{meas} = I_{6D_{5/2}-5P_{3/2}} + I_{6D_{3/2}-5P_{3/2}}$ and the total population N_{6D} of the 6^2D doublet takes the form:

$$I_{6D}^{meas} = \xi N_{6D}\left(\frac{g_{5/2}}{g_{5/2}+g_{3/2}} A_{6D_{5/2}-5P_{3/2}} + \frac{g_{3/2}}{g_{5/2}+g_{3/2}} A_{6D_{3/2}-5P_{3/2}}\right), \qquad (15)$$

where N_{6D} is given by eq. (13). The experimental $6^2D_{3/2,5/2} \rightarrow 5^2P_{3/2}$ fluorescence signal exclusive of the background (Fig. 3b) was fitted with eq. (15). $R_{8S \rightarrow 6D}$ coming in from eq. (13) was the only parameter of fit. Einstein coefficients $A_{6D_{5/2}-5P_{3/2}}$ and $A_{6D_{3/2}-5P_{3/2}}$ were taken according to [23]. Besides the direct ET, the two additional channels via the 7^2P and 8^2P states were included in (13). With the quenching cross section of the 8^2S state (see section 4.3) taken as an upper limit for $\sigma_{8S \rightarrow 5F}$, we estimated that population transfer via the 5^2F state

can be neglected because of the unfavourable $5^2F \rightarrow 6^2D$ branching ratio. Radiative rates $T_{8S\rightarrow *}$ and $T_{k\rightarrow 6D}$ (12a,b) were obtained by using the Einstein coefficients based on [26]. Γ_{8S} and $\xi N_{20} \equiv \xi N^0_{8S}$ were obtained by fitting eq. (8a) to the respective direct fluorescence signals (section 4.3). Γ_{7P} and Γ_{8P} were taken according to [18].

Due to the presence of helium the values of $R_{8S\rightarrow 6D}/N_{\mathrm{Rb}}v_{\mathrm{Rb-Rb}}$ exhibited a similar, though less pronounced, dependence on N_{Rb} (Fig. 4b) as in the case of J-mixing discussed above. By fitting a function of type (14) to this dependence, the cross section for Rb induced ET, $\sigma^{\mathrm{Rb-Rb}}_{8S\rightarrow 6D} = 3.4(1.2)\times 10^{-14}\mathrm{cm}^2$, was obtained (see Table 1). In the same time the cross section for He induced ET was estimated as $\sigma^{\mathrm{Rb\ He}}_{8S\rightarrow 6D} = 4.2(2.6)\times 10^{-16}\mathrm{cm}^2$. This is to be compared with the value $1.3(0.5)\times 10^{-16}\mathrm{cm}^2$, given in [11].

It should be noted that the BBR mediated processes contribute significantly to the observed $8^2S \rightarrow 6^2D$ population transfer. Since the Rb number density is strongly dependent on temperature (Nesmeyanov's relation [21]), the relative contributions of BBR and collisionally mediated processes vary significantly with N_{Rb} (i.e., with temperature). The ratio of both contributions (BBR mediated transfer to ET in Rb-Rb collisions) varies from a few at lowest N_{Rb} values to about one at highest N_{Rb} of the present experiment [27]. Therefore disregard of the BBR influence in the analysis of the experimental results can lead to considerable errors.

4.2.2 ET from 6^2D to 8^2S

With both 6^2D_J fine structure components consecutively excited, the direct $6^2D_J \rightarrow 5^2P$ and sensitised $8^2S \rightarrow 5^2P$ fluorescence was observed. However, in some cases we were unable to obtain a reliable fit of the function based on (13) to the 8^2S time-resolved fluorescence signals. In these cases, the fluorescence appeared to be considerably stronger than expected from the detailed balancing principle. According to (13), the shape of the time-resolved sensitised fluorescence (inclusive of the BBR contribution) should be essentially the same for ET in directions opposite to each other. The difference is only in the amplitude scaling factor, which is unfavourable for the $6^2D \rightarrow 8^2S$ direction (ca 18 times smaller). The process which might be responsible for the observed excess population of the 8^2S state is a superradiant (SR) transition from the laser excited 6^2D state to the 7^2P state, followed by the BBR induced transition to the 8^2S state. With the spectral sensitivity range of our detection system we were unable to observe IR fluorescence to verify this possibility. We modelled this SR channel by introducing extra terms in (13), which allowed us to reproduce the shape of the 8^2S

fluorescence signals [27]. Nevertheless we have omitted the results for $6^2D \rightarrow 8^2S$ transfer as less reliable. For the $8^2S \rightarrow 6^2D$ ET the extra terms revealed negligible effect on the $R_{8S \rightarrow 6D}$ values, showing that SR was not significant in that case.

4.3 Lifetimes and collisional quenching

Fitting of eq. (8a) to the observed direct fluorescence signals provided the $N_{Rb}v_{Rb\text{-}Rb}$-dependent total decay rates Γ_{8S}, $\Gamma_{6D_{3/2}}$ and $\Gamma_{6D_{5/2}}$. Besides the predominant contribution of the spontaneous radiative decay, these rates contain also deexcitation rates due to (*i*) the presence of BBR, (*ii*) quenching induced by collisions with He atoms, and (*iii*) quenching induced by collisions with the ground state Rb atoms:

$$\Gamma_i = \frac{1}{\tau_i} + \Gamma_i^{bb} + K_i^{Rb\text{-}He} + K_i^{Rb\text{-}Rb}$$

Here, τ_i is the natural radiative lifetime; Γ_i^{bb} - the BBR induced transition rate [22]; $K_i^{Rb\text{-}He} = \sigma_{q,i}^{Rb\text{-}He} N_{He} v_{Rb\text{-}He}$ and $K_i^{Rb\text{-}Rb} = \sigma_{q,i}^{Rb\text{-}Rb} N_{Rb} v_{Rb\text{-}Rb}$ are the quenching rates in Rb-He and Rb-Rb collisions, respectively.

For each temperature, we calculated the corrected rates $\Gamma_i^c = \Gamma_i - \Gamma_i^{bb} - K_i^{Rb\text{-}He}$. The BBR corrections were performed as described in Ref. [28]. They amounted about 1% of the total decay rates. The contribution of He induced quenching was calculated for the $6^2D_{3/2}$ and $6^2D_{5/2}$ states using the respective quenching cross sections, $\sigma_{q,6D_{3/2}}^{Rb\text{-}He} = 6.6(1.0)\times10^{-14}\text{cm}^2$ and $\sigma_{q,6D_{5/2}}^{Rb\text{-}He} = 4.9(0.7)\times10^{-14}\text{cm}^2$, given in [24]. For the $8^2S_{1/2}$ state we have not found in the literature any data on quenching by He. Therefore we adopted as a safe upper limit for this quenching cross section a value of 10^{-14}cm^2, which is based on available data for higher n values. The reliability of this assumption is supported by the results of the theoretical modelling presented in [29]. For the He number density we used the value $N_{He}=1.5(0.3)\times10^{13}\text{cm}^{-3}$ determined in Sect. 4.1. Contributions to the observed rates due to collisions with He were on average 4%, 3% and 0.3% for the $6^2D_{3/2}$, $6^2D_{5/2}$ and $8^2S_{1/2}$ states, respectively.

Extrapolation of thus obtained corrected rates $\Gamma_i^c = 1/\tau_i + \sigma_{q,i}^{Rb\text{-}Rb} N_{Rb} v_{Rb\text{-}Rb}$ (Stern-Volmer plots) to the collisionless limit ($N_{Rb}v_{Rb\text{-}Rb} \rightarrow 0$) allowed us to obtain the natural lifetimes τ_i for for all states of interest: $8^2S_{1/2}$, $6^2D_{3/2}$ and $6^2D_{5/2}$. From the slopes of $N_{Rb}v_{Rb\text{-}Rb}$-

dependencies, the respective quenching cross sections $\sigma_{q,i}^{Rb-Rb}$ were determined. The results are listed in Tables 1 and 2 along with results available from other studies.

5 Discussion

Inelastic cross sections measured in this work (Table 1) are, with the exception of the cross section for the $8^2S \rightarrow 6^2D$ ET, in good agreement with the experimental values of other authors. The quenching cross sections agree approximately (within a factor of two) with the geometrical cross sections. For the 6^2D_J states, quenching is largely due to ET to the other J sublevel, though the contribution of ET out of the doublet is not negligible. A similar trend has been observed also for the other lowest ^2D states of rubidium (see, e.g., the data compiled in [30]). The cross section for ET from 8^2S to 6^2D amounts to only ¼ of the total quenching cross section for the 8^2S state. As far as other processes contributing to the quenching of 6^2D and 8^2S states are concerned, we can mention ET to the 5^2F and 5^2G states, the infrared fluorescence from which was beyond the sensitivity range of our detection (PMT), and associative ionisation in collisions with the ground state Rb atoms [15]. $Rb^+ + Rb^-$ ion par formation seems to be relatively inefficient as a quenching process [31].

The value for the $8^2S \rightarrow 6^2D$ ET cross section obtained by us is almost 20 times smaller than that measured in [11], and also somewhat smaller than the value (obtained as a side product of an ionisation experiment) reported in [15]. In neither of the studies [11], [15] care was taken to account for the presence of thermal radiation. In present experiment the analysis of the shapes of time resolved signals drew our attention to considerable contribution of extra channels due to the BBR-induced transitions. Account for the BBR mediated population transfer in the thermal conditions of experiments [11], [15] would significantly lower the relevant cross sections. In particular, the cross section reported in [15] would become close to the present result, while value of [11] would remain about ten times larger [27].

As mentioned in sect.1, the $8^2S \rightarrow 6^2D$ ET process is interesting, since here ET takes place between two configurations, which are not coupled by the dipole-dipole interaction. In the absence of calculated molecular terms correlating to these states, it is impossible to make definitive conclusions about the mechanism of this ET process. For the lower 7^2S and 5^2D states efficient mutual ET is possible thanks to the near lying 5^2P+5^2P configuration which enables the dipole coupling between the 7^2S+5^2S and 5^2D+5^2S configurations [13]. For the 8^2S and 6^2D states, which are energetically distant from 5^2P+5^2P, ET was not expected to be

particularly efficient. However, our measured cross section for this process actually exceeds that for the ET from 7^2S to 5^2D. The relatively efficient $8^2S \rightarrow 6^2D$ ET may possibly be influenced by the 7^2P+5^2S and 8^2P+5^2S configurations. The ionic $Rb^+ + Rb^-$ term, which crosses the initial and final covalent states at large internuclear distances (R>60 a.u.), may also contribute, although one would expect that this coupling is weak [13].

Our measured lifetimes (see Table 2) are, within their uncertainty limits, in good agreement with those calculated by Theodosiou [18] and Hansen [19], and for the 6^2D state also with the theoretical lifetime of He et al. [20]. The agreement with the other experimental results [32-34] is good for the $8^2S_{1/2}$ state and less satisfactory for the 6^2D_J states.

In conclusion, we have measured the natural lifetimes and quenching cross sections for $6^2D_{5/2,3/2}$ and $8^2S_{1/2}$ states, the 6^2D state J-mixing cross section and the cross section for ET from the 8^2S to 6^2D state. The analysis of time resolved sensitised fluorescence signals allowed us to access information about the processes involved in the population transfer. The influence of the BBR on the population transfer can be significant even for such low lying states as 8^2S and 6^2D.

Acknowledgements

This work was partially supported by the Polish Committee for Scientific Research (grant No. 2 P03B 065 11) and by the Latvian Science Council. We gratefully acknowledge Prof. M. Auzins for helpful discussions and Prof. J. Migdałek for calculations of Rb oscillator strengths.

References

1. I. L. Beigman, and V. S. Lebedev, Phys. Rep. **250**, 95 (1995).
2. P. H. T. Philipsen, J. H. Nijland, H. Rudolph, and H. G. M. Heideman, J. Phys. B **26**, 939 (1993), and references therein.
3. Z. J. Jabbour, R. K. Nakimota, J. Huennekens, M. Allegrini, S. Miloševic, and F. de Tomasi, Phys. Rev. A **54**, 1372 (1996).
4. F. de Tomasi, S. Miloševic, P. Verker, A. Fioretti, M. Allegrini, Z. J. Jabbour, and J. Huennekens, J. Phys. B **30**, 4991 (1997).
5. V. Horvatic, C. Vadla, and M. Movre, Z. Phys. D **27**, 123 (1993).

6. G. De Filippo, S. Guldberg-Kjær, S. Miloševic, J. O. P. Pedersen, and M. Allegrini, Phys. Rev. A 57, 255 (1998).
7. V. M. Borodin, and I. V. Komarov, Opt. i Spektrosk. **36**, 250 (1974).
8. L. Barbier, M. Chéret, J. Phys. B **16**, 3213 (1983).
9. S. Geltman, Phys. Rev. A **40**, 2301 (1989).
10. P. Kowalczyk, J. Phys. B **17**, 817 (1984).
11. A. D. Sharma, H. A. Schuessler, and R. H. Hill, Jr, Phys. Rev. A **37**, 4649 (1988).
12. Luo Caiyan, A. Ekers, J. Klavins, and M. Jansons, Physica Scripta **53**, 306 (1996).
13. V. Grushevsky, M. Jansons, and K. Orlovsky, Physica Scripta **56**, 245 (1997).
14. A. Ekers, Proceedings of the Latvian Academy of Sciences, Section B, 1995, No. 7/8 (576/577) p. 130.
15. L. Barbier, M. Chéret, J. Phys. B **20**, 1229 (1987).
16. P. Hannaford, and R. M. Lowe, Optical Engineering **22**, 532 (1983).
17. W. Schade, L. Wolejko, and V. Helbig, Phys. Rev. A **47**, 2099 (1993).
18. C. E. Theodosiou, Phys. Rev. A **30**, 2881 (1984).
19. W. Hansen, J. Phys. B **17**, 4833 (1984).
20. X. He, B. Li, A. Chen, and C. Zhang, J. Phys. B **23**, 661 (1990).
21. A. N. Nesmeyanov, *Vapor pressure of the chemical elements* (Elsevier, Amsterdam/London/New York, 1963).
22. T. F. Gallagher, in: *Rydberg states of atoms and molecules*, edited by R. F. Stebbings and F. Barry Dunning (Cambridge University Press, 1982).
23. J. Migdałek, and W. E. Baylis, Can. J. Phys. **57**, 1708 (1979).
24. J. Supronowicz, J. B. Atkinson, and L. Krause, Phys. Rev. A **31**, 2691 (1985).
25. J. Groszkowski, *Technika wysokiej próżni* (High Vacuum Technique - in Polish), 2nd edn. (Wydawnictwa Naukowo-Techniczne, Warszawa, 1978).
26. J. Migdałek (private communication - the oscillator strengths calculated by using a fully relativistic model potential appeared to be quite close to the ones obtained with Coulomb approximation by A. Lingård and S. E. Nielsen, At. Data Nucl. Data Tables, **19**, 533 (1977)).
27. B. Bieniak, A. Ekers, M. Głódź, and J. Szonert (unpublished).
28. J. Szonert, B. Bieniak, M. Głódź, and M. Piechota, Z. Phys. D **33**, 177 (1995).
29. V. S. Lebedev, Zh. Eksp. Teor. Fiz. [Sov. Phys. - JETP] **103**, 50 (1993).
30. J. Supronowicz, J. B. Atkinson, and L. Krause, Phys. Rev. A **30**, 112 (1984).
31. M. Chéret and L. Barbier, Phys. Rev. A **30**, 1132 (1984).

32. J. Marek and P. Münster, J. Phys. B **13**, 1731 (1980).

33. H. Lundberg and S. Svanberg, Phys. Letters **56A**, 31 (1976).

34. G. Waligórski, P. Kowalczyk, and C. Radzewicz, Z. Phys. D **3**, 79 (1986).

35. J. W. Parker, H. A. Schuessler, R. H. Hill, Jr., and B. G. Zollars, Phys. Rev. A **29**, 617 (1984).

Table captions.

Table 1. Inelastic cross sections for Rb*+Rb collisions, in units of 10^{-14}cm^2.

Table 2. Natural lifetimes for the $8^2S_{1/2}$, $6^2D_{3/2}$ and $6^2D_{5/2}$ states of Rb, in ns.

Figure captions.

Fig. 1. Schematic diagram of the experimental apparatus: MCS - multichannel scaler; PM photomultiplier; SM - stepping motor; PD - fast photodiode; LM - laser power meter; NDF - neutral density filter; L1-L3 - lenses; A1,A2 - apertures; PPR - polarisation plane rotator; P - polariser; BS - beam splitter; PR - prism.

Fig. 2. Energy diagram of Rb and illustration of mechanisms of population transfer from the 8^2S to 6^2D state. "Spont." denotes prevailing spontaneous emission accompanied with few per cent of stimulated emission.

Fig. 3. Sensitised fluorescence signals: (a) from $6^2D_{3/2}$ at laser excitation of the $6^2D_{5/2}$ state; (b) from $6^2D_{3/2,5/2}$ at laser excitation of $8^2S_{1/2}$. Solid lines are least squares fits of eq. (8b) and eq. (15) (with (13)), respectively.

Fig. 4. $R_{6D_{5/2}\to 6D_{3/2}}/N_{\mathrm{Rb}}\,v_{\mathrm{Rb\ Rb}}$ dependence on N_{Rb} for (a) $6^2D_{5/2}\to 6^2D_{3/2}$ J-mixing, (b) $8^2S\to 6^2D$ ET. • - experiment; solid line - least squares fit of eq. (14) in case (a), and of an analogous one in case (b).

Initial state	Final state		Quenching cross section $\sigma_{q,i}^{Rb-Rb}$	Geometrical cross section σ_{geom}
	$6^2D_{3/2}$	$6^2D_{5/2}$		
$8^2S_{1/2}$	3.4(1.2)[‡,a] 67(30)[‡,d] 6.1(2.1)[‡,f]		12.8(3.4)[a] 8.1(2.0)[e]	15.7[g]
$6^2D_{3/2}$		13.8(3.2)[†,a] 10.4(2.1)[†,b] 17.3(3.5)[c]	22.8(2.9)[a] 25.3(5.3)[c]	11.7[g]
$6^2D_{5/2}$	9.2(2.1)[a] 6.9(1.4)[b] 11.6(2.3)[c]		14.1(5.7)[a] 15.6(3.3)[c]	

[a] This work.
[b] Parker et al., Ref. [35].
[c] Supronowicz et al., Ref. [24].
[d] Sharma et al., Ref. [11].
[e] Waligórski et al., Ref. [34].
[f] Barbier, Cherét, Ref. [15].
[g] Geometrical cross section is defined as, e. g., in Ref. [35].
[†] Recalculated using detailed balancing principle.
[‡] 6^2D fine structure not distinguished.

Ekers et al., Table 1.

State	Experimental				Theoretical, 0 K		
	This work	MM[a,†]	LS[b,†]	WKR[c]	HLCZ[d]	Theodosiou[e]	Hansen[f]
$8^2S_{1/2}$	161(3)	154(7)	153(8)	166(4)	148	158.3	162.4
$6^2D_{3/2}$	256(4)		285(16)	234(7)[‡]	251[‡]	253.6	258.5
$6^2D_{5/2}$	249(5)	237(15)				243.7	244.1

[a] Marek, Münster, Ref. 32
[b] Lundberg, Svanberg, Ref. 33
[c] Waligórski et al., Ref. 34
[d] He et al., Ref. 20
[e] Theodosiou, Ref. 18
[f] Hansen, Ref. 19
[†] Not corrected for blackbody radiation
[‡] 6^2D fine structure not distinguished

Ekers et al., Table 2.

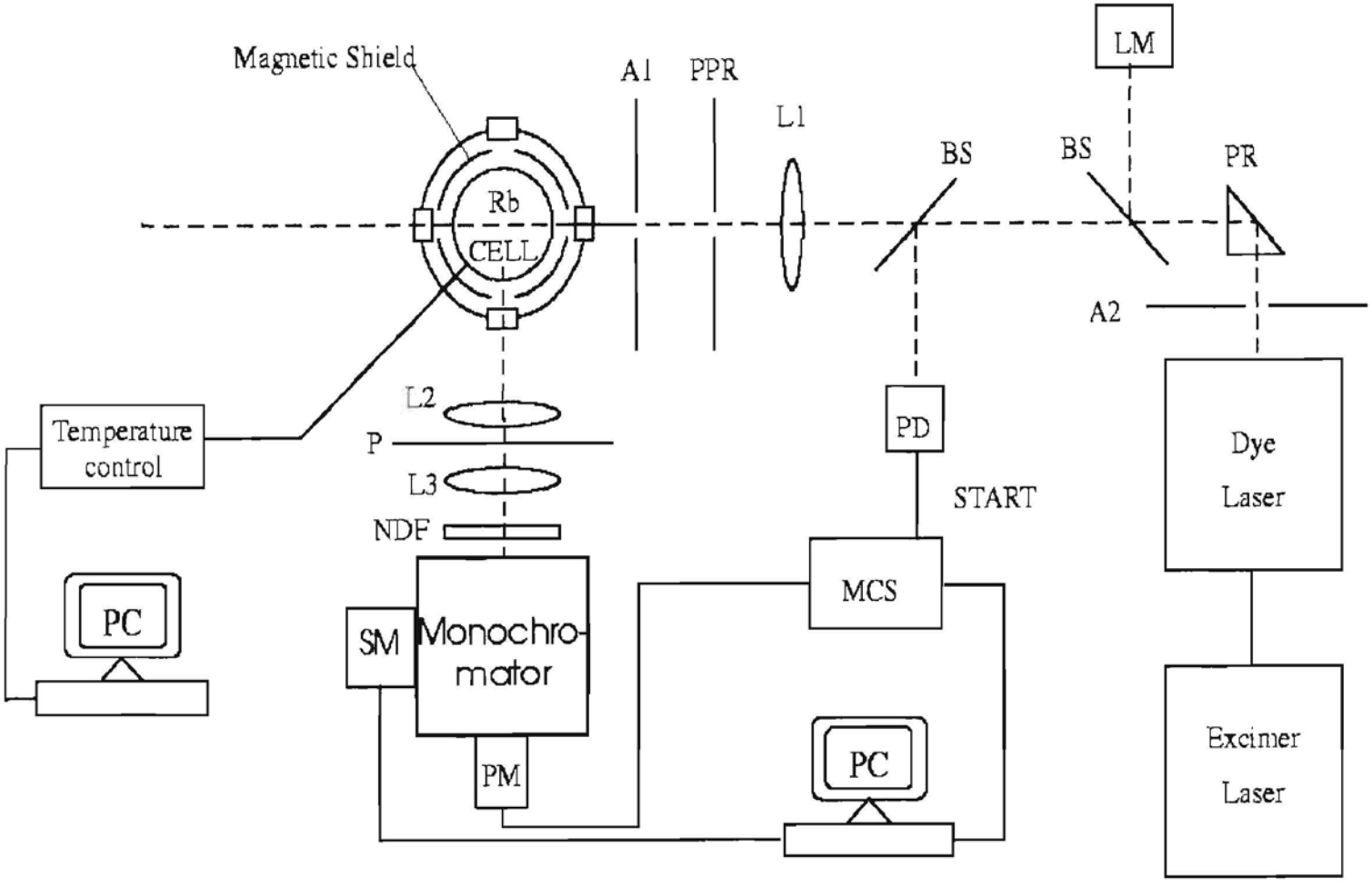

Ekers et al., Fig. 1

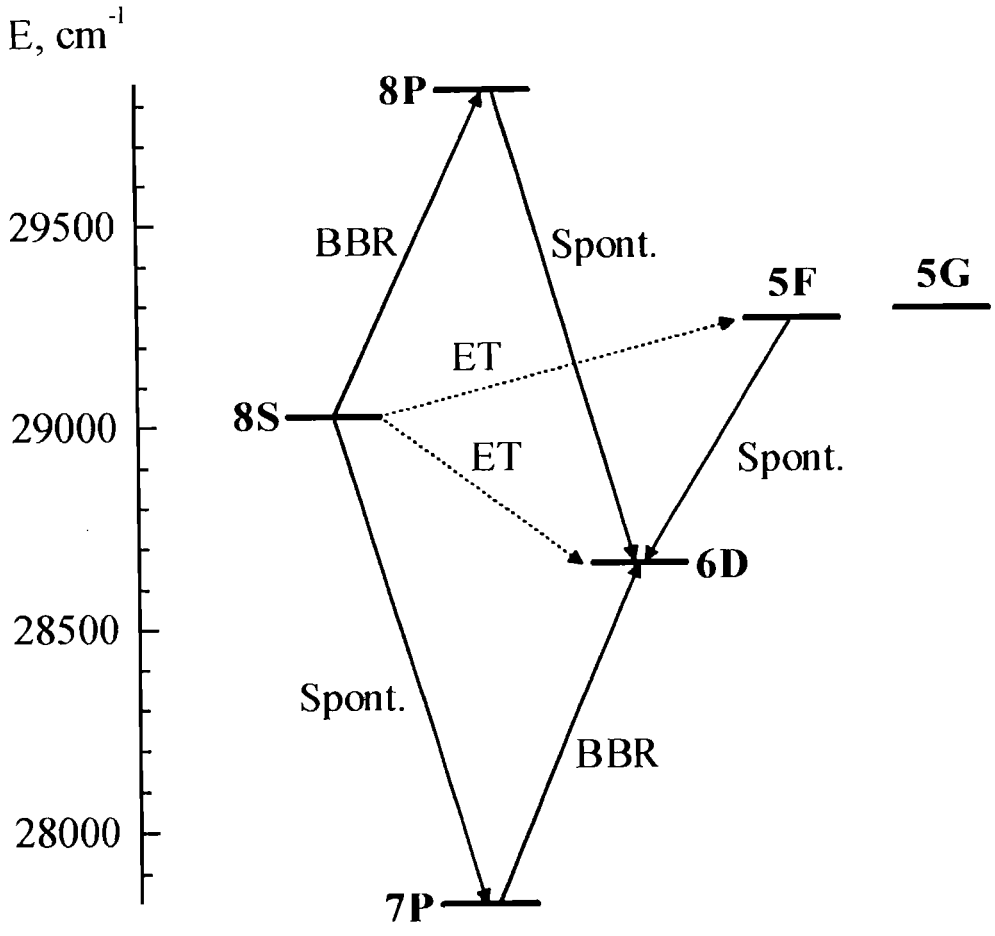

Ekers et al., Fig. 2.

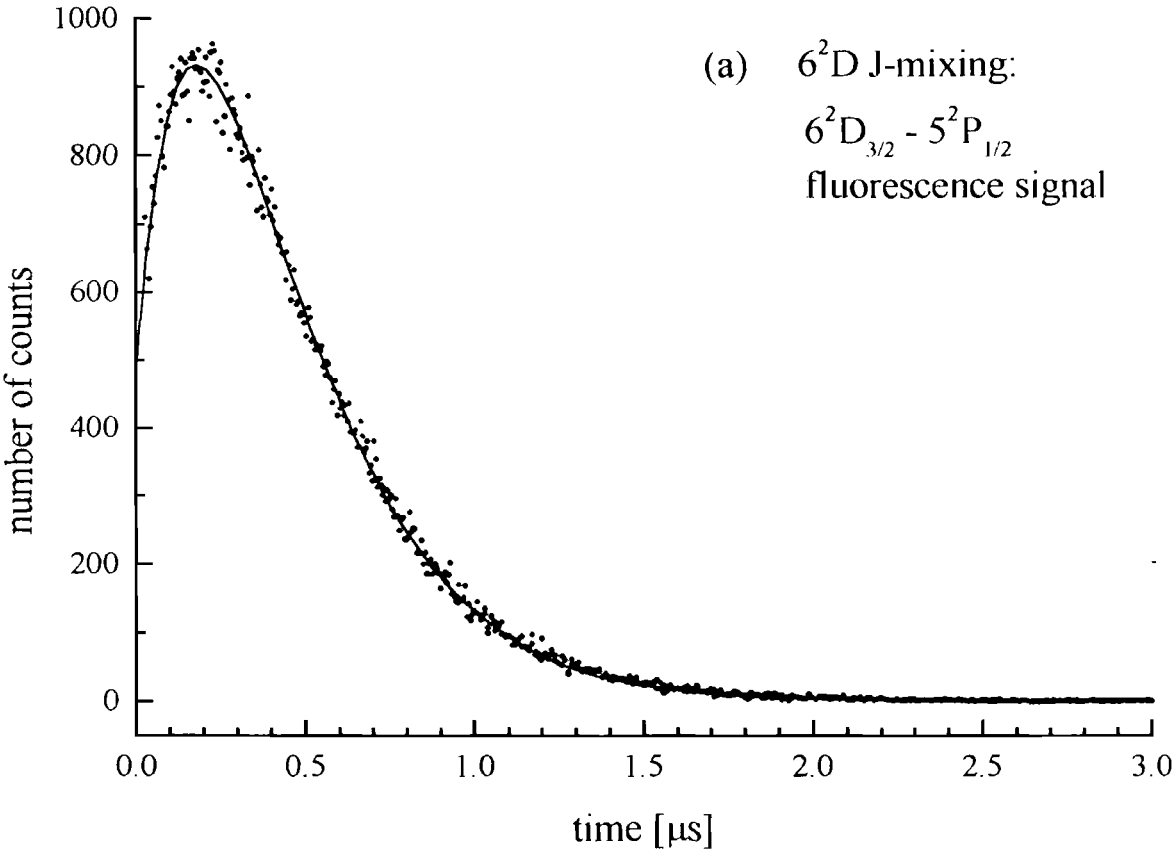

Ekers et al., Fig. 3a.

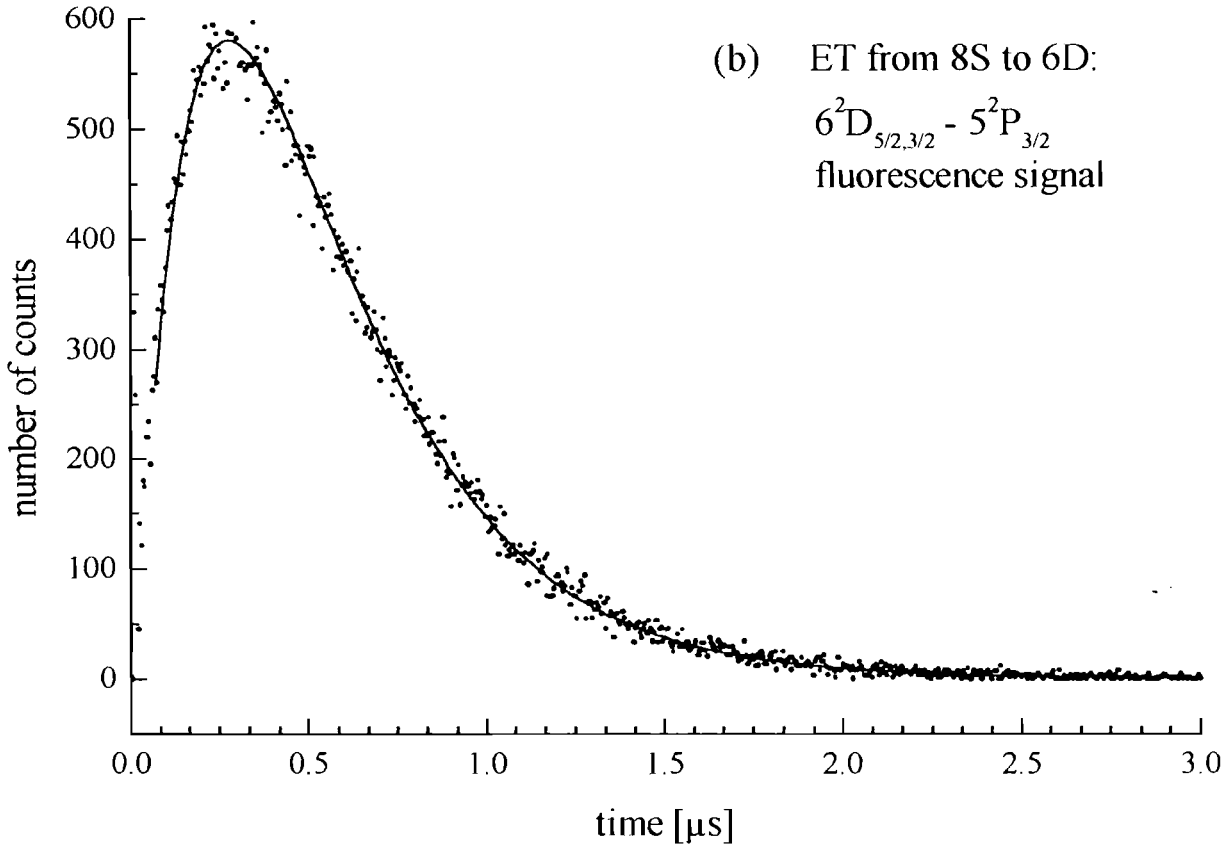

Ekers et al., Fig. 3b.

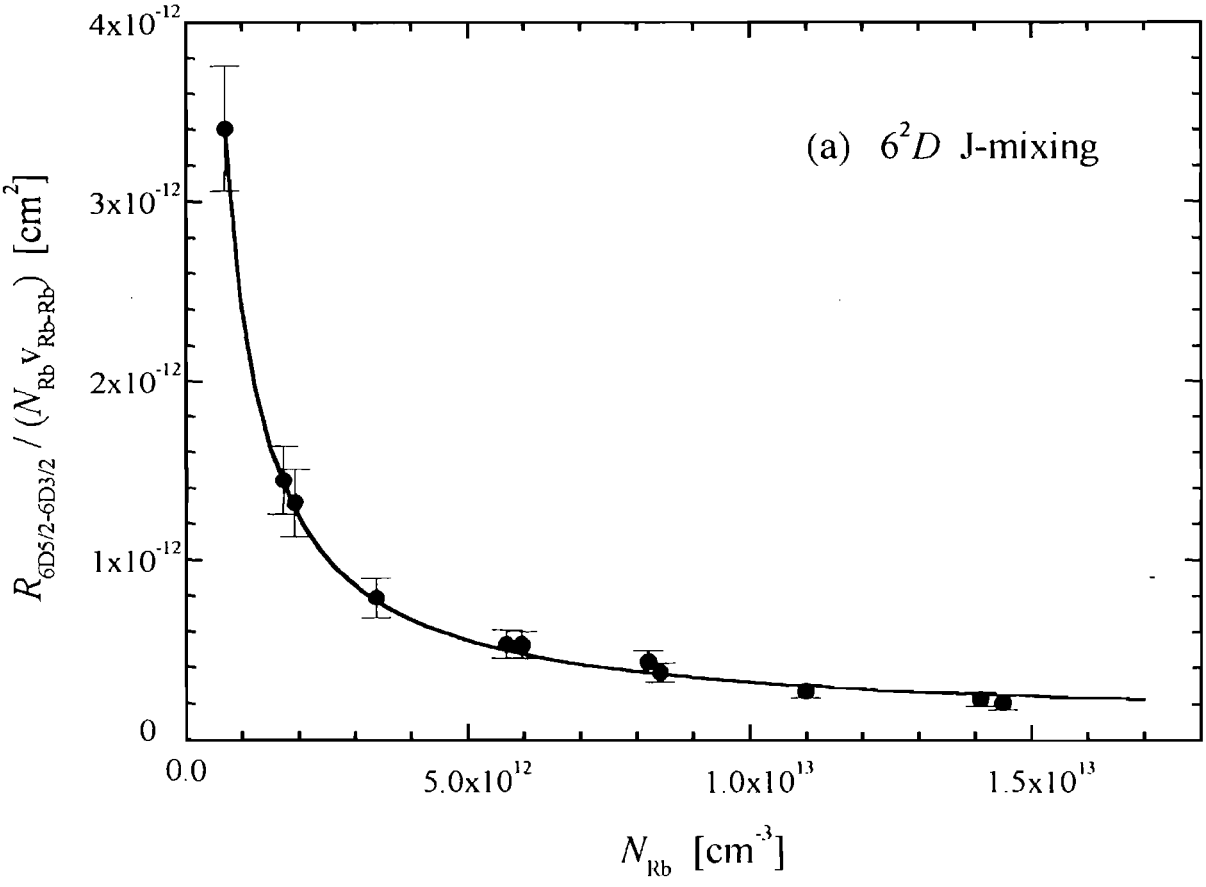

Ekers et al., Fig. 4a.

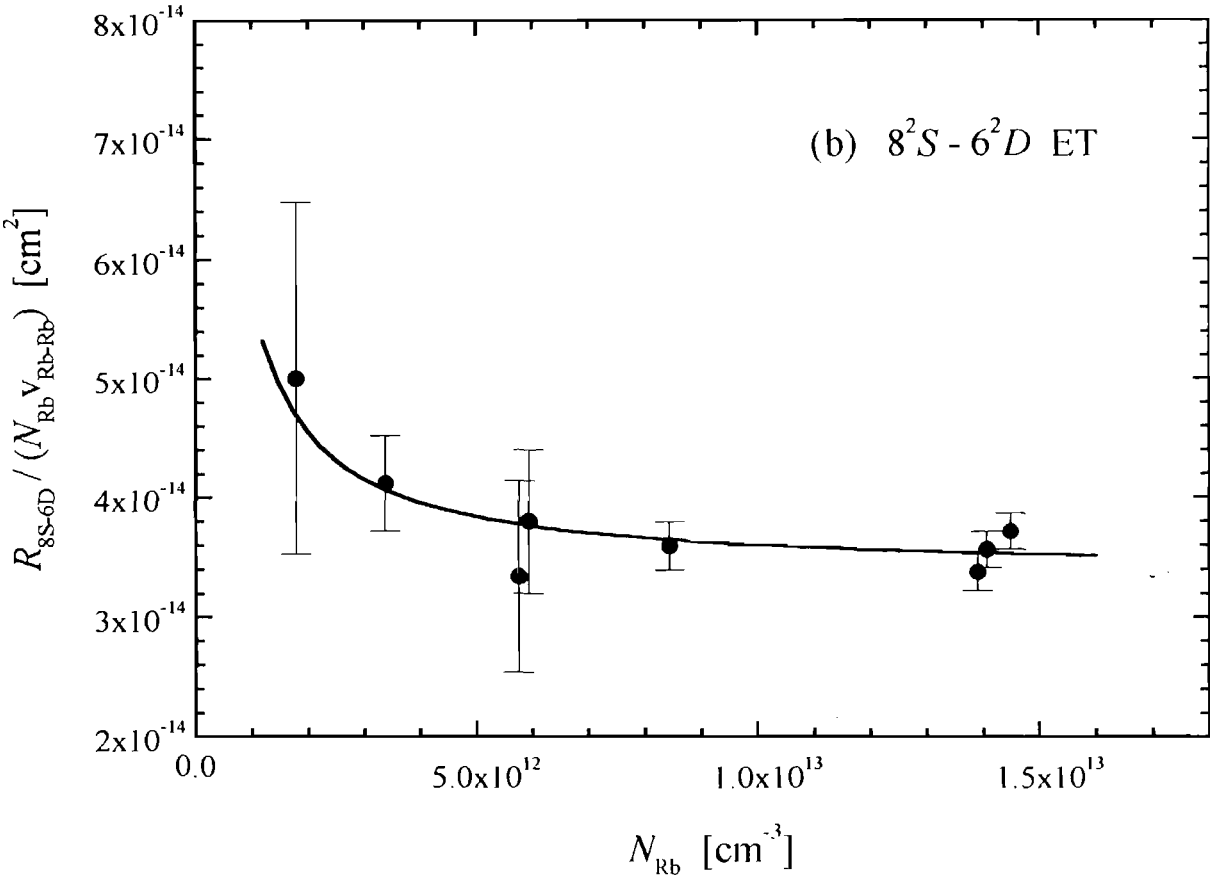

Ekers et al., Fig. 4b.

Non-dipole excitation transfer between the 6^2S and 4^2D states in potassium.

A. Ekers and J. Alnis

University of Latvia, Institute of Atomic Physics and Spectroscopy, Raina bulv. 19, LV-1586 Riga, Latvia; e-mail: aekers@latnet.lv

Abstract

We report an experimental study of collisional excitation transfer between the 6^2S and 4^2D states in potassium. The experiment was performed in potassium vapour, using two-step laser excitation of the 6^2S state. The cross sections of excitation transfer from the 6^2S to 4^2D state and of the 4^2D state quenching in collisions with ground state atoms were determined as $\sigma_{6S\to 4D} = (1.8\pm0.6)\times10^{15}\text{cm}^2$ and $\sigma^q_{4D} = (2.7\pm1.2)\times10^{14}\text{cm}^2$, respectively.

PACS: 34.50.Fa, 32.50.+d

1. Introduction

Among the large variety of collisional excitation transfer (ET) processes the most detailed studied, both experimentally and theoretically, are the so called energy pooling (EP) collisions of two excited alkali atoms resulting in population of high-lying states:

$$M^*(^2P) + M^*(^2P) \rightarrow M^{**}(^2S \text{ or } ^2D) + M(^2S) + \Delta E. \qquad (1)$$

For details concerning experimental studies of these processes we refer the interested reader to publications [1-4] and references therein. A theoretical approach to the EP processes has been developed in [5] for EP in caesium, and later elaborated and applied to other alkalis by various authors [6-10]. A common feature of the processes of type (1) is that they proceed efficiently thanks to the strong dipole-dipole interaction between the intital ($^2P+^2P$) and final ($^2S+^2D$ or $^2D+^2S$) configurations of atoms.

Already in the early studies of ET processes it had been noticed that the cross sections (i.e., rate constants) of different reactions possess a common dependence on the energy defect ΔE [11]. The presently existing data on the EP allows to establish an empirical relation between the reaction rate constant k and energy defect ΔE [12]:

$$k = A \times \exp\left(-\frac{\Delta E}{k_B T}\right), \qquad (2)$$

where $A = (5.0\pm0.6)\times10^{-9}\mathrm{cm^3s^{-1}}$. This relation is valid for the processes with positive ΔE. Moreover, if one compares the rates of other ET process, they also seem to obey the relation (2), no matter if the dipole-dipole interaction between the initial and final configurations is present or not.

One may expect that the ET processes between the atomic ^{2}S and ^{2}D states (hereafter referred to as *SD-transfer*),

$$M^{**}(^2S) + M(^2S) \rightarrow M^{**}(^2D) + M(^2S),$$

will be inefficient because of the lack of interactions that would couple the (^{2}S+^{2}S) and (^{2}D+^{2}S) configurations. However, the existing studies [13-15] on the SD-transfer processes show that they also obey, within uncertainty limits, the relation (2). Theoretical studies [16,17] of the process

$$Rb^{**}(7^2S) + Rb(5^2S) \rightarrow Rb^{**}(5^2D) + Rb(5^2S), \qquad (3)$$

for which an experimental cross section of $8\times10^{-15}\mathrm{cm^2}$ has been reported [14], attributed the efficient ET in this case to the proximity of the (5^2P+5^2P) configuration, which introduces a strong dipole coupling between the initial (7^2S+5^2S) and final (5^2D+5^2S) configurations. In order to clarify the role of interaction in the ET, we are interested in pairs of close lying ^{2}S and ^{2}D states which are energetically well isolated from the ^{2}P states. Such isolation would eventually allow to exclude effects like that of the perturbing (5^2P+5^2P) configuration in the case of SD-transfer process (3), and, hence, the dipole-dipole interaction. The pair of the 6^2S and 4^2D states in potassium (see Fig. 1) seems to be appropriate. The energy defect between these two states is only 53 $\mathrm{cm^{-1}}$. The 6^2P state lies 1548 $\mathrm{cm^{-1}}$ above 6^2S, and 4^2P+4^2P energy is 1311 $\mathrm{cm^{-1}}$ below the 4^2D. In the present work we are concerned with the ET process

$$K^{**}(6^2S) + K(4^2S) \rightarrow K^{**}(4^2D) + K(4^2S) + 53\ \mathrm{cm^{-1}}. \qquad (4)$$

The empirical relation (2) predicts for this process a cross section of $5.6\times10^{-14}\mathrm{cm^2}$ for the mean $k_B T$ of the present experiment.

2. Experiment and method

The experiment was performed in a potassium vapour cell, at temperatures $520\mathrm{K} \le T \le 600\mathrm{K}$. The cell was made of alkali resistant glass cell and placed in a two-chamber oven. The temperature of the side arm of the cell containing metallic potassium was kept 10 degrees below that of the main oven body. The potassium number densities were

calculated from the temperature-vapour pressure relation [18]. The atoms were excited to the 6^2S state using two-step laser excitation (cf Fig. 1). The frequency of the first step laser (Kr^+ pumped CR-590 dye laser with Oxazine 1 dye, $\Delta\nu_{L1} \approx 30GHz$) was detuned from the $4^2S_{1/2} \rightarrow 4^2P_{1/2}$ resonance by several Doppler widths in order to ensure homogeneous excitation of atoms along the beam axis. The second step laser (Ar^+ pumped CR-699 ring dye laser with DCM dye, $\Delta\nu_{L2} \approx 1MHz$) was set on resonance with the $4^2P_{1/2} \rightarrow 6^2S_{1/2}$ transition. The fluorescence was detected on the modulation frequency of the first step laser with a monochromator and a photomultiplier (RCA, model C31034-05) using lock-in technique.

The fluorescence was registered on the $6^2S_{1/2} \rightarrow 4^2P_{3/2}$ (6938.8 Å) and $4^2D_{3/2,5/2} \rightarrow 4^2P_{3/2}$ (6964.7 Å) transitions at various potassium number densities ($8.5\times10^{14}cm^{-3} \leq N_0 \leq 1\times10^{16}cm^{-3}$). The fluorescence intensities provide information about the relative populations in the 6^2S and 4^2D states. The $4^2D_{3/2} \rightarrow 4^2P_{1/2}$ spectral line (6936.3 Å) was not resolved from the comparatively strong $6^2S_{1/2} \rightarrow 4^2P_{3/2}$ fluorescence. It is important to note that the strongly edothermic EP process [3]

$$K^*(4^2P) + K^*(4^2P) \rightarrow K^{**}(4^2D) + K(4^2S)$$

did not contribute to the 4^2D fluorescence signal: with the second step laser blocked, no fluorescence from the 4^2D state was observable even at highest temperatures of the experiment.

Since the fluorescence from the 4^2D J=3/2 and J=5/2 components was not spectrally resolved, we do not distinguish the fine structure and assume that both J sublevels are populated according to statistical weights g_J. The latter assumption is justified because at the high K number densities of the present experiment collisional J-mixing is faster than radiative decay. The solution of rate equation for the 4^2D state allows to extract the cross section for the SD-transfer process (4) from intensity ratio of the $4^2D \rightarrow 4^2P$ and $6^2S \rightarrow 4^2P$ fluorescence lines. Under steady state conditions

$$\frac{dN_{4D}}{dt} = 0 = \sigma_{6S\rightarrow4D} N_0 v N_{6S} - \frac{1}{\tau_{4D}} N_{4D} - \sigma^q_{4D} N_0 v N_{4D}, \qquad (5)$$

where $\sigma_{6S\rightarrow4D}$ is the cross section for the process (4), σ^q_{4D} is the 4^2D state quenching cross section in collisions with ground state K atoms, τ_{4D} is the lifetime of the 4^2D state, $v = \sqrt{8k_B T/\pi\mu}$ is the mean relative velocity of colliding atoms, and N_{6S}, N_{4D} and N_0 are the number densities of the 6^2S, 4^2D and ground state atoms, respectively. From (5) we obtain for the ratio of number densities of excited atoms:

$$\frac{N_{4D}}{N_{6S}} = \frac{\sigma_{6S\to 4D}}{\sigma^{q}_{4D} + 1/(\tau_{4D} N_0 v)}. \qquad (6)$$

In order to relate this density ratio with the ratio of fluorescence intensities $I(4^2D_{5/2,3/2} \to 4^2P_{3/2})$ and $I(6^2S_{1/2} \to 4^2P_{3/2})$, measured in the experiment, a proportionality coefficient must be introduced to account for different transition probabilities of different transitions:

$$\alpha = \frac{g_{5/2} A(4^2D_{5/2} \to 4^2P_{3/2}) + g_{3/2} A(4^2D_{3/2} \to 4^2P_{3/2})}{(g_{5/2} + g_{3/2}) \times A(6^2S_{1/2} \to 4^2P_{3/2})}. \qquad (7)$$

Here A denote Einstein coefficients of the respective transitions, and $g_{5/2}$ and $g_{3/2}$ are the statistical weights of the $4^2D_{5/2}$ and $4^2D_{3/2}$, respectively. Using (6) and (7), the ratio of the measured fluorescence intensities can be expressed as

$$\eta = \frac{I(4^2D_{5/2,3/2} \to 4^2P_{3/2})}{I(6^2S_{1/2} \to 4^2P_{3/2})} = \alpha \frac{\sigma_{6S\to 4D}}{\sigma^{q}_{4D} + 1/(\tau_{4D} N_0 v)}. \qquad (8)$$

Thus, the SD-transfer and quenching cross sections can be obtained from the measured intensity ratio η. In (7) and (8) we are using the values for the Einstein coefficients from [19], and lifetime τ_{4D} given in [20].

3. Results and discussion

The experimental dependence of the intensity ratio η on the product of number density N_0 and collision velocity v, $N_0 v$, is shown in Fig. 2. By fitting eq. (8) to the experimental points (solid line, Fig. 2), the cross section for the process (4), $\sigma_{6S\to 4D} = (1.8\pm0.6)\times10^{-15}\text{cm}^2$, and the 4^2D state quenching cross section, $\sigma^{q}_{4D} = (2.7\pm1.1)\times10^{-14}\text{cm}^2$, were determined. If one compares the available cross sections of different SD-transfer processes (Table I), it is evident that the process in potassium is the least efficient despite the smallest energy defect. Also note that the experimental cross section for the SD-transfer process (4) is more than 30 times smaller than predicted by the empirical relation (2). The relatively small value of this cross section may be explained by the lack of strong interactions, which would couple the initial (6^2S+4^2S) and final (4^2D+4^2S) configurations. The dipole-dipole interaction mediated by the (4^2P+4^2P) configuration can be eventually excluded because of its large energy separation from the 6^2S+4^2S and 4^2D+4^2S states of separated K atoms. This would explain why the cross section of the process (4) is smaller than it would be expected from the relation (2). The latter was obtained for EP processes dominated by the dipole-dipole interaction, which is absent in

the present case. Possibly, the process (4) is governed by interaction of $K(6^2S)+K(4^2S)$ and $K(4^2D)+K(4^2S)$ quasi-molecular states with the ionic $K^+ + K^-$ state at large internuclear distances $R > 60$ a.u. (see the potential curves calculated in [21]).

As about the quenching of the 4^2D state, we can mention few possible processes which could be responsible for it. The quenching with the ground state K_2 molecules we exclude because of the following considerations. Assuming that the excited atoms are being quenched in collisions with the molecules, we obtain for the 4^2D quenching cross section a value of $4.3\times10^{-12}cm^2$, which is unrealistically large. Moreover, with the molecules as the quenching actors we could not reproduce the experimental $\eta(N_0 v)$-dependence as good as in the case of quenching with atoms. Therefore we conclude, that the 4^2D state is quenched in collisions with ground state K atoms. One of the possible processes is the associative ionisation leading to formation of K_2^+. Another possibility is ET to the 4^2F state. To best of our knowledge, there is no data available in the existing literature about these processes. It should be noted, however, that both above mentioned processes are strongly endoergic (by $-923cm^{-1}$ and $-730cm^{-1}$, respectively), and therefore they are not expected to be particularly efficient. A more likely explanation of the quenching is capture of the colliding $K(4^2D)$ and $K(4^2S)$ atoms on the attractive molecular terms at small internuclear distances [17].

In conclusion, we have experimentally determined the cross sections for ET between the 6^2S and 4^2S states of potassium, and the 4^2D state quenching cross section in collisions with the ground state atoms. The former cross section is more than 30 times smaller than predicted by the empirical relation of the cross section with energy defect (2). A theoretical work on these processes is in progress, and will be reported elswhere.

Acknowledgements

This work was partially supported by the Latvian Science Council. We are grateful to Prof. K. Bergmann, who provided the necessary experimental facilities. One of us (A.E.) thanks the Deutscher Akademischer Austauschdienst (DAAD) for support.

References

1. J. H. Nijland, J. A. de Gouw, H. A. Dijkerman, and H. G. M. Heideman, J. Phys. B **25**, 2841 (1992); J. H. Nijland, J. J. Blangé, H. Rudolph, H. A. Dijkerman, and H. G. M. Heideman, J. Phys. B **25**, 4835 (1992).
2. Z. J. Jabbour, R. K. Namiotka, J. Huennekens, M. Allegrini, S, Milošević, and F. de Tomasi, Phys. Rev. A **54**, 1372 (1996).
3. R. K. Namiotka, J. Huennekens, and M. Allegrini, Phys. Rev. A **56**, 514 (1997).
4. C. Vadla, Eur. Phys. J. D **1**, 259 (1998).
5. V. M. Borodin and I. V. Komarov, Opt. Spectrosc. **36**, 145 (1974) [Opt. Spektrosk. **36**, 250 (1974)].
6. L. Barbier, M. Chéret, J. Phys. B **16**, 3213 (1983).
7. P. Kowalczyk, J. Phys. B **17**, 817 (1984); Chem. Phys. Lett. **68**, 203 (1979).
8. S. Geltman, Phys. Rev. A **40**, 2301 (1989).
9. P. H. T. Philipsen, J. H. Nijland, H. Rudolph, and H. G. M. Heideman, J. Phys. B **26**, 939 (1993).
10. I. Yu. Yurova, O. Dulieu, S. Magnier, F. Masnou-Seeuws, and V. N. Ostrovskii, J. Phys. B **27**, 3659 (1994).
11. L. Krause, Adv. Chem. Phys. **28**, 267 (1975).
12. G. De Filippo, S. Guldberg-Kjær, S, Milošević, J. O. P. Pedersen, and M. Allegrini, Phys. Rev. A **57**, 255 (1998).
13. A. Ekers, Proceedings of the Latvian Academy of Sciences B **7/8**, 130 (1995).
14. Luo Caiyan, A. Ekers, J. Klavins, M. Jansons, Physica Scripta **53**, 306 (1996).
15. A. Ekers, M. Głódź, J. Szonert, B. Bieniak, K. Fronc, and T. Radelitski, Eur. Phys. J. D (submitted).
16. V. Grushevsky, M. Jansons, and K. Orlovsky, Physica Scripta **56**, 245 (1997).
17. K. Orlovsky, V. Grushevsky, and A. Ekers, Eur. Phys. J. D (submitted).
18. A. N. Nesmeyanov, in *Vapor Pressure of the Chemical Elements*, edited by R. Gary (Elsevier, Amsterdam / London / New York, 1963).
19. A. Lingård and S. E. Nielsen, At. Data Nucl. Data Tables **19**, 533 (1977).
20. C. E. Theodosiou, Phys. Rev. A **30**, 2881 (1984).
21. S. Magnier and Ph. Millié, Phys. Rev. A **54**, 204 (1996).

Table captions

Table 1. Energy defects and cross-sections for SD-transfer processes in Rb and K.

Figure captions

Fig. 1. Energy level diagram for the lowest and intermediate excited states of potassium. Solid arrowlines depict two steps of the laser excitation. Detuning of the first step laser Δ is exaggerated on this picture. Dotted arrowlines mark the observed fluorescence transitions.

Fig. 2. Dependence of the intensity ratio $I\left(4^2\mathrm{D}_{5/2,3/2} \rightarrow 4^2\mathrm{P}_{3/2}\right)/I\left(6^2\mathrm{S}_{1/2} \rightarrow 4^2\mathrm{P}_{3/2}\right)$ on $N_0 v$; •, experiment; solid line, least squares fit of eq. (8).

Process	ΔE, cm^{-1}	Cross section, cm^{-15}	
		Experimental	Theoretical
$Rb(7^2S)+Rb(5^2S) \rightarrow Rb(5^2D)+Rb(5^2S)$	607	8±4[a]	7.0[b]
$Rb(8^2S)+Rb(5^2S) \rightarrow Rb(6^2D)+Rb(5^2S)$	358	34±12[c]	
$K(6^2S)+K(4^2S) \rightarrow K(4^2D)+K(4^2S)$	53	1.8±0.6[d]	

[a] Luo Caiyan et al., Ref. [14]
[b] Orlovsky et al., Ref. [17]
[c] Ekers et al., Ref. [15]
[d] This work

Ekers and Alnis, Table 1.

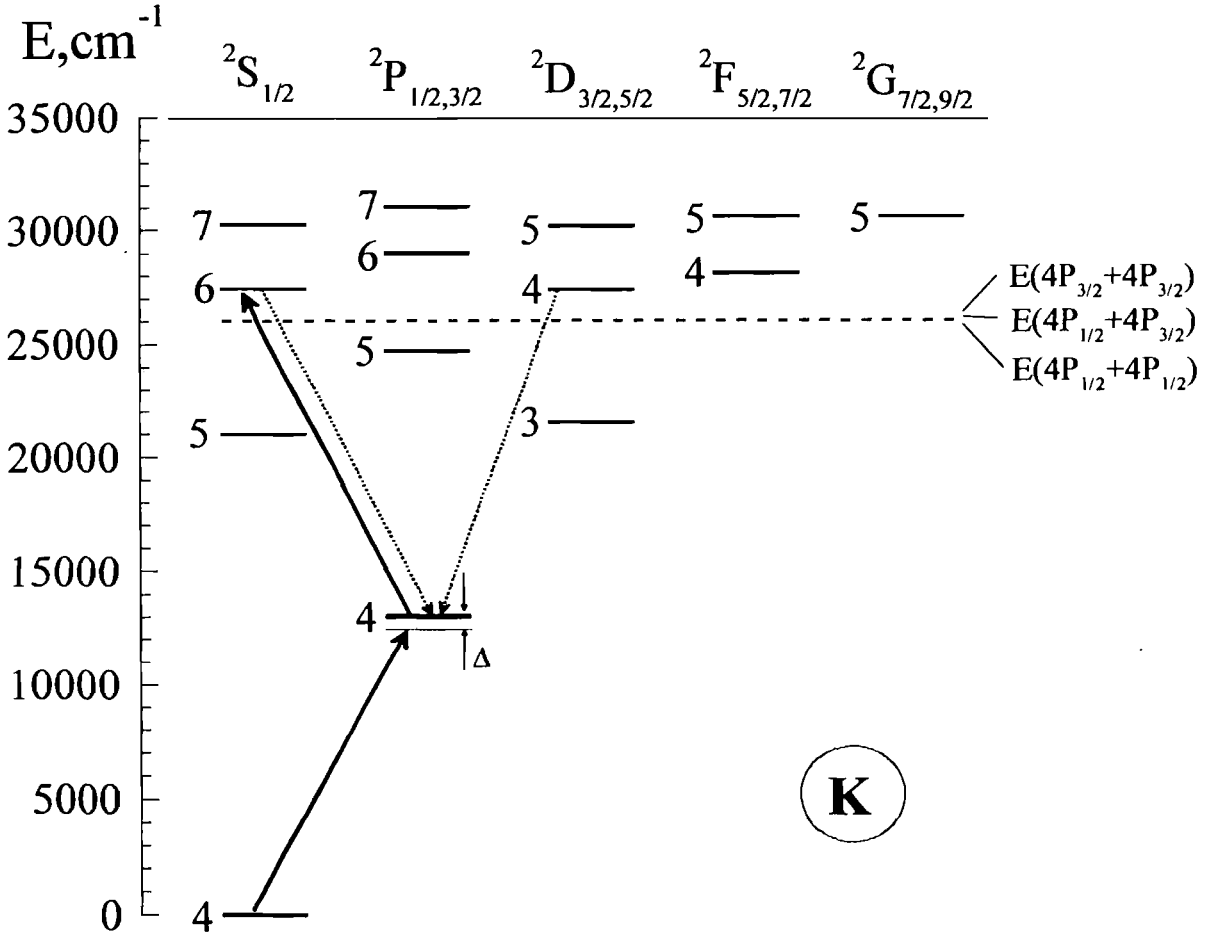

Ekers and Alnis, Fig. 1.

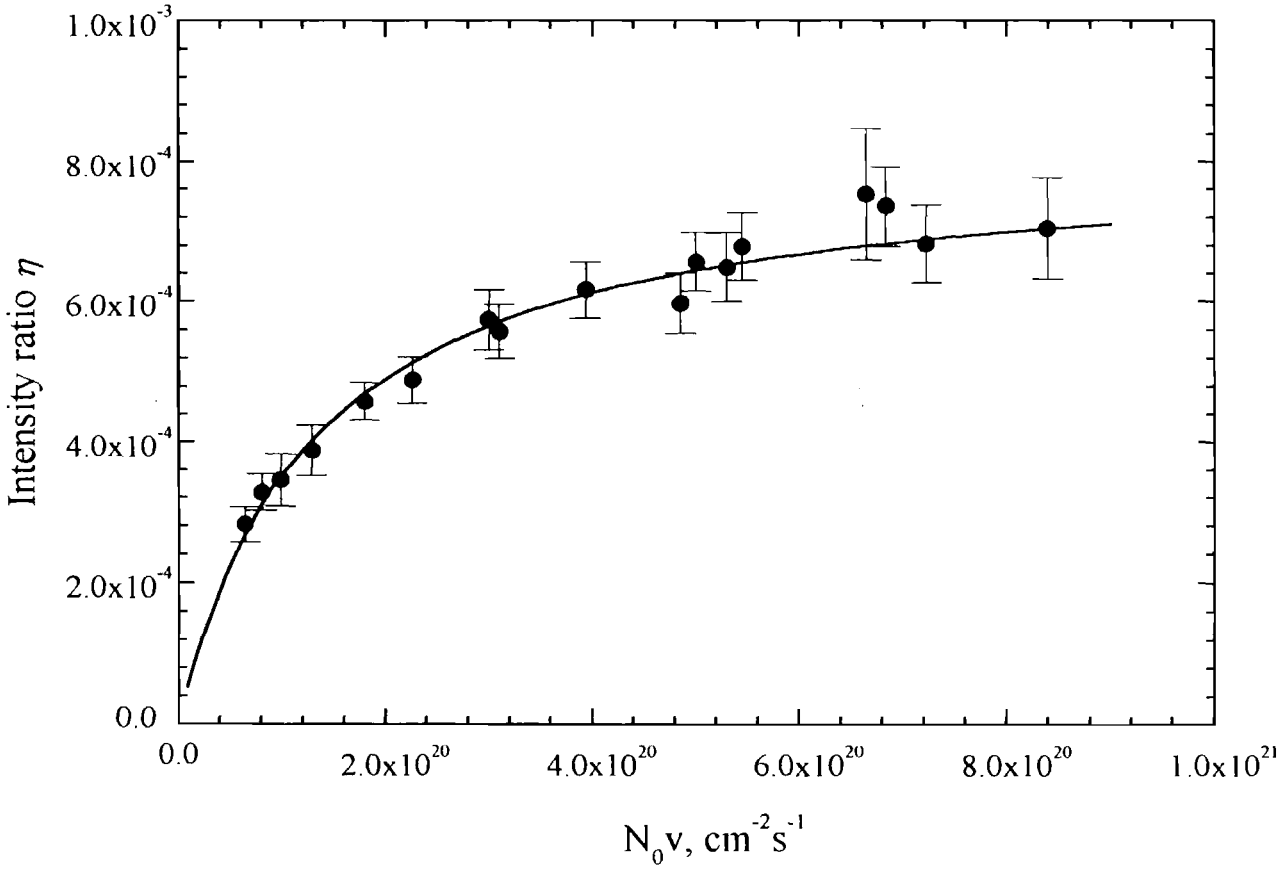

Ekers and Alnis, Fig. 2.

7 October 1994

ELSEVIER

Chemical Physics Letters 228 (1994) 346–350

CHEMICAL PHYSICS LETTERS

Ionization in collisions between excited sodium dimers and atoms

J. Klavins [a,b], M. Jansons [a], A. Ekers [a], Luo Caiyan [b], S. Svanberg [b]

[a] *Department of Spectroscopy, University of Latvia, Rainis Boulevard 19, 1586 Riga, Latvia*

[b] *Department of Physics, Lund Institute of Technology, Box 118, S-221 00, Sweden*

Received 16 May 1994; in final form 19 July 1994

Abstract

Associative ionizing molecule–atom collisions $Na_2(A\,^1\Sigma_u^+) + Na(3p) \rightarrow Na_3^+ + e$ have been observed at simultaneous excitation of dimers and atoms by means of two lasers. Measurements of the relevant ionization current show that the cross section of molecule–atom ionizing collisions exceeds by an order of magnitude the cross section of the well-known atom–atom associative ionization $Na(3p) + Na(3p) \rightarrow Na_2^+ + e$.

1. Introduction

Production of sodium dimer ions Na_2^+ in associative ionizing (AI) collisions

$$Na(3p) + Na(3p) \rightarrow Na_2^+ + e \qquad (1)$$

has been considered in a number of studies at energies ranging from thermal collisions [1] to collisions of 'ultra-cold' Na atoms [2]. However, as far as we are informed, only in two papers [3,4] dimer–atom AI in sodium is reported to be observed under conditions when one of the colliding particles is highly excited while the other remains in the ground states,

$$Na(4d, 5s) + Na_2 \rightarrow Na_3^+ + e \text{ [3]}, \qquad (2)$$

$$Na + Na_2(C\,^1\Pi_u) \rightarrow Na_3^+ + e \text{ [4]}. \qquad (3)$$

The purpose of the present study is to confirm that sodium trimer ions can be produced in AI collisions between dimers and atoms in the case when both particles are in their lowest electronically excited states, namely

$$Na(3p) + Na_2(A\,^1\Sigma_u^+) \rightarrow Na_3^+ + e. \qquad (4)$$

Due to the low ionization potential of the sodium trimer [5], the Na_3^+ ions can become dominating in the alkali plasma [6,7]. A high density of atoms and dimers in the lower excited levels is helpful for the channel (4) of trimer ion production. The reversed process of trimer ion dissociative recombination, is, in a number of cases [6,8], responsible for the well-known diffuse band emission in alkali dimers.

2. Experimental

We have analyzed the laser-induced ionization in sodium vapour by continuous wave laser excitation of atomic 3p states whilst another, chopper-modulated laser beam was used to excite the $A\,^1\Sigma_u^+$-state of sodium dimers. The ion current was measured by a lock-in amplifier, thus excluding the constant, unmodulated part of the total ion current produced in AI collisions of excited atoms (1). In preliminary experiments [9] such an excitation of $Na_2(A\,^1\Sigma_u^+)$ molecules by a Kr^+ laser (647.1/676.3 nm) allowed us to distinguish the part of ion current produced by simultaneous laser excitation of Na_2 and Na. The ion

0009-2614/94/$07.00
SSDI 0009-2614(94)00946-5

current appeared to be a linear function of the power of both lasers. In case when only the atoms were excited (by a modulated laser beam) the Na ion current was proportional to the squared laser power in accordance with reaction (1).

However, the simultaneous energy transfer (ET) from dimers to atoms is also possible, which did not allow to make unambiguous conclusion that the ionization signal induced by both lasers is caused by Na_3^+ ions produced in dimer–atom AI collisions (4). The aim of the present study was to separate the contribution of $Na_2^* + Na^*$ AI collisions (4) from the total ion signal, without the use of a mass spectrometer, as well as to evaluate the efficiency of the Na_3^+ production.

3. Experimental setup

The general scheme of the experiment is shown in Fig. 1. Sodium vapor was contained in a cylindrical glass cell equipped with a sapphire window to transmit the laser beams, and with electrodes to collect the ions. The cell was made out of alkali-resistant glass to make the observation of laser-induced fluorescence (LIF) possible. The glass walls were degassed and saturated with Na vapor at 450°C, and afterward a portion of pure Na had been distilled into the cell before it was detached from the vacuum system. Thus, the interaction of Na vapor and the glass during the experimental produce was minimized. Typical densities of $[Na] \approx 10^{15}$ cm^{-3} and $[Na_2] \approx 10^{13}$ cm^{-3} correspond to a temperature range of 340–380°C in the experiment.

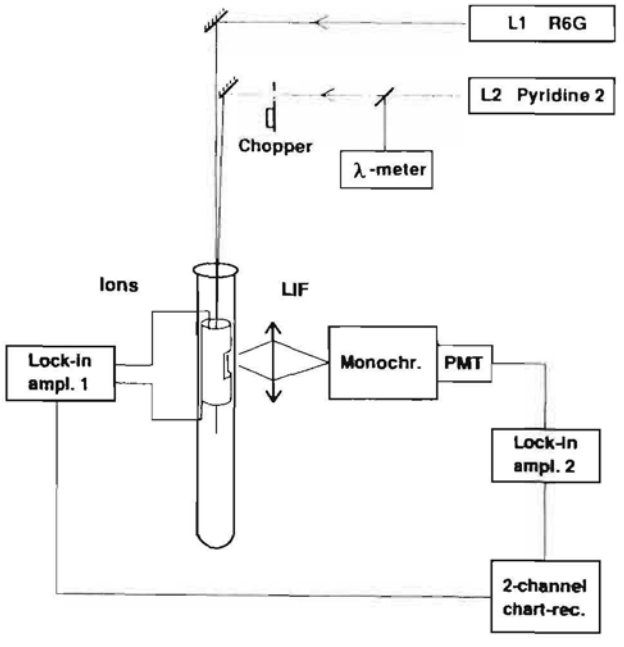

Fig. 1. Experimental arrangement for AI and LIF registration in sodium vapor. Monochr.: Jobin-Yvon model HR-100. Lock-in ampl. 1: Princeton Appl. Research model HR-8. Lock-in ampl. 2: Princeton Appl. Research model 5209. PMT: Hamamatsu model R943-02.

To excite Na atoms a CW broad band ($\Delta\lambda \approx 0.025$ nm) 30 mW R6G dye laser L1 (Coherent Radiation model CR-599) was used. Because of the high optical density of the vapor, the laser was tuned at the wing of Na D_2 line. This allows to improve the signal/noise ratio in the registration, since the rather high signal ($\sim [Na^*]^2$) of the $Na^* + Na^*$ AI, regardless of the blocking by a lock-in amplifier, is a source of noise, the level of which strongly depends on the concentration of excited Na atoms.

The Na_2 molecule were excited by a single-frequency ring dye laser L2 (Coherent Radiation model CR-699), with pyridine 2 dye, the generation interval of which allowed selective excitation of different rotational levels of the $A\,^1\Sigma_u^+$ lower vibrational states $v'=0$ and $v'=1$. The laser was chopper-modulated (730 Hz), the reference signal being applied to separate lock-in amplifiers for the ion current and LIF registration channels. The laser power was about 100 mW. The wavelength of the Na_2 absorption $v''J'' \rightarrow v'J'$ was calculated from known spectroscopic constants of the A and X states, and a λ meter (home built) was used for tuning. The laser beams ($\phi \approx 2$–3 mm) were crossing each other at a very small angle in the ionization detector. A voltage difference of 2–3 V was applied between the electrodes of the detector. A small opening in the cylindrical ion collector enabled the observation of the LIF spectra.

4. Results and discussion

A typical laser-induced ionization signal for the case when only the laser L2 was modulated is shown in Fig. 2a. The registered ion current appears due to the simultaneous effect of both the lasers, i.e. to simultaneous excitation of Na_2 and Na. A similar ion sig-

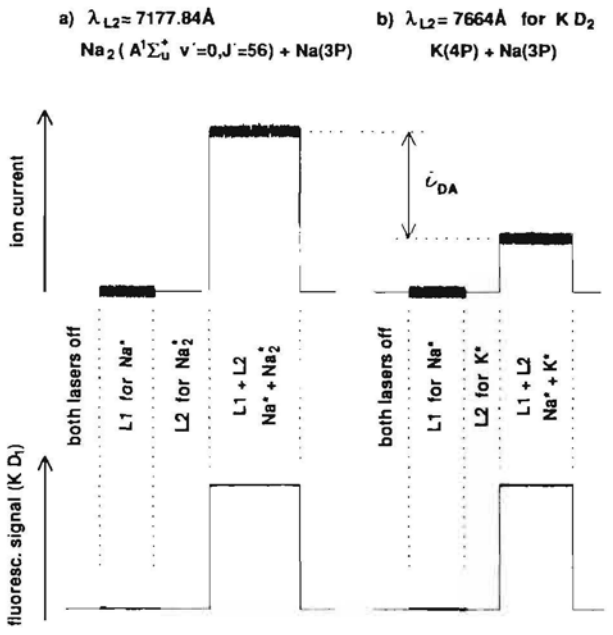

Fig. 2. Ion current and K D_1 line fluorescence signal: (a) at excitation of sodium dimers and atoms; (b) at excitation of potassium and sodium atoms.

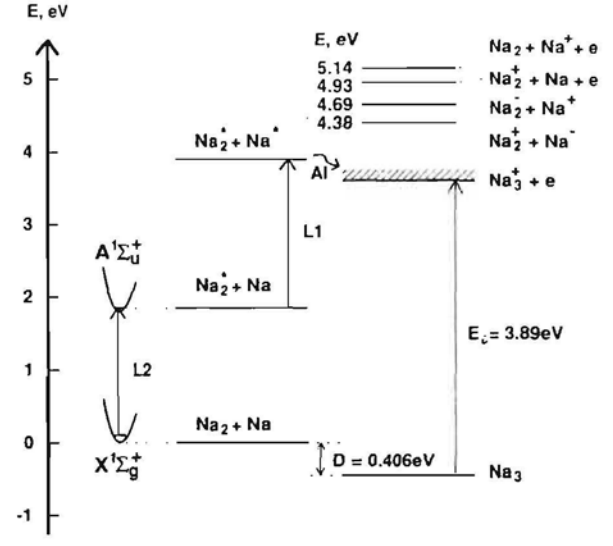

Fig. 3. Energy diagram of $Na_2(A\,^1\Sigma_u^+) + Na(3p)$ collisional ionization.

nal was obtained at excitation of a number of other $v'J'$ levels of the $A\,^1\Sigma_u^+$ states of Na_2.

The energy thresholds of possible ionization in $Na_2^* + Na^*$ collisions are shown in Fig. 3. The trimer ion Na_3^+ produced in dimer–atom AI process is the only energetically possible direct mechanism. The registered signal of the two laser-induced ionization may contain a contribution from the atom–atom AI following the ET in dimer–atom collisions,

$$Na_2(A\,^1\Sigma_u^+) + Na \rightarrow Na_2(X\,^1\Sigma_g^+) + Na(3p)\,, \quad (5)$$

$$Na(3p) + Na(3p) \rightarrow Na_2^+ + e\,. \quad (6)$$

To exclude the ET from Na_2^* to Na, the sodium dimers were excited to the lower $v' = 0$, $v' = 1$ levels, the energy defect of which, with regard to ET, is rather large ($\Delta E \geqslant 0.3$ eV), thus making the ET probability small. No Na D lines were observed in the fluorescence spectrum induced by the L2 laser even at the maximum sensitivity of the LIF registration system.

The presence of a small potassium impurity in the sodium vapor is unavoidable, and weak potassium D line emission was detected in the LIF spectrum. In an earlier study [10] we have obtained a large cross section of ET from a number of $Na_2(A\,^1\Sigma_u^+, v'J')$ levels to the 4p levels of K atoms. The following AI process in $Na(3p) + K(4p)$ collisions is able to provide a contribution to the registered ion current,

$$Na_2(A\,^1\Sigma_u^+) + K \rightarrow Na_2(X\,^1\Sigma_g^+) + K(4p)\,, \quad (7)$$

$$K(4p) + Na(3p) \rightarrow NaK^+ + e\,. \quad (8)$$

By scanning of the L2 laser frequency a certain correlation was observed between the registered ion current and K atoms D lines intensity. The $Na_2^* + Na^*$ direct AI collisions not being excluded, such a correlation, however, suggests the necessity to determine the contribution of NaK^+ ion molecules to the measured ion signal. It was carried out in the following way. In a cell containing a minimum of K atom admixture, the $A\,^1\Sigma_u^+$ state $v'J'$ levels of Na_2 molecules were excited, for which the ET to 4p levels of potassium atoms has the smallest cross section [10]. The NaK^+ contribution into the total ionization signal has been fixed in the following way. First, the ion current produced by simultaneous excitations of Na_2 (laser L2) and Na (laser L1) was measured (Fig. 2a). Then the laser L2 was tuned to direct optical excitation of K atoms in the wing of D_2 line and attenuated ($\geqslant 30$ times) to provide an K atom D_1 emission intensity to be equal to that observed at excitation of K(4p) by ET from Na_2^* (see Fig. 2b). In this case the density of K(4p) atoms excited by ET is equal to (or, at least, does not exceed) the density of optically excited K(4p). The ion current in the latter case is deter-

mined by Na^*+K^* AI collisions only, since the sodium dimers are not excited. The difference in ion signals (Fig. 2) in both cases is equal to (or, at least, is not less than) the ion current of Na_3^+ in AI $Na^*+Na_2^*$ collisions (4).

The rate of Na_3^+ ions production is equal to

$$K_{DA}^{AI}\int [Na^*]\,[Na_2^*]\,dV. \tag{9}$$

For volume averaged densities of excited particles the rate constant of the AI reaction (4) can be written as

$$K_{DA}^{AI}=\frac{i_{DA}}{e[Na_2^*]\,[Na^*]V_1}, \tag{10}$$

where i_{DA} is the ion current and V_1 is the volume of the ionization region. The rate constant of AI of two Na (3p) atoms

$$K_{AA}^{AI}=\frac{i_{AA}}{0.5\,e[Na^*]^2V_2} \tag{11}$$

was measured in Ref. [1]. The ratio of both constants is then

$$\frac{K_{DA}^{AI}}{K_{AA}^{AI}}=\frac{i_{DA}}{i_{AA}}\frac{0.5[Na^*]}{[Na_2^*]}\frac{V_2}{V_1}. \tag{12}$$

From the measured Na^*+Na^* AI current and the known K_{AA}^{AI} value the average density of excited atoms was estimated as $[Na^*]\approx 5\times 10^{10}\,cm^{-3}$.

To obtain the excited dimer density the system of population balance equations was solved with regard to the laser coupled levels. In the case of Na_2 the solution is determined not only by the probabilities of stimulated ($B_{ki}\rho\approx 450\ \mu s^{-1}$) and spontaneous ($A_{ik}\approx 5\ \mu s^{-1}$) transitions between the upper (i) and the lower (k) level. Spontaneous emission to other ground-state levels $v''J''$ levels ($\sum_k A_{ik}=1/\tau_i$) is very important, as well as repopulation of the laser-depleted lower state in dimer–atom collisions, having the cross section $Q=4\times 10^{-14}\,cm^2$ for Na_2+Na [11]. Even at rather high saturation values, in our experiment reaching $S\approx 100$ [1], most of the absorbing molecules are redistributed through the upper level to other $v''J''$ levels of the ground state $X\,^1\Sigma_g^+$, whilst only $\approx 6\%$ remain in the upper level $v'J'$. The ground state Na_2 $v''J''$ molecules have Maxwellian velocity distribution ($\Delta\nu_D\approx 1.6$ GHz), therefore only a part of them is able to absorb the single frequency linear polarized laser radiation. Power-broadened homogeneous linewidth of the molecular transition is $\Delta\nu_{sat}\approx 0.14$ GHz, so we finally estimate the excited dimer density in our experiment as $[Na_2^*]\leqslant 10^8\,cm^{-3}$.

Hence, the $Na_2^*+Na^*$ AI rate constant appears to exceed that of the Na^*+Na^* AI at least by an order of magnitude, as it follows from expression (12) according to obtained experimental data and estimated excited particle densities. The corresponding cross section of the sodium dimer–atom AI collisions (4) attains the value of $Q\geqslant 10^{-15}\,cm^2$, which is a rather high one for collisional ionization.

5. Conclusion

We have separated experimentally the contribution of light-induced ionization signal of Na_3^+ ions produced in AI collisions $Na_2(A\,^1\Sigma_u^+)+Na(3p)$. An estimation of the first experimental results shows that the cross section of those AI collisions exceeds considerably the well-known rather high cross section of the $Na(3p)+Na(3p)$ AI collisions. A large efficiency of dimer–atom AI as compared to atom–atom AI has been also observed in Ref. [3], in collisions between ground-state Na_2 molecules and highly excited Na atoms. The experimental studies of the AI cross-section dependence on $v'J'$ quantum number of the excited $A\,^1\Sigma_u^+$ state of Na_2 are now in progress, which would provide more information on the AI process.

Acknowledgement

This work was supported by the Swedish Natural Science Research Council and Latvian Science Council. Laser assistance by S. Kroll is gratefully acknowledged. One of us (JK) would like to thank the Swedish Institute for a stipend supporting his stay in Sweden.

[1] S is the so called saturation parameter, which could be found from $\Delta N=\Delta N_0(1+S)^{-1}$, where ΔN and ΔN_0 are the population difference between the lower and upper molecular levels in presence of, and without laser radiation, respectively.

References

[1] N.N. Bezuglov, A.N. Klyucharev and V.A. Sheverev, J. Phys. B 20 (1987) 2497, and references therein.
[2] M.E. Wagshul, K. Helmerson, P.D. Lett, S.L. Rolston, W.D. Phillips, R. Heather and P.S. Julienne, Phys. Rev. Letters 70 (1993) 2074, and references therein.
[3] C. Tapalian and W.W. Smith, Chem. Phys. Letters 211 (1993) 425.
[4] C.-C. Tsai, J.T. Bahns and W.C. Stwalley, Rev. Sci. Instrum. 63 (1992) 5576.
[5] A. Herman, S. Leutwyler, E. Schumacher and L. Wöste, Helv. Chimica Acta 61 (1978) 453.
[6] J.T. Bahns and W.C. Stwalley, Appl. Phys. Letters 44 (1984) 826.
[7] J.T. Bahns, M. Koch and W.C. Stwalley, Laser Part. Beams 7 (1989) 545.
[8] D. Xing, K.I. Udea and H. Takuma, Laser Part. Beams 11 (1993) 3.
[9] M. Jansons, J. Klavins and V. Grushevsky, in: Abstracts of the Fourth European Conference on Atomic and Molecular Physics, Part 2 (EPS, Riga, 1992) p. 359.
[10] M. Jansons, J. Klavins, V. Grushevsky, C. Luo and S. Svanberg, Z. Physik D in press.
[11] D. Zevgolis, Rev. Roum. Phys. 32 (1987) 205.

Chem. Phys. Lett. (1999) in press

Vibrational effects in $Na_2(A^1\Sigma_u^+, v') + Na(3p_{3/2})$ associative ionization.

A. Ekers[a,b], O. Kaufmann[a], K. Bergmann[a], J. Alnis[a,b], J. Klavins[b]

[a] University of Kaiserslautern, Department of Physics, D-67653 Kaiserslautern, Germany

[b] University of Latvia, Institute of Atomic Physics and Spectroscopy, LV-1586 Riga, Latvia

ABSTRACT.

Associative ionizing $Na_2(A^1\Sigma_u^+, v') + Na(3p_{3/2})$ collisions have been studied in a single supersonic beam with respect to the influence of the initial vibrational excitation of the molecules on the reaction efficiency. An enhancement of trimer ion yield of nearly one order of magnitude has been observed as the vibrational excitation increases from v'=0 to v'=14.

From the large variety of atom-atom associative ionization (AI) processes, the best studied is the reaction of Na(3p) atoms,

$$Na(3p) + Na(3p) \rightarrow Na_2^+ + e, \qquad (1)$$

the detailed studies of which have contributed significantly to the understanding of mechanisms of the AI processes (see for details [1] and references therein). Molecule-atom AI has been observed recently for three different situations: (*i*) in collisions of ground state atoms with highly excited molecules [2]; (*ii*) in collisions of highly excited atoms with ground state

molecules [3]; (*iii*) in collisions of excited atoms with the molecules excited in their first electronically excited state [4]. In the latter work, the process

$$Na_2(A^1\Sigma_u^+) + Na(3p_{3/2}) \rightarrow Na_3^+ + e, \qquad (2)$$

was studied in a vapour cell with excitation of only the lowest vibrational levels v'=0 and 1 in the $A^1\Sigma_u^+$ state. The cross section was found to be about one order of magnitude higher than that of the AI process (1). None of the studies [2-4] considered the influence of vibrational excitation of the molecules on the Na_3^+ yield.

It is well known, that initial vibrational excitation affects the reactivity in atom-molecule exchange reactions [5]. The cross section may increase [6] or decrease with increasing excitation. A dramatic increase with v" has been observed in the process of dissociative attachment of low energy electrons to the vibrationally excited molecules [7-9]. Recently vibrational effects have also been observed for the process of dissociative charge transfer in collisions between sodium dimers and atoms proceeding through highly excited Na_3 potential surfaces [9]. There was evidence [10] that vibrational effects do play a role also in the case of molecule-atom AI. The complexity of such processes is, however, increased because of the additional degrees of freedom of the triatomic molecule which is formed.

The present study is performed using a single supersonic Na/Na_2 beam arrangement with time-of-flight mass analysis (TOF) to distinguish the trimer ions from Na_2^+ ions produced in the atomic AI process (1). Low intra-beam collision energies and concentration of the molecules in their lowest vibrational level provide favourable experimental conditions. They help to establish a relatively high density of molecules in the excited states by optical excitation. The beam expands from an oven operated at T = 900 K, through a 0.4-mm-diam nozzle, the temperature of which is held 50 K higher than the oven temperature. The divergence of the beam is reduced to about 1° by two skimmers, which results in a residual transverse Doppler-width of 40 MHz. The density of the atoms and molecules in the reaction

region 20 cm downstream from the nozzle are correspondingly $n_{Na} \approx 2\times10^{11}\text{cm}^{-3}$ and $n_{Na_2} \approx 2\times10^{10}\text{cm}^{-3}$. Most of the Na_2 molecules in the beam (99%) are concentrated in the lowest vibrational level (v"=0) while about 1% are in v"=1. The population distribution over the rotational levels reaches its maximum for J"=7, as determined by laser induced fluorescence measurements. The flow velocity of the particles in the beam, and the velocity distribution of atoms and molecules are readily measured by means of the Doppler shift technique [11,12]. The beam velocity is 1340 m/s and the mean relative velocity of molecules and atoms is 112 m/s, which corresponds to a mean collision energy of $\overline{E} \approx 1.6$ meV.

Two linearly polarised laser beams L_1 and L_2 (diameter 3 mm), with the direction of their linear polarisation adjusted parallel to the particle beam axis, were overlapped in the collision region (Fig. 1). The frequency of the first laser L_1 (a CR-699 cw single mode ring dye laser operated with Rh6G dye) was tuned to the $3s_{1/2} \rightarrow 3p_{3/2}$ ($F"=2 \rightarrow F'=3$) transition. The laser L_1 beam was directed in the reaction region through a diaphragm to provide a homogeneous intensity profile. The loss of atoms to the $F"=1$ level of the ground state, which is not accessible for laser excitation, was small because the power of the laser L_1 was kept below the saturation limit, the typical intensity being 10 mW/cm^2. At higher laser intensities, power broadening leads to simultaneous excitation of the F'=2 hyperfine component, from which spontaneous decay to the $F"=1$ is possible.

The second laser L_2 (a CR-699 cw ring dye laser, DCM dye) was used to excite the molecules from the ground $X^1\Sigma_g^+$ state to individual vibrational levels ($0 \le v' \le 14$) of the $A^1\Sigma_u^+$ state, using the R transition J"=9→J'=10. A sharp edge cuts the upstream part of the L_1 and L_2 intensity profiles and prevents optical pumping of molecules upstream from the reaction region. A third laser L_3 (a CR-699 cw ring dye laser, DCM dye), which intersects the molecular beam 20 cm downstream from the reaction region, is used to verify the molecular

excitation. Its frequency is tuned to v"=0→v'=5 R transition with J"=9. When the molecules are excited in the reaction region, optical pumping leads to a reduction of the L_3 induced fluorescence signal. This provides, in combination with the wavemeter readings, an unambiguous verification that the desired molecular transition is excited.

The power of laser L_2 was chosen high enough to saturate the molecular transition in order to ensure an excitation efficiency of unity for molecules in the level v"=0, J"=9 during the passage through the laser beam. This allowed us to disregard the different Franck-Condon factors (FCF) of the various v"=0→v' transitions.

The production rate of trimer ions produced in the reaction volume V is given by

$$\frac{dN_{Na_3^+}}{dt} = K_{MA}^{Al} \int_V [\,Na^*\,][\,Na_2^*\,]dV\,, \qquad (3)$$

where K_{MA}^{Al} is the rate constant of the molecule-atom Al reaction (2), while $[\,Na^*\,]$ and $[\,Na_2^*\,]$ are the densities of excited atoms and molecules, respectively. Since there is only negligible optical pumping in the atomic excitation process, the density of excited atoms $[\,Na^*\,]$ follows the laser L_1 spatially filtered intensity profile (weak excitation limit), which is assumed to be constant over the reaction volume. Provided that the molecular transitions are saturated and all the molecules of the lower (v"J")-level are pumped, the integral $\int_V [\,Na_2^*\,]dV$ is independent on the FCF for the respective transition and does not depend on the laser power. Therefore, any variation of the Na_3^+ ion signal on v' measured at constant power of laser L_1 ($3s$-$3p$ excitation) reflects the v' dependence of the rate constant K_{MA}^{Al}.

The experimentally observed dependence of the Na_3^+ ion yield on the vibrational quantum number v' is given in Fig. 2. All the data points are normalised to the same density of $Na(3p_{3/2})$, which is proportional to the square root of the simultaneously observed Na_2^+ signals resulting from process (1). This accounts for the slight variations in the flux of excited

atoms due to frequency jitter of laser L_1. The rate constant of trimer ion formation is nearly independent of the vibrational excitation in the range $0 \le v' \le 10$. For $v' \ge 11$ it increases significantly with v'. For v'=14 the ion yield is about 7 times larger than for $v' \le 10$. Several pairs of $v''=0 \rightarrow v'$ transitions possess very similar FCF. For instance, for excitation of v'=3 and v'=14, or v'=5 and v'=11, the FCF are nearly the same. In that case, conclusions about the relative Na_3^+ yields do not rely on assumptions about the vibrational dependence of the integral in eq. (3).

Even for v'=0 the reaction (2) is exoenergetic (Fig. 3). Reliable information on the potential surfaces for the $Na_2(A^1\Sigma_u^+) + Na(3p_{3/2})$ collision complex is not available at present. A quantitative interpretation of the results is therefore not possible. However, we mention two possible reasons for the observed vibrational dependence of the reaction rate constant. On one hand, the increase of the rate constant with v' could be related to a potential barrier in the entrance channel which is overcome by vibrational energy of the molecules. This would lead to a vibrational dependence of the formation of Na_3^+ ions in their ground $^1A_1'$ state of triangular configuration of the nuclei with a distinct onset at a specific vibrational energy. On the other hand, the vibrational dependence could result from the opening of a new exit channel which is energetically not accessible for molecules in their low vibrational levels. In particular, formation of a linear Na_3^+ molecule in $^3\Sigma_u^+$ (first excited) state is energetically possible at enhanced vibrational excitation of the Na_2 molecule. In fact, we find from the Na_3 ionisation potential according to [13] and relative positioning of the Na_3^+ states given in [14] that vibrational excitation to levels $v' \ge 14$ provides enough energy to open the channel leading to the formation of the Na_3^+ in the $^3\Sigma_u^+$ state. However, more precise computational results are needed to verify the latter statement.

We have observed vibrational effects also in AI of the ground state $Na_2(v'')$ molecules with Na($3d$) atoms. It is interesting to note that a distinct increase of the rate of Na_3^+ formation is observed for those levels v"=26-29, which coincide energetically with the distinct change of the slope of the rate constant with increasing v' for the reaction (2) at v'=11–14. This seems to support the hypothesis about the formation of Na_3^+ in its $^3\Sigma_u^+$ state. Studies of the AI with Na($3d$) atoms are in progress and will be reported elsewhere.

ACKNOWLEDGEMENTS.

We are grateful to Prof. W. Meyer for helpful discussions. Partial support by the Deutsche Forschungsgemeinschaft, Latvian Science Council, and the EU-HCM network (ERB-CHR-XCT-94-0603) is acknowledged. One of us (A.E.) thanks the Deutscher Akademischer Austauschdienst (DAAD) for support.

REFERENCES.

1. B. Huynh, O. Dulieu, and F. Masnou-Seeuws, Phys. Rev. A 57 (1998) 958.
2. C.-C. Tsai, J. T. Bahns, and W. C. Stwalley, Rev. Sci. Instrum. 63 (1992) 5576.
3. C. Tapalian and W. W. Smith, Chem. Phys. Lett. 211 (1993) 425.
4. J. Klavins, M. Jansons, A. Ekers, Luo Caiyan, and S. Svanberg, Chem. Phys. Lett. 228 (1994) 346.
5. H.-G. Rubahn and K. Bergmann, Ann. Rev. Phys. Chem. 41 (1990) 735.
6. P. Dittmann, F. P. Pesl, J. Martin, G. W. Coulston, G. Z. He, and K. Bergmann, J. Chem. Phys. 97 (1992) 9472.

7. M. Külz, M. Keil, A. Kortyna, B. Schellhaaß, J. Hauck, K. Bergmann, W. Meyer, and D. Weyh, Phys. Rev. A 53 (1996) 3324.

8. M. Allan and S. F. Wong, Phys. Rev. Lett. 41 (1978) 1791.

9. M. Keil, Dissoziative Elektronenanlagerung an schwingungsangeregte Moleküle, Dissertation (Universität Kaiserslautern, 1998).

10. A. Ekers, O. Kaufmann, M. Keil, K. Bergmann, and J. Klavins, Europhysics Conference Abstracts 22D (1998) 4-48.

11. K. Bergmann, W. Demtröder, and P. Hering, Appl. Phys. 8 (1975) 65.

12. U. Hefter and K. Bergmann, in *Atomic and Molecular Beam Techniques*, edited by G. Scoles (Oxford University Press, New York-Oxford, 1988), p. 193.

13. W. Meyer, personal communication.

14. G.-H. Jeung, M. Broyer, and P. Labastie, Chem. Phys. Lett. 165 (1990) 494

Figure captions.

Fig. 1. Schematic arrangement of the experiment with the lasers for excitation of atoms (L_1) and molecules (L_2) as well as for monitoring (L_3).

Fig. 2. Experimental dependence of the Na_3^+ ion yield on the vibrational quantum number v' of the $A^1\Sigma_u^+$ state.

Fig. 3. Energy diagram for the $Na_2(A^1\Sigma_u^+) + Na(3p_{3/2})$ colliding system. Na_3^+ ground $^1A_1'$ state energy is given according to [13]. ν_1 and $\nu_{2,3}$ correspond to different Na_3^+ vibrational modes (anharmonicity is not accounted for).

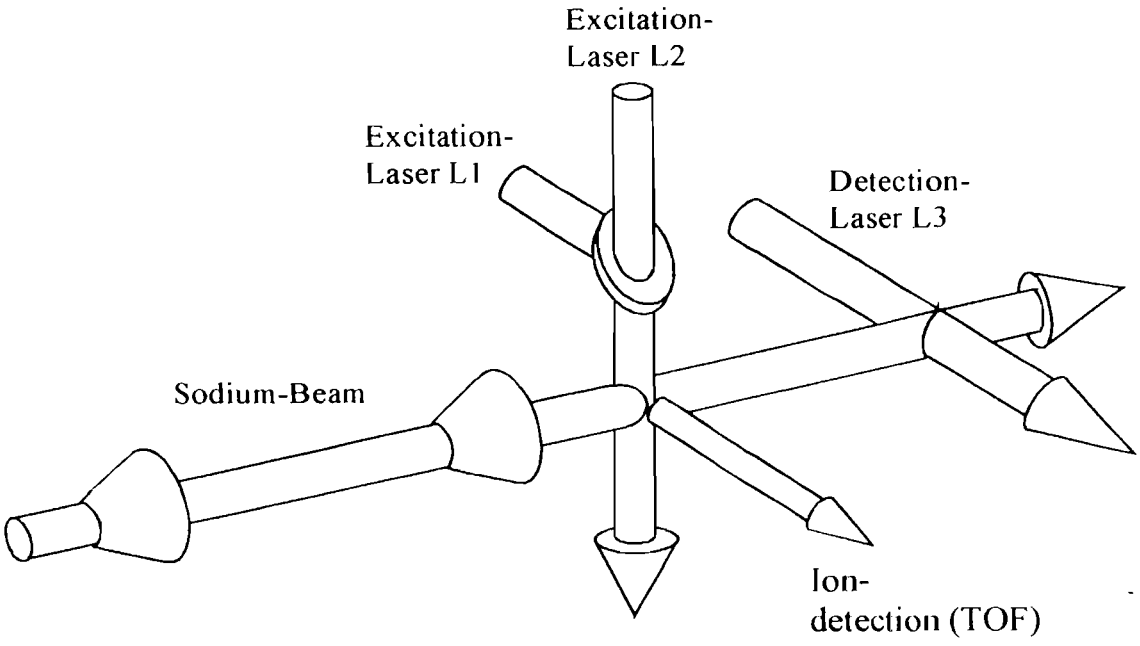
Excitation-
Laser L2
Excitation-
Laser L1
Detection-
Laser L3
Sodium-Beam
Ion-
detection (TOF)

Fig. 1

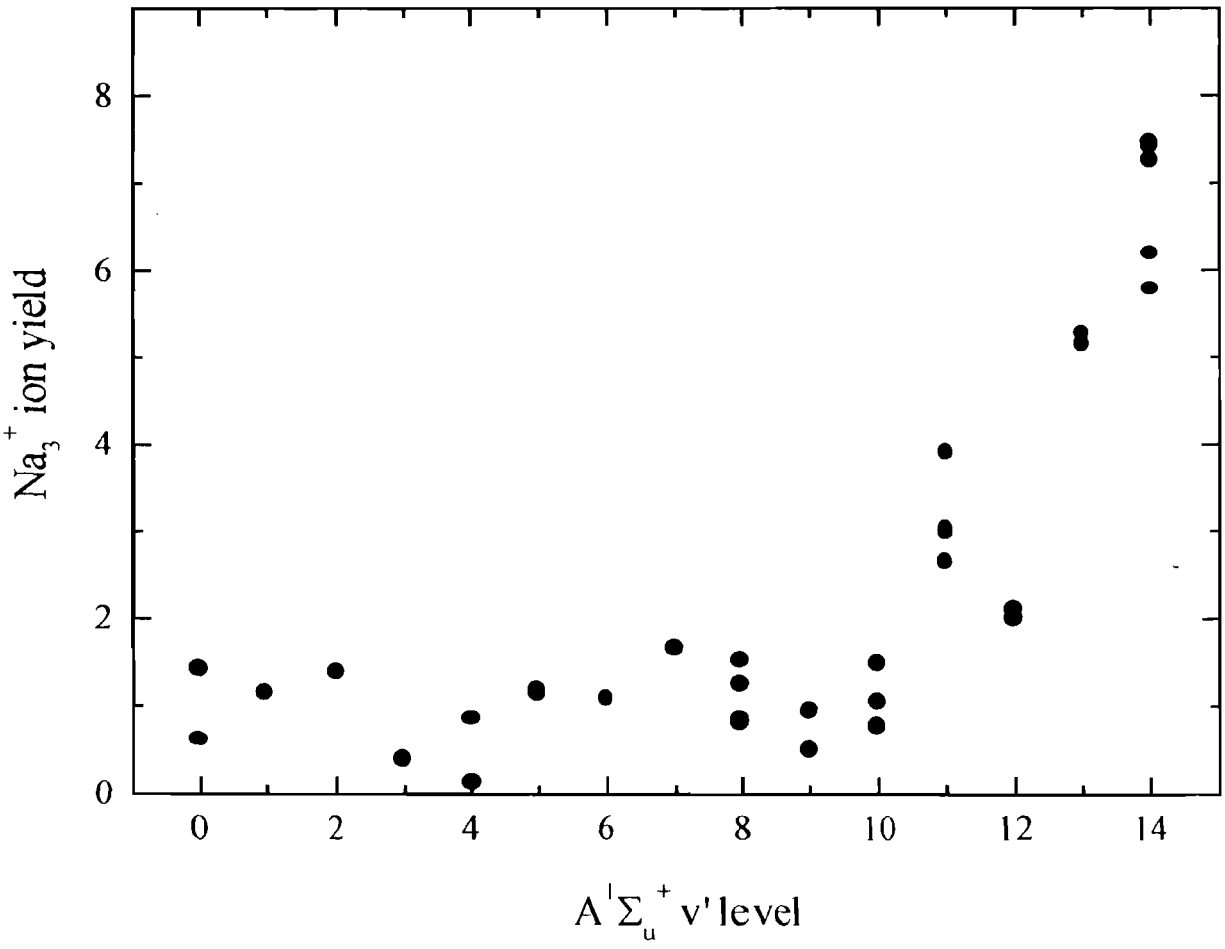

Fig. 2

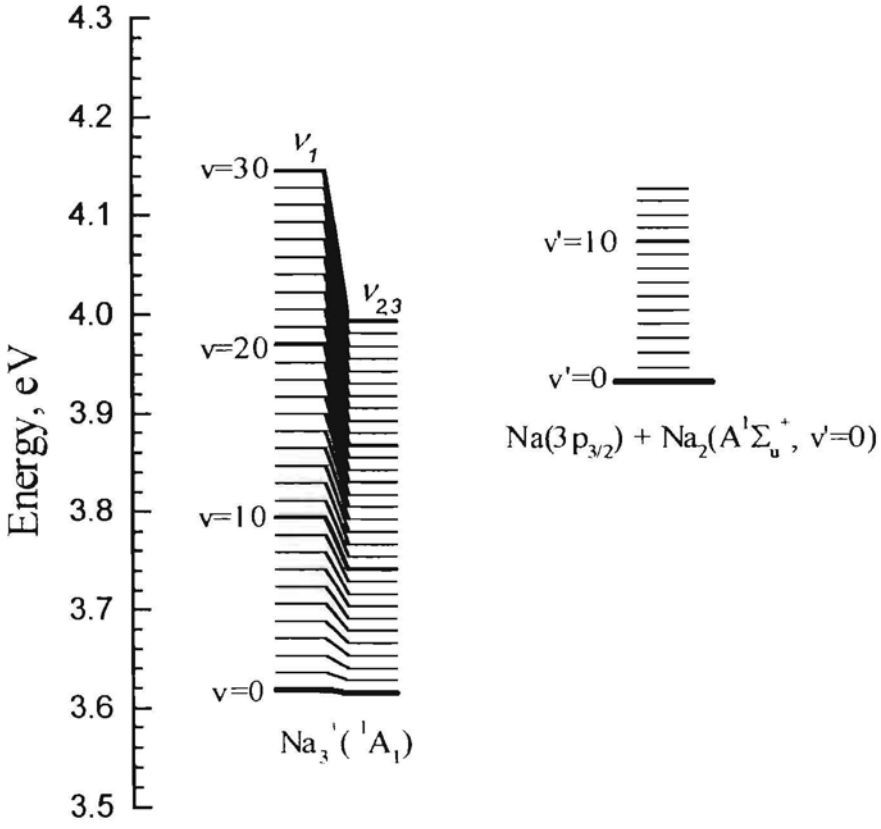
4.3
4.2
4.1
4.0
3.9
3.8
3.7
3.6
3.5
Energy, eV
v=30
v=20
v=10
v=0
ν_1
ν_{23}
Na_3 ($^1A_1$)
v'=10
v'=0
$Na(3p_{3/2}) + Na_2(A^1\Sigma_u^+, v'=0)$

Associative ionization in collisions of electronically excited Na atoms with vibrationally excited $Na_2(v'')$ molecules.

A. Ekers[a,b], O. Kaufmann[a], M. Keil[a], and K. Bergmann[a]

[a] Universität Kaiserslautern, Fachbereich Physik, Postfach 3049, D-67653 Kaiserslautern, Germany

[b] University of Latvia, Institute of Atomic Physics and Spectroscopy, Raina bulv. 19, LV-1586 Riga, Latvia

Abstract

We have studied the formation of Na_3^+ ions in collisions of Na($3d$,$5s$,$4d$) atoms with vibrationally excited $Na_2(v'')$ molecules in their electronic ground state in a supersonic beam. The cross section of the Na($4d_{5/2}$) + Na_2 associative ionization is found to be about six times larger than that of the corresponding atomic reaction Na($4d_{5/2}$) + Na($3s$) $\rightarrow$ Na_2^+. Associative ionization in collisions of Na($3d$) with $Na_2(v'')$ is observed only with vibrationally excited Na_2 molecules. The cross section $\sigma(v'')$ of this reaction increases only slightly with v'' for low vibrational excitation, while a strong increase with v'' is observed for $v'' \geq 26$. The latter observation suggests the opening of the channel leading to the formation of Na_3^+ ions in the first electronically excited state for $v'' \geq 26$.

PACS: 34.50

1 Introduction

Contrary to the well known associative ionization (AI) in collisions of sodium atoms, (see [1] for details and references therein), atom-molecule AI has not been studied until

recently. The formation of Na_3^+ ions in Al has been observed for the first time in collisions of electronically excited molecules with ground state atoms [2]:

$$Na_2(2^1\Pi_g) + Na(3s) \rightarrow Na_3^+ + e. \quad (1)$$

Two other studies consider Al in collisions of ground state molecules with electronically excited atoms [3],

$$Na_2(X^1\Sigma_g^+) + Na(4d) \rightarrow Na_3^+ + e; \quad (2)$$

$$Na_2(X^1\Sigma_g^+) + Na(5s) \rightarrow Na_3^+ + e, \quad (3)$$

and in collisions of molecules and atoms excited in their first excited states [4,5]

$$Na_2(A^1\Sigma_u^+) + Na(3p) \rightarrow Na_3^+ + e. \quad (4)$$

The authors of [2] used process (1) as an ion source for a space-charge limited diode ionisation detector. They made no attempt to further study the formation of trimer ions. Processes (2), (3) and (4) were considered in more detail. The processes (2) and (3) were studied in an effusive beam, using time-of-flight (TOF) mass spectrometry to distinguish different ionic products. The cross sections were determined relative to the corresponding atom-atom Al reactions

$$Na(3s) + Na(4d) \rightarrow Na_2^+ + e, \quad (5)$$

$$Na(3s) + Na(5s) \rightarrow Na_2^+ + e. \quad (6)$$

It was found that the atom-molecule Al cross section is two times larger than the cross section of the respective atomic reaction in case of the $4d_{5/2}$ state, and 10 times larger in case of the $5s_{1/2}$. The cross sections for the reactions (5) and (6) have been measured in sodium vapour in an earlier study [6]. An estimate of the cross section for the process (5) is also available, based on electron spectrometric studies in an effusive beam [7].

Process (4) was studied in a vapour cell, with excitation of the molecules to the lowest vibrational levels, $v' = 0$ and 1, in the $A^1\Sigma_u^+$ state [4]. The cross section was estimated to be $\sigma \approx 10^{-15}\,cm^2$, which is an order of magnitude larger than that of the process [1]:

$$Na(3p) + Na(3p) \rightarrow Na_2^+ + e. \quad (7)$$

A more detailed study [5] in a supersonic beam revealed that the rate constant for the reaction (4) is essentially independent of v' at small vibrational excitation ($v' = 0 \ldots 10$), but increases significantly with v' for $v' \geq 11$. For $v' = 14$ the reaction is nearly one order of magnitude more efficient than for low v'.

It is well known that vibrational excitation affects the cross section for inelastic collisions [8], for atom-molecule exchange reactions [9], or for dissociative attachment of low energy electrons to molecules [10-12]. The sensitivity of the process of charge transfer from Rydberg states to the vibrational level of the molecule has also been confirmed recently [12]. Observations of AI of ground state Na_2 molecules with Na($3d$) atoms in a supersonic beam suggested that vibrational excitation of molecules may significantly enhance the trimer ion production rate [13]. In particular, Na_3^+ ions were observed from the process Na($3d$) + $Na_2(X^1\Sigma_g^+, v'')$ only for $v'' > 0$, although the energy of the $3d$ state lies 13 meV above the Na_3 ionisation threshold.

Our present study is concerned with the consequences of the initial molecular vibrational excitation for the process of AI in collisions of Na atoms excited to their $3d$, $5s$ or $4d$ states with $Na_2(X^1\Sigma_g^+, v'')$.

2 Experiment

2.1 Supersonic beam setup

The experiment is done in a single supersonic Na/Na_2 beam with TOF mass analysis to distinguish the trimer ions from Na_2^+ and Na^+ ions. The latter ions are produced in atomic associative ionization or by the process of Penning ionization. The experimental setup is described in detail in Ref. [11]. Briefly, the beam expands from an oven operated at 900K temperature through a 0.4-mm-diam nozzle, the temperature of which is held 50K higher than that of the oven. The beam is collimated by two skimmers to a divergence of about 1°, which limits the residual transverse Doppler broadening to 40MHz. The concentrations of atoms and molecules in the reaction region 20cm downstream from the nozzle are $n_{Na} \approx 2.3\times10^{11}\text{cm}^{-3}$ and $n_{Na_2} \approx 2\times10^{10}\text{cm}^{-3}$, respectively.

In our supersonic beam, 99% of the dimers are concentrated in their lowest vibrational level, $v'' = 0$, and about 1% are found in $v'' = 1$. The maximum of the population distribution over the rotational levels is found at $J'' = 7$. This level contains about 9% of the total population. The velocity and the velocity distribution of atoms or molecules in the beam are readily measured by the Doppler shift technique [14,15]. The beam velocity is 1340 m/s, and the width of the distribution function is 300 m/s for atoms or 260 m/s for molecules (full width at 1/e). The mean relative velocity of atom-atom or atom-molecule collisions is v_{AA} =

120 m/s or v_{MA} = 112 m/s, which corresponds to a mean collision energy $\overline{E}_{AA}$ = 1.4 meV or $\overline{E}_{MA}$ = 1.6 meV.

2.2 Optical preparation of atoms and molecules.

The experimental arrangement of particle and laser beams is shown in Fig. 1. All the lasers used in the experiment are cw single mode ring lasers (CR-699 or CR-899) with a line width of about 1MHz. Atoms are optically excited in the reaction region in $3d$, $5s$ or $4d$ states by a two step excitation scheme. One laser drives the $3s_{1/2} \rightarrow 3p_{3/2}$ ($F'' = 2 \rightarrow F' = 3$) transition, while the other laser excites atoms from $3p_{3/2}$ to the desired higher lying states. Radiative cascading from these states leads to the population of all hyperfine sublevels, and a loss of atoms to the $F'' = 1$ sublevel of the $3s_{1/2}$ state by optical pumping is inevitable.

One consequence of optical pumping is a variation of the location of highest density of atoms in the excited state with laser power. When the excitation probability is small compared to unity, the density of Na^* is highest near the axis of the laser beam. However, with increasing excitation probability because of increasing laser power, the region of highest Na^* density moves upstream with respect to the propagation of the particles in the beam and is found in the wings of the laser beam profile [16] and thus away from the region of highest detection efficiency for the time-of-flight analysis. In order to assure the independence of the detection efficiency with regard to a variation of the laser intensity, the latter was kept sufficiently low to prevent saturation. As a test, the Na_2^+ ions from process (5) or from

$$Na(3p) + Na(5s) \rightarrow Na_2^+ + e, \qquad (8)$$

$$Na(3p) + Na(3d) \rightarrow Na_2^+ + e, \qquad (9)$$

were observed to determine the saturation limits (see Fig. 2a). At the given low collision energy in our experiment, the contribution of process (7) to the ion signal is negligibly small compared to the processes (5), (8) and (9).

To prepare vibrationally excited Na_2 molecules in their electronic ground state, either Franck-Condon pumping (FCP) [15] or stimulated Raman adiabatic passage (STIRAP) [17] is used. In the case of FCP, molecules are excited to different v′ levels of the $A^1\Sigma_u^+$ state on $A^1\Sigma_u^+(v',10) \leftarrow X^1\Sigma_g^+(0,9)$ transitions. Depending on v′ in the electronically excited state, spontaneous decay of the molecules creates different population distributions $f_{v'}(v'')$ over vibrational levels (v″) of the $X^1\Sigma_g^+$ state (Fig. 3), which are unambiguously determined by

the corresponding transition rates (which include the variation of the transition dipole moment with internuclear distance). To avoid collisions of electronically excited molecules with the excited atoms, the pump laser beam intersects the particle beam 15 cm upstream of the reaction region (see Fig. (1)). With the molecular transition being saturated, FCP leads to efficient (≈100%) optical pumping of the molecules to the vibrationally excited levels of the molecular ground state. To verify the molecular excitation, a probe laser resonant with the $A^1\Sigma_u^+(5,10) \leftarrow X^1\Sigma_g^+(0,9)$ transition intersects the particle beam downstream from the reaction region. The lower (v",J")-level is the same for pump and probe lasers. Therefore the probe laser induced fluorescence signal decreases whenever the pump laser is resonant with the chosen transition. This together with the wavemeter readings provides an unambiguous verification that the desired molecular transition is excited.

Contrary to the FCP, STIRAP allows one to selectively transfer the population from v"=0 to excited vibrational levels in the electronic ground state. In STIRAP, a Stokes laser field couples the intermediate (v',10)-level in the $A^1\Sigma_u^+$ state with the final (v''_f,9)-level in the $X^1\Sigma_g^+$ state prior to the interaction of molecules with the pump laser field, which couples the initial (0,9) and intermediate levels. The sequence of interactions is controlled by the spatial displacement of the axes of the pump and Stokes lasers [17]. With properly adjusted displacement all the population of the initial level is transferred to the chosen final level. The lasers are detuned from the resonance with the respective molecular transitions by an equal amount of 200 MHz, maintaining the two photon resonance for the $(v''=0,J''=9) \rightarrow (v',J'=10) \rightarrow (v''_f, J''_f=9)$ transitions. The population transfer efficiency by STIRAP, which in the present experiment was reaching up to 99%, is monitored with the probe laser on $A^1\Sigma_u^+(v'_{pr},10) \leftarrow X^1\Sigma_g^+(v''_f,9)$ transitions.

3 Results and analysis

3.1 $Na_2(v'')$ + Na(4*d*) collisions

Upon excitation of the Na $4d_{3/2}$ and $4d_{5/2}$ states, Na^+, Na_2^+, and Na_3^+ ions are observed in the mass spectrum (see Fig. 4). The Na^+ ions are formed in atomic Penning and photoionization processes [7,18]:

$$Na(3p,4d) + Na(4d) \rightarrow Na^+ + Na + e, \qquad (10)$$

$$Na(4d) + h\nu \rightarrow Na^+ + e. \qquad (11)$$

The Na_2^+ ions are formed in atomic AI processes (5) and (7). At the low collision energies of our experiment, the process (7) is relatively inefficient, and gives about two orders of magnitude smaller contribution to the observed Na_2^+ signal than the process (5). This was verified by measuring the Na_2^+ signal with the laser beam for the $3p \rightarrow 4d$ excitation blocked, in agreement with observations by the authors of [7].

The formation of Na_3^+ ions is due to AI of $Na_2(X^1\Sigma_g^+, v'')$ molecules and Na($4d$) atoms according to process (2). The Na_3^+ signal varies linearly with the power of the laser for the 3s→3p excitation (see Fig. 2b). This confirms that one Na($4d$) atom is needed to form Na_3^+. Since the densities of ground state atoms and molecules are known, and Na($4d$) atoms participate also in the formation of Na_2^+, the atom-molecule AI cross section can be determined relative to the cross section for the atom-atom AI process (5) [3]. The rates of production of Na_2^+ and Na_3^+ ions in the processes (5) and (2) are correspondingly

$$\dot{N}_{Na_2^+} = \sigma_{AA} v_{AA} \int n_{Na} n_{Na(4d)} dV_{AA} ;$$

$$\dot{N}_{Na_3^+} = \sigma_{MA} v_{MA} \int n_{Na_2} n_{Na(4d)} dV_{MA} ,$$

where σ_{AA} and σ_{MA} are the velocity averaged cross sections for the reactions (5) and (2), while the densities of the ground state atoms, ground state molecules and excited Na($4d$) atoms are n_{Na}, n_{Na_2}, and $n_{Na(4d)}$, respectively. The reaction volumes V_{AA} and V_{MA} are identical since they are both determined by the distribution of excited Na($4d$) atoms. Therefore the ratio of the rates of formation of Na_3^+ and Na_2^+ ions is

$$\frac{\dot{N}_{Na_3^+}}{\dot{N}_{Na_2^+}} = \frac{\sigma_{MA}}{\sigma_{AA}} \frac{v_{MA} n_{Na_2}}{v_{AA} n_{Na}} .$$

The latter equation connects the atom-molecule AI cross section and the corresponding atom-atom AI cross section,

$$\sigma_{MA} = \sigma_{AA} \frac{\dot{N}_{Na_3^+}}{\dot{N}_{Na_2^+}} \frac{v_{AA} n_{Na}}{v_{MA} n_{Na_2}} ,$$

since the ratio of the ion signals is measured, and the other parameters (particle densities and relative velocities) are known. Furthermore, we have assumed that the detection efficiency is the same for both the dimer and the trimer ions. We find for the cross sections for AI in collisions of $Na_2(X^1\Sigma_g^+, v''=0)$ molecules with Na($4d_{3/2}$) and Na($4d_{5/2}$) states

$\sigma_{MA}(4d_{3/2}) = 7.2\sigma_{AA}(4d_{3/2})$ and $\sigma_{MA}(4d_{5/2}) = 5.9\sigma_{AA}(4d_{5/2})$.

We have also applied vibrational excitation to the Na_2 molecules. No noticeable change in the efficiency of trimer ion formation was observed when the molecules were vibrationally excited.

3.2 $Na_2(v'')$ + Na(5*s*) collisions

Formation of Na^+, Na_2^+, and Na_3^+ ions was also observed in collisions of Na_2 with $Na(5s_{1/2})$. The Na^+ ions are formed in a Penning process or by a photoionization, in analogy to the processes (10) and (11) [7,18]. The atom-atom AI process (6), involving atoms in their 5*s* and 3*s* states, is endothermic by 42 meV, which exceeds the mean atom-atom collision energy in our experiment (1.4 meV) by a factor of 30 and thus does not contribute to the formation of Na_2^+ ions.

The dependence of the Na_2^+ signal was nearly quadratic with respect to the power of laser 1 ($3s \rightarrow 3p$ excitation, see Fig. 2c), but linear with respect to the power of laser 2 ($3p \rightarrow 5s$ excitation, see Fig. 2d). This suggests that the Na_2^+ ions are formed in the AI process (8). Quadratic dependence on the power of laser 1 is expected for process (8) since laser 1 is not only involved in the population of the 3*p* level, but also in the population of the 5*s* level. The determination of the cross section of the atom-molecule AI process (3) yielding Na_3^+ ions in collisions of $Na_2(X^1\Sigma_g^+, v'')$ and Na(5*s*), following the procedure discussed in Section 3.1, is not possible since the absolute concentration of atoms in the 3*p* state is not known. Within the given signal-to-noise ratio no variation of the Na_3^+ signal was observed when the Na_2 molecules where excited to vibrational levels $v'' > 0$ using the FCP method.

3.3 $Na_2(v'')$ + Na(3*d*) collisions

Only Na^+ and Na_2^+ ions were observed when the atoms were excited to the $3d_{5/2}$ level but the Na_2 molecules remained in their vibrational ground state. The formation of atomic ions are due to Penning and photoionization processes [18,19]:

$$Na(3p,3d) + Na(3d) \rightarrow Na^+ + Na + e, \qquad (12)$$

$$Na(3d) + h\nu \rightarrow Na^+ + e. \qquad (13)$$

The Na_2^+ ions are formed in the AI process (9).

Ions from the atom-molecule AI reaction,

$$Na_2(X^1\Sigma_g^+, v'') + Na(3d_{5/2}) \rightarrow Na_3^+ + e, \qquad (14)$$

were observed only with vibrationally excited Na_2 molecules. The variation of the Na_3^+ signal with vibrational excitation, while the density of $Na(3d_{5/2})$ atoms was kept constant, is given in Fig. 5. Franck-Condon pumping establishes a vibrational distribution $f_{v'}(v'')$, which depends on the level v' excited in the $A^1\Sigma_u^+$ electronic state (see also Fig. 3). From $f_{v'}(v'')$ a mean value $\langle v'' \rangle_{v'}$ of vibrational excitation can be determined. The ion yield increases smoothly with $\langle v'' \rangle_{v'}$, with a marked increase of the slope found for $\langle v'' \rangle_{v'} > 15$.

The rate of trimer ion formation is determined by a convolution of the v'' dependent cross section $\sigma(v'')$ for the process (14) with the population distribution $f_{v'}(v'')$ of the Na_2 molecules:

$$\dot{N}_{Na_3^+}^{FCP}(v') = \kappa \sum_{v''} \sigma(v'') f_{v'}(v''), \qquad (15)$$

where κ is a constant factor relating the cross section to the signal. The distribution function $f_{v'}(v'')$ is normalised such that $\sum_{v''} f_{v'}(v'') = 1$. The population of the optically pumped level of the molecules was always fully depleted during their interaction time with the pump laser, therefore the factor κ does not depend on v' or v''.

The attempts to model the vibrational dependence of the atom-molecule AI cross section in (15) using a step function

$$\sigma(v'') = \begin{cases} 0, & v'' < v_{th} \\ \sigma_{max}, & v'' \geq v_{th} \end{cases}$$

fail to reproduce the observed trimer ion signal v'-dependence. The experimental v'-dependence suggests a smooth increase of the cross section with v'', the slope of which increases for high v''. The v''-dependence of the trimer ion signals, $\dot{N}_{Na_3^+}^{STIRAP}$, was also measured using the STIRAP technique for selective excitation of the levels $v'' = 7$, 10 and 11 (see Fig. 6). From the data of Fig. 4 we find

$$\dot{N}_{Na_3^+}^{STIRAP}(v'') = \kappa\sigma(v''),$$

with

$$\kappa\sigma(v'') = \begin{cases} 0, & v'' < 5; \\ -160 + 34.5v'', & v'' \geq 5. \end{cases} \qquad (16)$$

The use of eq. (16), with the parameters determined from the STIRAP data, in eq. (15) nicely reproduces the results obtained by the FCP method up to v′ = 11 or $\langle v'' \rangle_{v'} = 15$ (see the solid line of Fig.5). The distribution function $f_{v'}(v'')$ is negligibly small for v″ > 25 and v′ ≤ 11. Therefore we assume eq. (16) to be valid for v″ ≤ 25. For levels 12 ≤ v′ ≤ 14 significant population is established in vibrational levels in the range 26 ≤ v″ ≤ 29. Judging from the deviation of the observed ion signal from the solid line [which is based on eqs (15) and (16)] for v′ > 11, we conclude that the cross sections for trimer ion formation increases strongly for v″ ≥ 26.

4 Discussion

This work deals with the dependence of the atom-molecule associative ionisation process yielding Na_3^+ ions in $Na^* + Na_2(X^1\Sigma_g^+, v'')$ collisions on the initial vibrational excitation of the molecules while the atoms are excited to the 3*d*, 5*s* or 4*d* levels. The cross sections for the AI process involving Na(4*d*) atoms could also be determined by comparison with previously measured cross sections for atom-atom associative ionisation [6] in collisions of Na (4*d*) and Na (3*s*) atoms, yielding Na_2^+ ions. The cross sections for atom-molecule AI was found to be 7.2 and 5.9 times larger, for atoms in the $4d_{3/2}$ and $4d_{5/2}$ level, respectively, as compared to the atom-atom AI process. The cross section for the $Na(4d_{5/2}) + Na_2(X^1\Sigma_g^+, v'')$ is by about a factor of three larger than the one reported in [3]. In the case of the 5*s* state determination of the atom-molecule AI cross section was not possible because the main contribution to the Na_2^+ signal is due to the Na(3*p*) + Na(5*s*) collisions, and not due to the Na(3*s*) + Na(5*s*), as it was supposed in [3].

The atom-molecule AI process with the atoms excited to the 5*s* or 4*d* level proceeds efficiently with molecules in their vibrational ground states, v″ = 0. Considering the fact that only 9 % of the molecules are excited to higher lying vibrational levels when either the Franck-Condon-pumping technique or the STIRAP method is used, and for the given signal-to-noise ratio, we conclude that the cross section for the atom-molecule AI process varies by less than a factor of two in the range 0 ≤ v″ ≤ 29.

The formation of Na_3^+ ions in the atom-molecule AI process with atoms in the $3d_{5/2}$ level, process (14), was not observed for molecules in their vibrational ground state. In fact, the process is exothermic by only 13 meV (see Fig. 7) [20]. Additional energy seems to be

needed to form Na_3^+ ions. Based on the vibrationally selective data, obtained by the STIRAP technique, the data obtained by the FCP method were nicely reproduced (see Fig. 5). From that result we conclude that trimer ion formation requires vibrational excitation to levels $v'' \geq 5$. The cross section varies approximately linearly with v'' in the range $5 \leq v'' \leq 25$. The increasing density of states of the Na_3^+ ion with increasing energy may cause this vibrational level dependence. For $v'' \geq 26$ the cross section rises much faster with v'' than for $v'' \leq 25$. Thus, the character of the vibrational level dependence changes at a total (electronic and vibrational) energy of $4.078 \leq E_{tot} \leq 4.122$ eV. It is interesting to note that a similar vibrational level dependence of the atom-molecule AI was observed in the process $Na(3p_{3/2}) + Na_2(A^1\Sigma_u^+, v') \rightarrow Na_3^+ + e$, the character of which changed also at a total energy (electronic and vibrational) of $4.087 \leq E_{tot} \leq 4.127$ eV [5]. We tentatively attribute these observations to the opening of a new electronic channel at the product side. In fact, a theoretical study [21] suggests that the excited $^3\Sigma_u^+$ state of Na_3^+, with the nuclei in linear configuration, lies approximately 0.66 eV above the bend electronic ground state at total energies of 4.28 eV. More detailed information about the potential energy surfaces, and possibly new experiments which also determine the energy of the free electron after the AI process, are needed before final conclusions can be drawn.

Acknowledgements

We are grateful to Prof. W. Meyer and Prof. H. Hotop for helpful discussions, and Dr. C. Gebauer-Rochholz, L. Meyer and J. Alnis for assistance with the experiment. Partial support by the Deutsche Forschungsgemeinschaft, the Latvian Science Council, and the EU-HCM network (ERB-CHR-XCT-94-0603) is acknowledged. One of us (A. E.) thanks the Deutscher Akademischer Austauschdienst (DAAD) for support.

References

1. B. Huynh, O. Dulieu, and F. Masnou-Seeuws, Phys. Rev. A **57**, 958 (1998).
2. C.-C. Tsai, J. T. Bahns, and W. C. Stwalley, Rev. Sci. Instrum. **63**, 5576 (1992).
3. C. Tapalian and W. W. Smith, Rev. Chem. Phys. Lett. **211**, 425 (1993).

4. J. Klavins, M. Jansons, A. Ekers, Luo Caiyan, and S. Svanberg, Chem. Phys. Lett. **228**, 346 (1994).
5. A. Ekers, O. Kaufmann, K. Bergmann, J. Alnis, and J. Klavins, Chem. Phys. Lett. (to be published).
6. V. S. Kushawaha and J. J. Leventhal, Phys. Rev. A **25**, 346 (1982).
7. H. A. Meijer, S. Schohl, M. W. Müller, H. Dengel, M.-W. Ruf, and H. Hotop, J. Phys. B: At. Mol. Opt. Phys. **24**, 3621 (1991).
8. H.-G. Rubahn and K. Bergmann, Ann. Rev. Phys. Chem. **41**, 735 (1990).
9. P. Dittmann, F. P. Pesl, G. W. Coulston, G. Z. He, and K. Bergmann, J. Chem Phys. **97**, 9472 (1992).
10. M. Allan and S. F. Wong, Phys. Rev. Lett. **41**, 1791 (1078).
11. M. Külz, M. Keil, A. Kortyna, B. Schellhaaß, J. Hauck, K. Bergmann, W. Meyer, and D. Weyh, Phys. Rev. A **53**, 3324 (1996).
12. M. Keil, Dissertation, Universität Kaiserslautern, 1998.
13. A. Ekers, O. Kaufmann, M. Keil, K. Bergmann, and J. Klavins, in *Abstracts of the sixth European Conference on Atomic and Molecular Physics*, Siena, Italy, edited by V. Biancalana, P. Bicchi, and E. Mariotti (European Physical Society, Siena, 1998), p. 4-48.
14. K. Bergmann, W. Demtröder, and P. Hering, Appl. Phys. **8**, 65 (1975).
15. U. Hefter and K. Bergmann, in *Atomic and Molecular Beam Techniques*, edited by G. Scoles (Oxford University press, New York-Oxford, 1988).
16. K. Bergmann and E. Gottwald, Chem. Phys. Lett. **78**, 515(1981).
17. U. Gaubatz, P. Rudecki, S. Schiemann, and K. Bergmann, J. Chem. Phys. **92**, 5363 (1990); K. Bergmann, H. Theuer, and B. W. Shore, Rev. Mod. Phys. **70**, 1003 (1998).
18. B. Carré, F. Roussel, G. Spiess, J. M. Bizau, P. Gérard, and F. Wuilleumier, Z. Phys. D **1**, 79 (1986); B. Carré, G. Spiess, J. M. Bizau, P. Dhez, P. Gérard, F. Wuilleumier, J. C. Keller, J. L. Le Gouët, J. L. Picqué, D. L. Ederer, and P. M. Koch, Opt. Commun. **52**, 29 (1984).
19. H. Dengel, M.-W. Ruf, and H. Hotop, Europhys. Lett. **23**, 567 (1993).
20. W. Meyer (personal communication).
21. G.-H. Jeung, M. Broyer, and P. Labastie, Chem. Phys. Lett. **165**, 494 (1990).

Figure captions

Fig. 1. Schematic arrangement of particle and laser beams. Excitation lasers 1 and 2 excite atoms in the reaction region. Only the pump laser is used for vibrational excitation via Franck-Condon pumping (FCP). Both, the pump and the Stokes lasers are needed when the STIRAP method is implemented. The probe laser detects vibrational excitation of Na_2 molecules.

Fig. 2. Power dependence of the ion formation. Laser beams are focused to $\varnothing \sim 2$mm. Saturation is indicated in (a) and (b) for the ion signals due to processes Na($3s$) + Na($4d$) $\rightarrow$ Na_2^+ + e and $Na_2(X^1\Sigma_g^+)$ + Na($4d$) $\rightarrow$ Na_3^+ + e. Dependence of the Na_2^+ ion signal due to process Na($3p$) + Na($5s$) $\rightarrow$ Na_2^+ + e on the power of laser 1 is nearly quadratic (c), but linear on the power of laser 2 (d).

Fig. 3. Population distribution $f_{v'}(v'')$ established by Franck-Condon pumping for various v'.

Fig. 4. Time-of-flight mass spectrum obtained when Na atoms are excited to the $4d_{5/2}$ state.

Fig. 5. Vibrational dependence of the rate of trimer ion formation by the process (14) using the Franck-Condon pumping method. The lower horizontal scale gives the vibrational level v', which is excited in the $A^1\Sigma_u^+$ state. Fluorescence from this level establishes a population distribution $f_{v'}(v'')$ over vibrational levels in the electronic ground state. The corresponding mean vibrational excitation $\langle v'' \rangle_{v'}$ is given above the upper horizontal scale of the frame. The open circles give the experimental data. The solid line gives the expected vibrational level dependence, based on eq. (15) and using the parameters obtained from the STIRAP data, shown in Fig.4 [see also eq. (16)]. Good agreement is found up to levels v' = 11. For v' = 14, a fraction of 36% of the molecules in the initial state (v'' = 0, J'' = 9) is transferred to levels in the range $27 \leq v'' \leq 29$.

Fig. 6. Vibrational dependence of the Na_3^+ ion signal due to $Na_2(X^1\Sigma_g^+, v'')$ + Na($3d_{5/2}$) collisions. The level v'' is selectively populated by the STRAP method. Open circles are the

experimental points, normalised to 100% population transfer efficiency. The solid line is a linear least squares fit to the experimental data.

Fig. 7. Energy diagram for Na_2 + Na system. Zero energy is chosen at the Na($3s$) + $Na_2(X^1\Sigma_g^+)$ dissociation limit of the ground state Na_3 molecule. The dissociation energy and ionisation potential of Na_3 are taken according to [20]. The levels v″ and v′ correspond to the vibrational excitation energies in $X^1\Sigma_g^+$ and $A^1\Sigma_u^+$ states. The Na($3p_{3/2}$) + $Na_2(A^1\Sigma_u^+,v')$ collision system with $11 \leq v' \leq 14$ has the same energy as Na($3d_{5/2}$) + $Na_2(X^1\Sigma_g^+,v'')$ with $26 \leq v'' \leq 29$. Other relevant energies are given as well. The energy of the Na_3^+ $^3\Sigma_u^+$ state is not well known. The shaded area indicates the range of this energy, predicted by different studies.

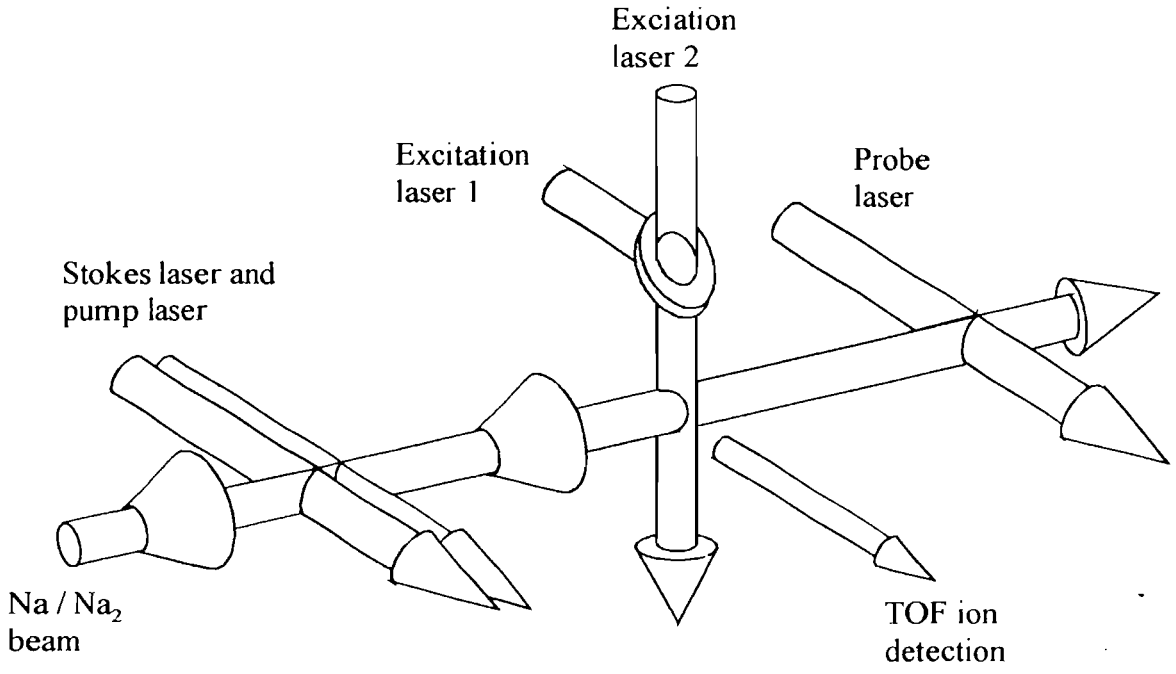
Exciation
laser 2
Excitation
laser 1
Probe
laser
Stokes laser and
pump laser
Na / Na_2
beam
TOF ion
detection

Fig. 1.

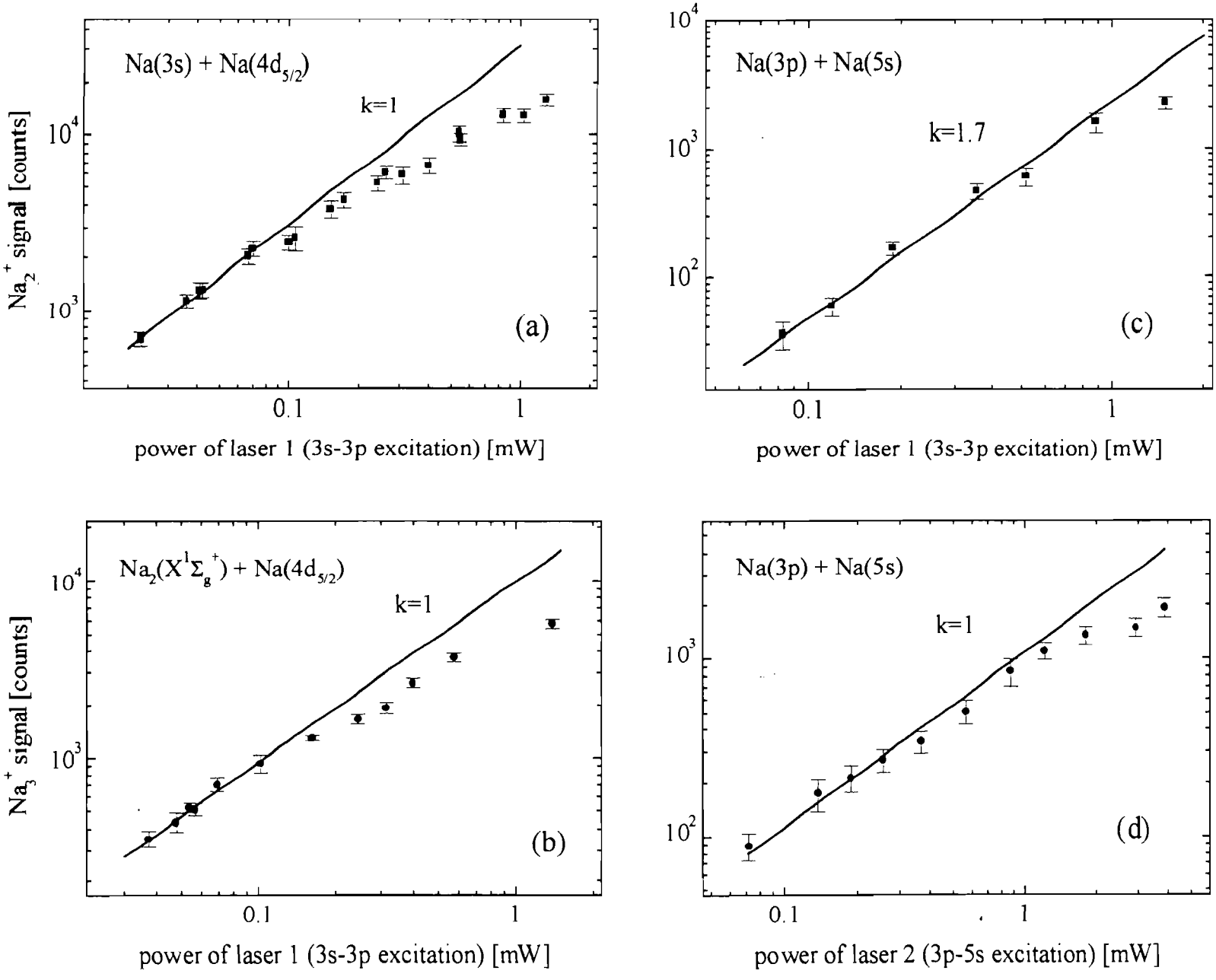
Na(3s) + Na(4d5/2)
k=1
(a)
Na2+ signal [counts]
power of laser 1 (3s-3p excitation) [mW]
Na(3p) + Na(5s)
k=1.7
(c)
power of laser 1 (3s-3p excitation) [mW]
Na2(X1Σg+) + Na(4d5/2)
k=1
(b)
Na3+ signal [counts]
power of laser 1 (3s-3p excitation) [mW]
Na(3p) + Na(5s)
k=1
(d)
power of laser 2 (3p-5s excitation) [mW]

Fig. 2

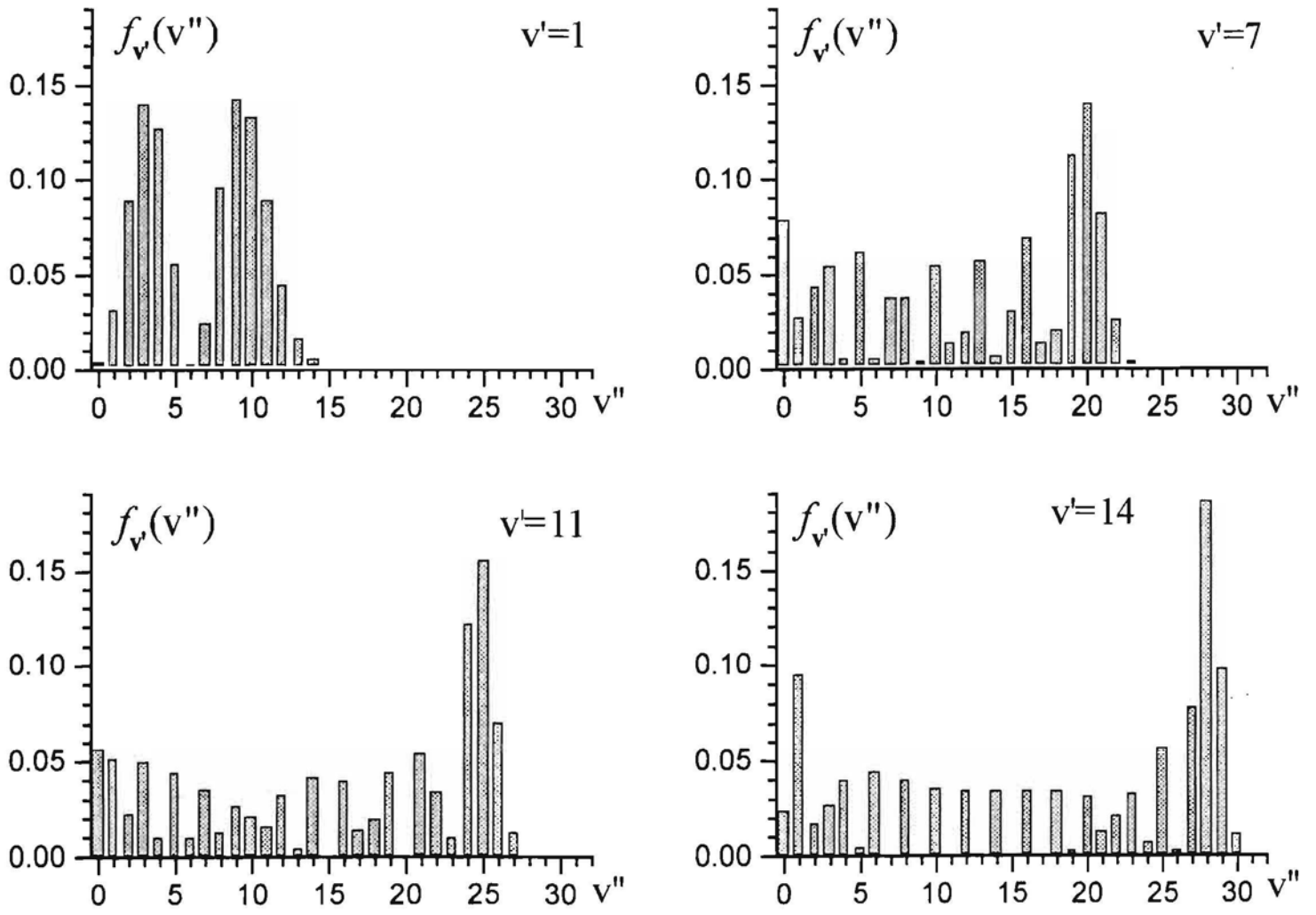

Fig. 3

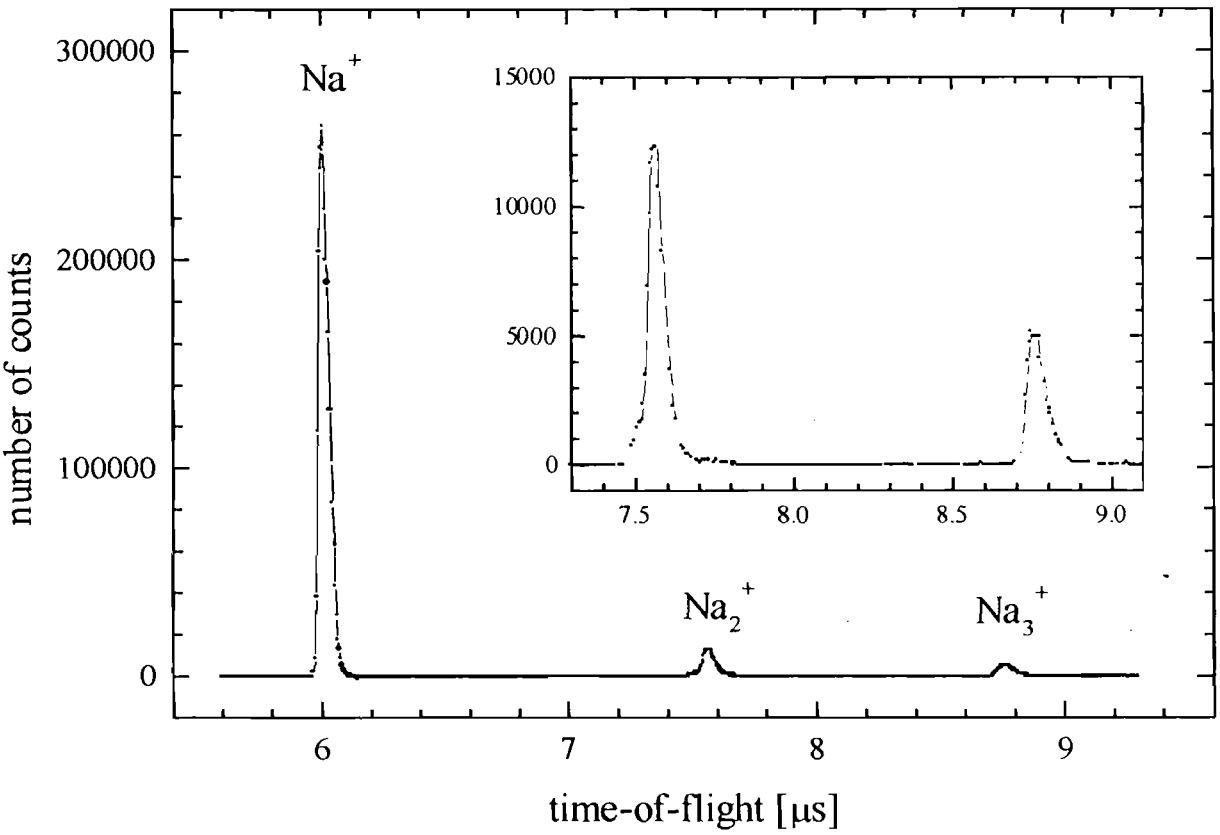
300000
200000
100000
0
number of counts
Na+
15000
10000
5000
0
7.5
8.0
8.5
9.0
Na2+
Na3+
6
7
8
9
time-of-flight [μs]

Fig. 4.

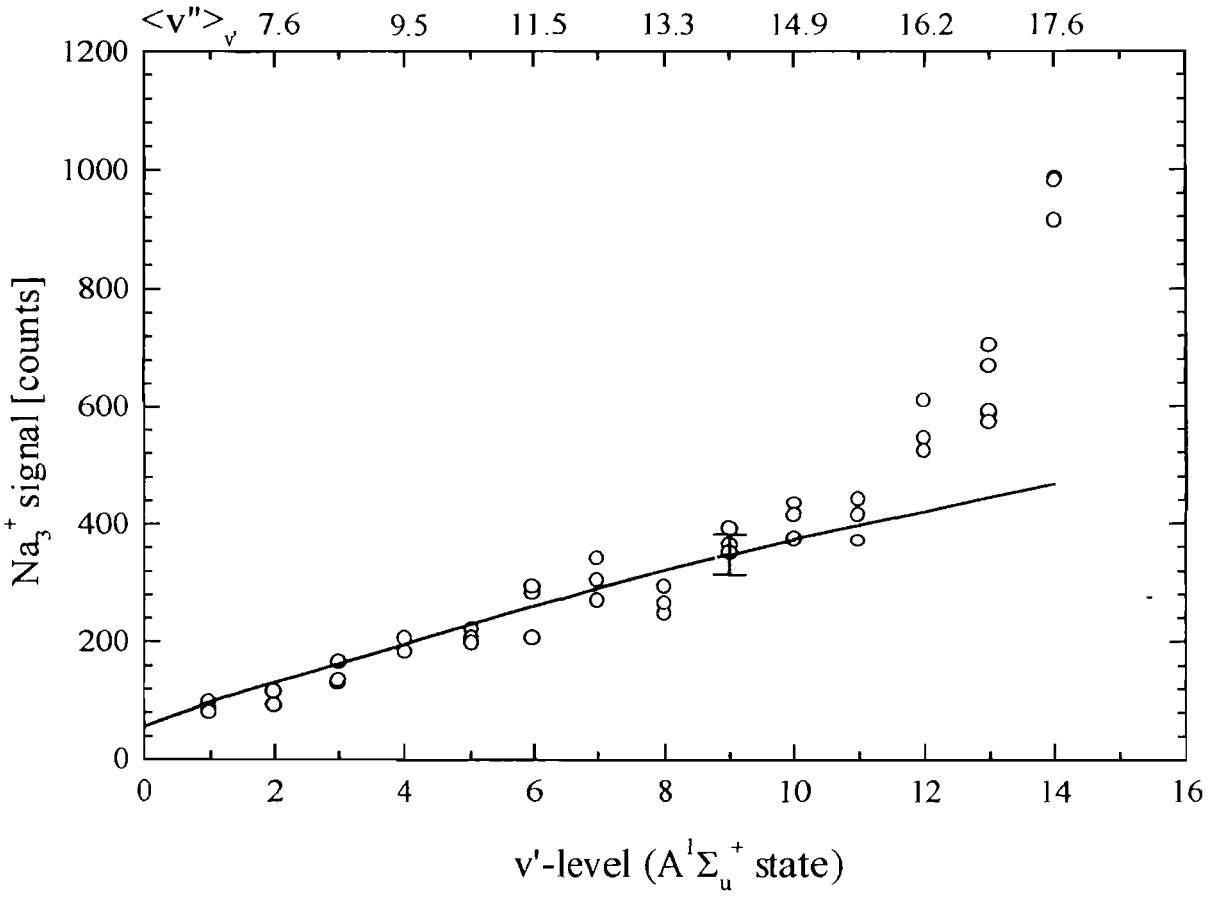
<v''>v' 7.6 9.5 11.5 13.3 14.9 16.2 17.6
1200
1000
800
600
400
200
0
Na3+ signal [counts]
0 2 4 6 8 10 12 14 16
v'-level (A1Σu+ state)

Fig. 5.

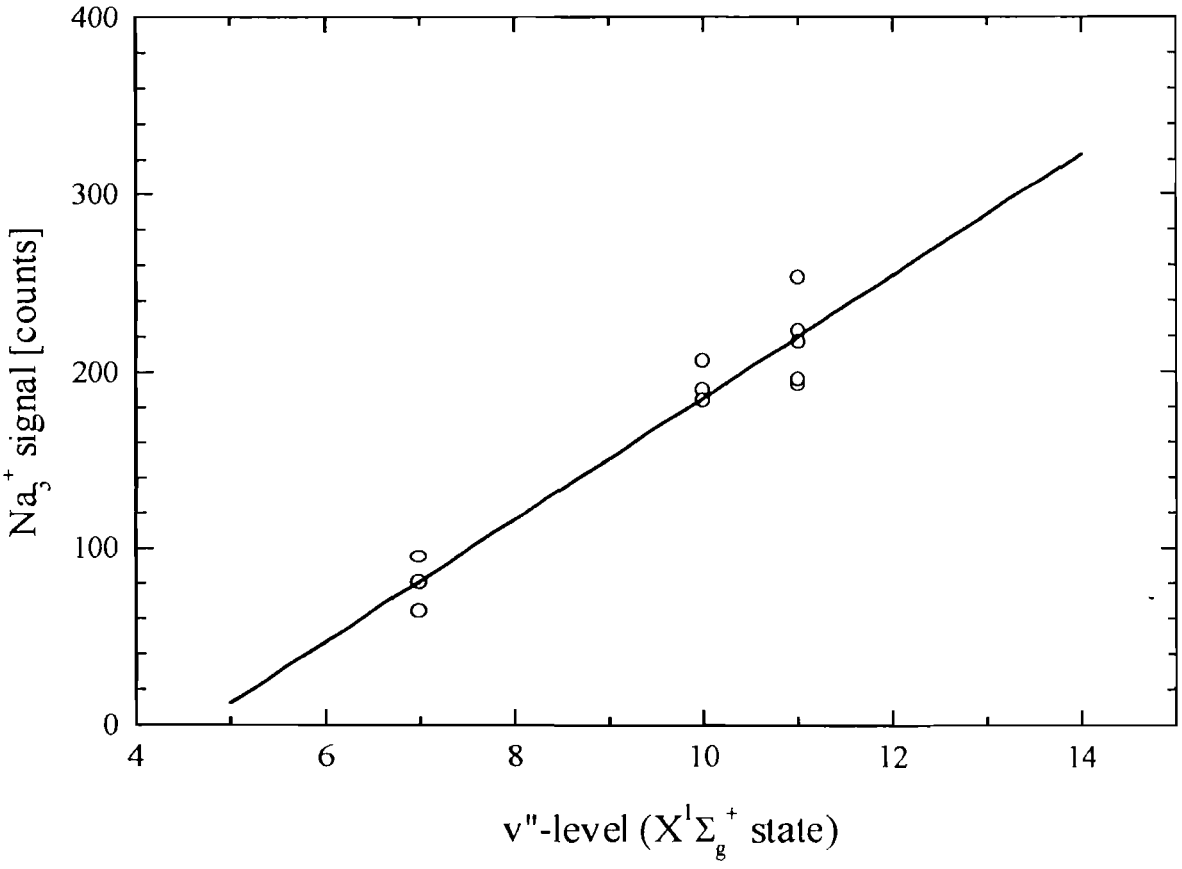
400
300
200
100
0
4
6
8
10
12
14
Na_3^+ signal [counts]
v"-level ($X^1\Sigma_g^+$ state)

Fig. 6.

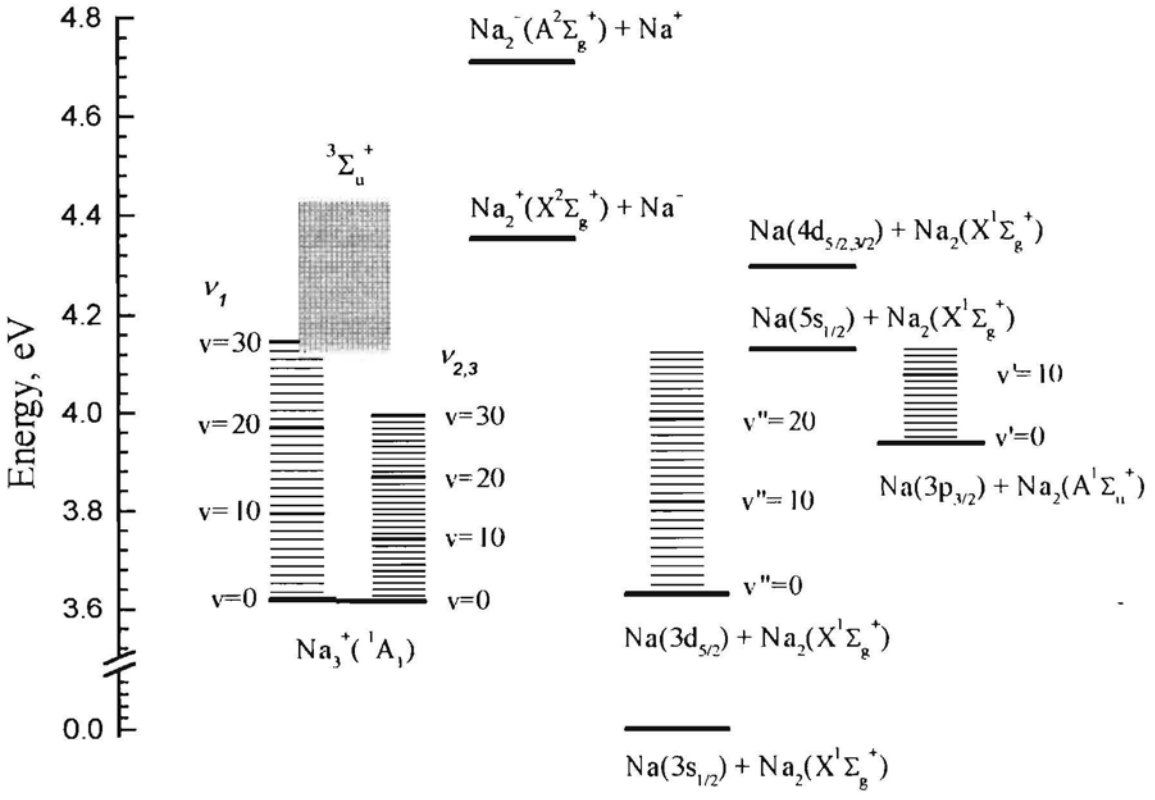
Energy, eV
4.8
4.6
4.4
4.2
4.0
3.8
3.6
0.0
$Na_2^-(A^2\Sigma_g^+) + Na^+$
$Na_2^+(X^2\Sigma_g^+) + Na^-$
$^3\Sigma_u^+$
ν_1
v=30
v=20
v=10
v=0
$\nu_{2,3}$
v=30
v=20
v=10
v=0
$Na_3^+(^1A_1)$
$Na(4d_{5/2,3/2}) + Na_2(X^1\Sigma_g^+)$
$Na(5s_{1/2}) + Na_2(X^1\Sigma_g^+)$
v''=20
v''=10
v''=0
$Na(3d_{5/2}) + Na_2(X^1\Sigma_g^+)$
$Na(3s_{1/2}) + Na_2(X^1\Sigma_g^+)$
v'=10
v'=0
$Na(3p_{3/2}) + Na_2(A^1\Sigma_u^+)$

Fig. 7.